Characterization of a novel Ser/Thr kinase/phosphatase pair in *Escherichia coli*

Krithika Rajagopalan

Submitted in partial fulfillment of the
requirements for the degree of
Doctor of Philosophy
in the Graduate School of Arts and Sciences

COLUMBIA UNIVERSITY

2018

ABSTRACT

Characterization of a novel Ser/Thr kinase/phosphatase pair in *Escherichia coli*

Krithika Rajagopalan

Regulatory protein phosphorylation is a well conserved mechanism of signal transduction in all biological systems. In bacteria, signal transduction by phosphorylation is thought to occur primarily on His and Asp residues. However, phosphoproteomic surveys in phylogenetically diverse bacteria over the past decade have identified numerous proteins that are phosphorylated on serine (Ser) and/or threonine (Thr) residues. Consistently, genes encoding Ser/Thr kinases are present in many bacterial genomes such as *E. coli*, which encodes at least three Ser/Thr kinases. Since Ser/Thr phosphorylation is a stable modification, a dedicated phosphatase is necessary to allow reversible regulation. Bacterial Ser/Thr phosphatases which have extensive sequence and structural homology to eukaryotic Ser/Thr PP2C-type phosphatases are referred to as eukaryotic-like Ser/Thr phosphatases (eSTPs). eSTPs have been identified in a number of bacteria, but none have been reported in *E. coli*. The work presented in this thesis was aimed at identifying and biochemically characterizing a eukaryotic-like Ser/Thr phosphatase and its partner Ser/Thr kinase in *E.coli*.

Chapter 3 describes the identification of a novel PP2C-like Ser/Thr phosphatase PphC encoded by an *E. coli* ORF, *yegK,* and characterization of its biochemical properties including kinetics, substrate specificity and sensitivity to known phosphatase inhibitors. I investigated differences in the activity of this protein in closely related *E. coli* strains. Finally, I demonstrated that this eSTP acts to dephosphorylate a novel Ser/Thr kinase which is encoded in the same operon suggesting that they most likely function as a pair in regulating Ser/Thr phosphorylation.

Chapter 4 describes the biochemical characterization of a Ser/Thr kinase YegI in *E. coli*. I show that YegI is an active kinase with significant structural homology to eukaryotic Ser/Thr kinases. The YegI kinase domain is tethered to a cytoplasmic C-terminal domain containing two non-specific DNA binding Helix-hairpin helix motifs. I have identified enolase and elongation factor-Tu (EF-Tu) as potential physiological substrates of YegI and have demonstrated that phosphorylation of EF-Tu by YegI inhibits protein translation *in vitro*.

TABLE OF CONTENTS

LIST OF FIGURES

LIST OF TABLES

ACKNOWLEDGEMENTS

I would like to thank my thesis advisor Jonathan Dworkin for giving me this opportunity to pursue my graduate work under his able guidance. He was a mentor in the truest sense, and I will forever be grateful for his enduring support and belief in my abilities as a scientist. His positivity and clear thinking is something that I would like to carry forward with me throughout my scientific career.

I would also like to thank all the members of the Dworkin lab past and present- Elizabeth Libby, Zak Frentz, Heather Feaga, Simon Diez, Paushali Chaudhury and Chris Thoroughgood for inspiring me to be a better scientist. Thank you for the countless hours of scientific and non-scientific discussions. This thesis would not be possible without your scientific advice and constructive criticism. Above all thank you for making the lab an enjoyable and fun place to work.

I would like to thank my committee, Lorraine Symington, and Max Gottesman, for always asking insightful questions and for patiently listening to my experimental ideas. I also thank Lars Dietrich and Anu Janakiraman for serving on my thesis committee.

I would like to thank Emily Chen from the HICCC proteomics shared resources at CUMC for identifying phosphorylation sites and performing the data analysis. I would like to thank our collaborator, Ljiljana Pasa-Tolic at PNNL, WA and Jared Shaw for performing comparative phosphoproteomics and data analysis. I would also like to thank members of the Symington lab and the Gottesman lab for kindly providing reagents and experimental advice.

I am indebted to my masters' program mentor Prakash Kulkarni for introducing me to scientific research and for teaching me how to think and design my experiments. I would also like to thank all my colleagues from my master’s program especially Sindu for her unconditional support and trust in me.

I would like to thank my family. Thank you, Mom and Dad, for your enormous moral support and for always inspiring me to work harder every day of my life. I am also grateful to my in-laws for sharing their valuable time with me during graduate school and always encouraging me to do better. Thank you, Nikhil, for being the best brother and a great in-house motivational speaker.

Lastly, I would like to thank my husband, Sohil for being the best support system I could have ever asked for during these crucial years of graduate school. Thank you for your enormous love and moral support. I am truly blessed and thankful to have you in my life.

Dedication

I would like to dedicate this thesis in memory of my grandfather (“thatha”) T.R. Srinivasan for being my biggest cheerleader.

CHAPTER 1

Introduction

1.1 Protein phosphorylation

Post-translational modifications control the activity of many proteins in the cell. Protein phosphorylation is one of the most widely studied post-translational modifications and has emerged as a crucial mechanism for signal transduction and regulation of protein function (1). Protein phosphorylation involves covalent attachment of a phosphate group to an amino acid side chain in the protein. Addition of a phosphate group enhances the charge density and hydrophilicity of the amino acid side chain thereby causing a change in conformation and protein function.

Phosphorylation is a rapid and reversible process mediated by the action of two opposing classes of enzymes: protein kinases and protein phosphatases. Protein kinases catalyze the hydrolysis of adenosine triphosphate (ATP) and generally transfer the $\boldsymbol{\gamma}$ phosphoryl group of ATP to phospho acceptor amino acids on a target protein. In eukaryotic cells, phospho acceptor amino acids are mostly hydroxyl group-containing amino acids such as serine, threonine and tyrosine. In several lower organisms such as bacteria, aspartate and histidine residues also act as phospho acceptor amino acids. Removal of a phosphate group from the phospho acceptor amino acids is catalyzed by protein phosphatases thereby restoring the target protein to its original state. This process is referred to as dephosphorylation.

If the target protein is an enzyme, then phosphorylation/dephosphorylation can alter its enzymatic activity, potentially acting as an ON/OFF switch. Additionally, phosphorylation can regulate protein function by facilitating or disrupting protein-protein interactions; stabilizing protein structure or marking protein for proteasomal degradation. Phosphorylation plays a key role in several metabolic pathways including cell growth, cell division, cell cycle, transcription,

translation and hormonal responses. The first evidence of a regulatory role of phosphorylation was observed in glycogen metabolism. Krebs and Fisher, as well as Wosilait and Sutherland in two independent studies, demonstrated that glycogen phosphorylase, an enzyme that plays a key role in glycogen metabolism, is subject to phosphorylation and dephosphorylation that affect its activity (2-5). Subsequently, over the years, many kinases, phosphatases, and phosphoproteins have been identified and characterized in phylogenetically diverse organisms, thereby establishing protein phosphorylation as a broadly important mechanism in regulating cellular processes.

1.2 Protein phosphorylation in bacteria

Historically, protein phosphorylation has been associated with eukaryotic cells (6). In fact, the question of whether this modification even existed in bacteria was a matter of debate. Initial studies to address this question were carried out in *Escherichia coli*, where the authors detected protein kinase activity by a cyclic AMP-dependent enzyme and subsequent phosphorylation of histone-like nucleoid structuring proteins (H-NS) (7). Cyclic AMP-dependent kinase activity was also detected in oral streptococci (8). However, due to a lack of chemical identity of residues and issues with reproducibility, these studies failed to conclude the presence of protein phosphorylation.

Eventually, studies in the late 1970s demonstrated that this mechanism is not exclusive to eukaryotes but can also be observed in bacteria (9, 10). The first bacterial phosphoprotein detected was an NADP-dependent isocitrate dehydrogenase (IDH), an enzyme that catalyzes the metabolism of isocitrate in the Krebs cycle. Two forms of IDH were isolated, phosphorylated and unphosphorylated, and it was observed that the phosphorylated form of IDH was completely inactive (11, 12). Although IDH was phosphorylated on a serine residue, the kinase responsible

for this modification had no similarity to eukaryotic type Ser/Thr kinases (13). These results suggested that bacteria may lack the eukaryotic-like signal transduction mediated by Ser/Thr phosphorylation. Subsequently, studies in the mid-1980s discovered the presence of histidine kinases that lacked any sequence homology to eukaryotic kinases (14, 15). These kinases became part of the two-component systems that established protein phosphorylation by histidine kinases as a global mechanism of signal transduction in bacteria (16).

1.3 Two-component systems: His/Asp phosphorylation

Unlike eukaryotes where signal transduction predominantly operates through phosphorylation on Ser/Thr/Tyr residues, signal transduction in bacteria was found to take place primarily by the addition of a phosphate group to histidine or aspartate residues. This mechanism involves two main components: a sensor molecule and a response regulator. In response to external stimulus, a sensor protein, most often a membrane-spanning histidine kinase, dimerizes and undergoes autophosphorylation on a conserved histidine residue. The autophosphorylated sensor kinase catalyzes the transfer of this phosphate group to a conserved aspartic acid residue in the response regulator. Upon phosphorylation, response regulators attain an active conformation and can affect the expression of genes via DNA binding (Fig.1.1) (17, 18).

In comparison to Ser/Thr kinases that create phosphoester intermediates, histidine kinases generate phosphoramide intermediates that are relatively labile. Therefore, they do not necessarily require a dedicated phosphatase to reverse the reaction. Interestingly, histidine kinases are thought to possess phosphatase activity (19). While the details of this activity remain somewhat mysterious, the general assumption in the field is that the balance between the kinase and phosphatase activity of the histidine kinase determines the phosphorylation state of the target

response regulator. Both Gram-positive and Gram-negative bacteria possess histidine kinases that regulate a range of bacterial cellular processes including sporulation, virulence, antibiotic resistance and chemotaxis (16, 20).

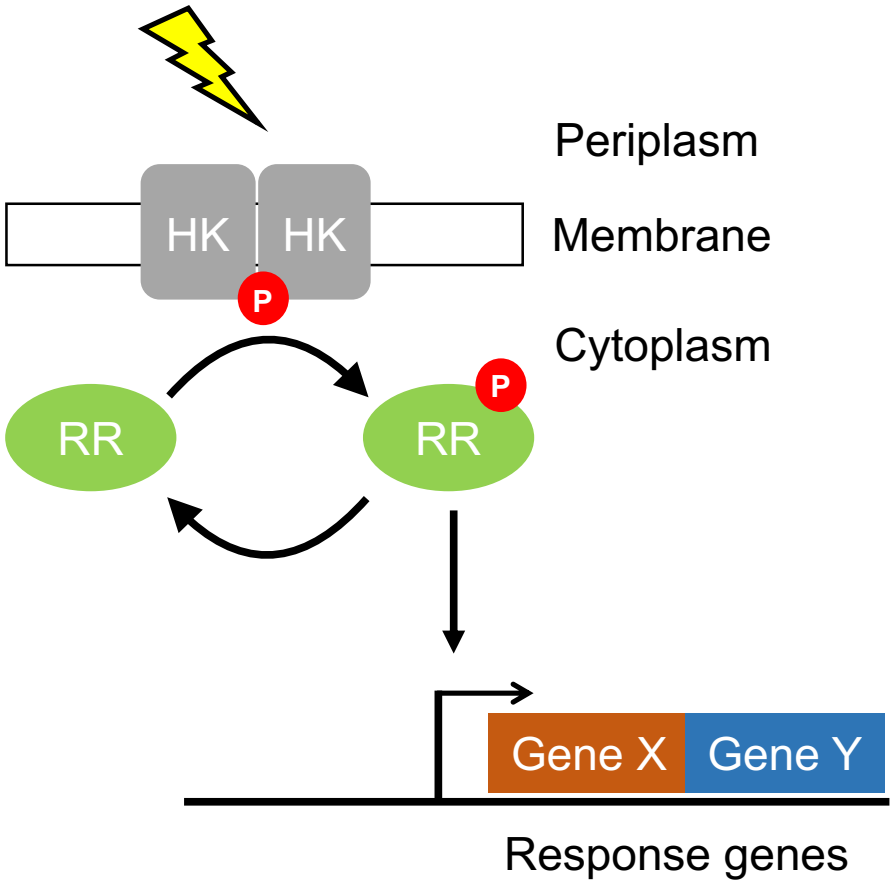

Figure 1.1: Phosphorylation by two-component systems
Inducing cues such as extra cytoplasmic stress (shown as yellow thunderbolt) are sensed by membrane bound histidine kinases (HK) that undergo dimerization and initiates autophosphorylation of Histidine residues and subsequent transfer of phosphoryl group to aspartate residues on response regulator (RR) in the cytoplasm. Phosphorylated response regulator functions as a transcriptional regulator by activating expression of target response genes (GeneX/ Y).

1.4 Ser/Thr phosphorylation in bacteria

The assumption that two component systems are only found in bacteria and that Ser/Thr kinase based systems are restricted to eukaryotes was found to be incorrect when studies emerged that plants and fungi have both these systems (21, 22). Similarly, the discovery of a gene (*pkn1*) encoding a Ser/Thr kinase in the Gram-negative bacterium *Myxococcus xanthus* indicated that Ser/Thr phosphorylation is not exclusive to eukaryotes. Specifically, the catalytic domain of Pkn1 shares significant sequence similarity to eukaryotic serine-threonine kinases (23). Although the knockout of *pkn1* did not affect viability, it was still important for the normal development of *M. xanthus*. A weak developmental defect and the lack of a difference in phosphorylation patterns between WT and Δ*pkn1* strains suggested that there could be additional kinases with redundant functions (23). Subsequently, using *pkn1* as a probe, the authors identified 26 additional genes with similarity to eukaryotic Ser/Thr kinases suggesting that Ser/Thr phosphorylation was important for normal development in *M. xanthus* (24-26). Following the identification of Ser/Thr kinases in *M. xanthus*, whole genome sequencing led to the discovery of these type of Ser/Thr kinases in several bacterial species suggesting that these proteins are widely prevalent in bacteria (27). Since these kinases share significant sequence and structural homology to catalytic domains of their eukaryotic counterparts they have been termed as eukaryotic-like serine-threonine kinases (eSTKs). These kinases are also referred to as Hanks-type kinases as they contain the conserved domain features described by Hanks *et al.* in 1988 (28).

eSTKs mediate phosphorylation of Ser/Thr residues, a modification that is relatively stable under physiological conditions as compared to phosphorylation on Asp/His residues. Therefore, a dedicated phosphatase is required to remove the phosphate group from Ser/Thr residues to reverse the phosphorylation reaction (Fig. 1.2). Consistently, whole genome sequencing of bacteria

revealed presence of eukaryotic-like Ser/Thr phosphatases (eSTPs) which bear a striking resemblance to a class of eukaryotic Ser/Thr phosphatases called Mg^{2+} or Mn^{2+} dependent protein phosphatases (PPM) (29). Genes encoding bacterial eSTPs often occur in the same operon as eSTKs and have been shown to counteract the kinase activity of eSTK by direct dephosphorylation of eSTK or eSTK substrates (30). The structural features and physiological role of eSTKs and eSTPs will be discussed in the following sections.

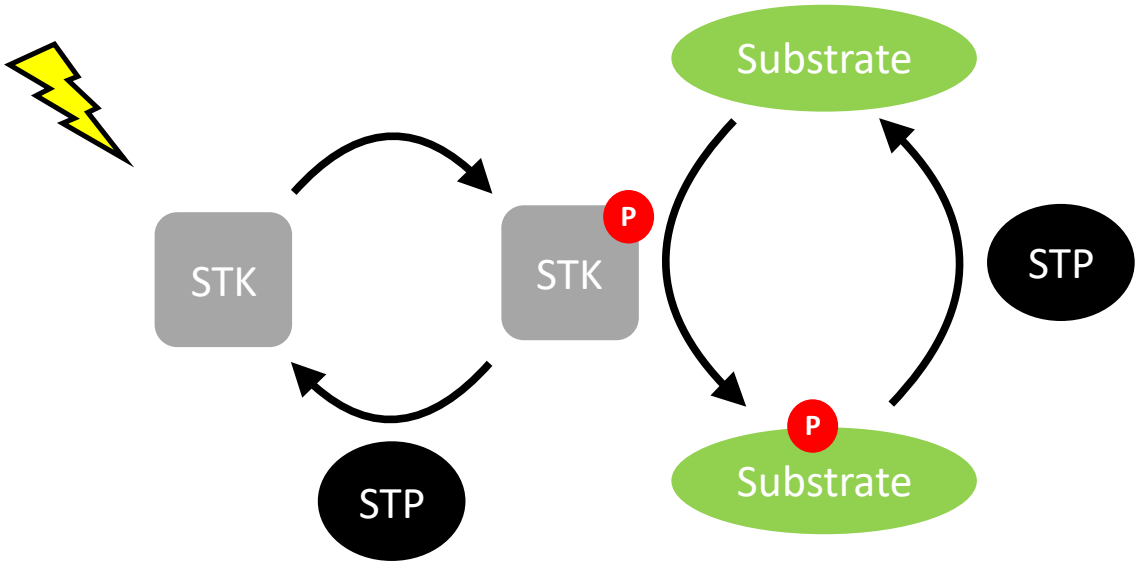

Figure 1.2: Ser/Thr phosphorylation
In response to external signal, the Ser/Thr kinase (STK) undergoes autophosphorylation on Ser/Thr residues and subsequently transphosphorylates a substrate on Ser/Thr residue. This stable phosphorylation on substrate is catalytically reversed by a Ser/Thr phosphatase (STP). STP can also remove phosphate group from STK.

1.5 Eukaryotic-like Ser/Thr kinases: Structural features

The catalytic domain of eSTKs is about 300 amino acids in length with sequence homology to eukaryotic protein kinases. The catalytic domain in eukaryotic Ser/Thr kinases is a bi-lobed structure containing a small N-terminal lobe primarily composed of β sheets and a large C-terminal lobe with mostly α helices (31). The catalytic site is present at the interface of the two lobes. While the N-terminal lobe orients and binds to ATP, the C-terminal lobe is responsible for binding to peptide substrate (Fig. 1.3A). The first crystal structure of an eSTK, *Mycobacterium tuberculosis* PknB, revealed significant structural homology to mouse cyclic AMP-dependent protein kinase (PKA), which is a member of eukaryotic Ser/Thr kinase superfamily (Fig.1.3B). The catalytic domain of eSTK contains twelve conserved Hanks subdomains numbered I-V, VIa, VIb and VII-XI. Hanks subdomains are characterized by the presence of twelve invariant and absolutely conserved residues responsible for positioning of the ATP molecule and catalysis (13).

The catalytic domain contains several essential structural features (Fig 1.3C). First, a nucleotide binding domain is present in between motifs I-IV. Nucleotide binding is mediated by motif I containing a glycine rich P-loop with sequence GXGXXGXV, a conserved lysine in motif II and a conserved glutamic acid in motif III. The P-loop is responsible for binding to the β and ɣ phosphates and catalyzes the transfer of the phosphate from ATP/ ADP during catalysis. Second, the catalytic loop present in motif VI is directly responsible for catalytic activity. The conserved aspartate residue in the catalytic motif D-X4-N is indispensable for catalytic activity and is conserved in all protein kinases. Third, the activation segment in the kinase domain is an important regulatory region that dictates activity of the kinase and it consists of the Mg^{2+}-binding loop (DFG motif), the activation loop and the P+1 loop. The aspartate residue in the DFG motif along with the conserved aspartate in the catalytic motif directly participate in catalysis by recognizing one of

the ATP bound Mg^{2+} ions. The activation loop is poorly conserved and is responsible for substrate specificity (32, 33). Activation of several eSTKs is achieved either by autophosphorylation or transphosphorylation of a threonine residue in the activation loop (34-36). Phosphorylation in the activation loop stabilizes the activation loop in a set conformation such that it promotes substrate binding and catalysis (32, 33). The activation loop also regulates protein-protein interactions. The P+1 loop lies at the interface of kinase and substrate and is responsible for specificity of kinase to serine/threonine phosphorylation (37).

Two possible mechanisms of kinase activation have been demonstrated: direct activation by ligand-promoted dimerization or indirect activation. The first evidence of ligand-promoted dimerization and activation of the kinase came from the crystal structure of *M. tuberculosis* PknB (35, 38). The PknB structure showed that it formed back-to-back dimers of the N-terminal lobe of the catalytic domain to undergo autophosphorylation. This mechanism of ligand-induced dimerization and activation was also observed for another *M. tuberculosis* eSTK, PknD (39), and the *Pseudomonas* eSTK PpkA (40). In cases where the kinase lacks a ligand binding domain, an indirect mechanism is proposed as a model for activation. For example, the crystal structure of the PknB kinase domain alone with an ATP competitive inhibitor revealed formation of asymmetric front-to-front dimers via interaction between the αG helix and an ordered activation loop on one domain and αG helix and a disordered activation loop of the second domain. Substitutions in the αG helix interface resulted in decreased autophosphorylation suggesting that αG helix in the C-terminal lobe of the kinase is important for activation. The conformation of the two proteins in the dimer is such that one monomer acts like an activator while the other monomer acts like a substrate very similar to a transphosphorylation model (41). This provides an alternate mechanism of activation especially for soluble kinases that lack a membrane bound domain.

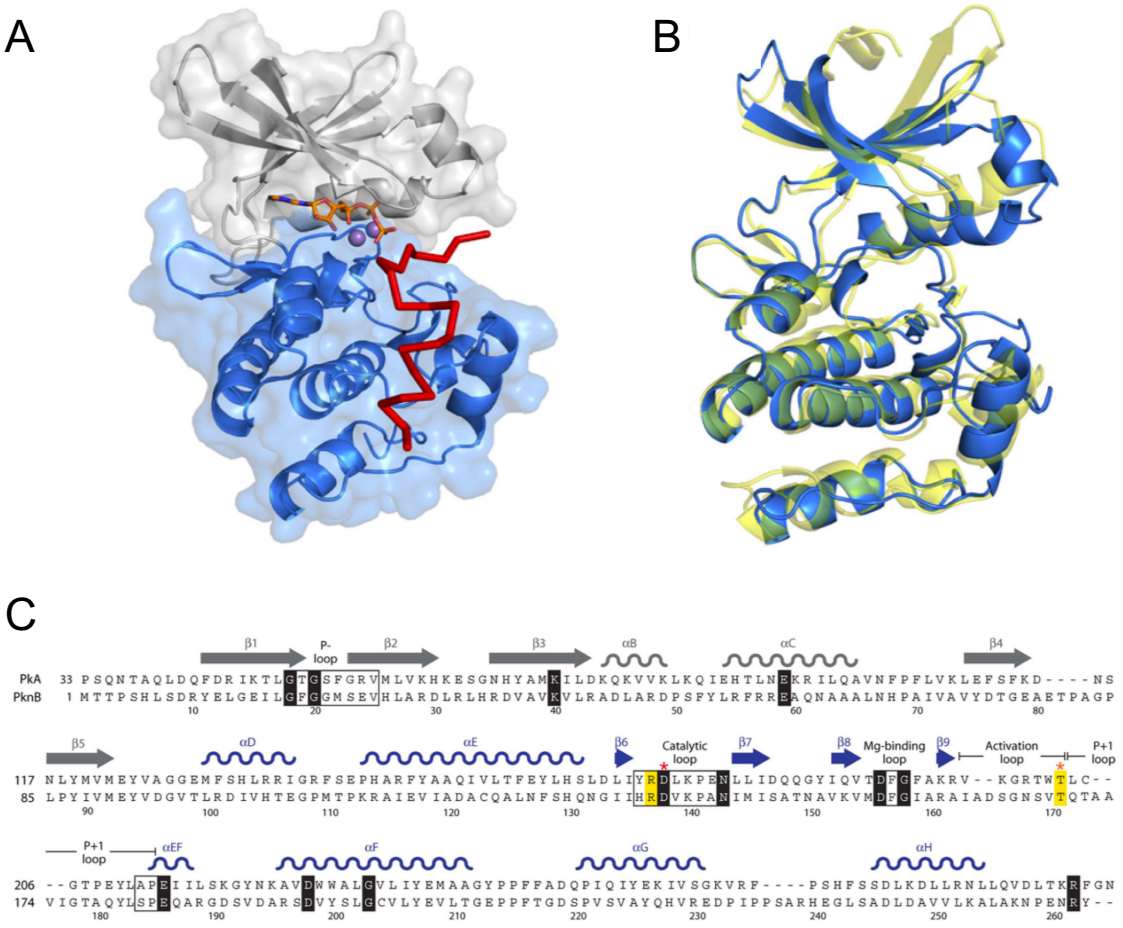

Figure 1.3: Structure of Eukaryotic-like Ser/Thr kinase (eSTK) catalytic domain (A)Crystal structure of mouse PKA catalytic domain in complex with ATP and an inhibitor peptide (PDB ID: 1ATP). The N-terminal lobe of PKA is depicted in gray and the C-terminal lobe is shown in blue. ATP molecule is shown as sticks, two manganese ions are shown as purple spheres, 20 residue inhibitor peptide is shown in red.
(B) Crystal structure of mouse PKA was superimposed on crystal structure of *M tuberculosis* eSTK PknB (PDB ID: 1MRU). Mouse PKA is shown in blue and PknB is shown in yellow.
(C) Amino acid sequence alignment of mouse PKA (residues 33-283) and PknB (1-266) catalytic domains. The secondary structure elements are represented on top of the sequence. Conserved structural features are shown in boxes, while invariant residues are highlighted in black. Red and orange asterisks indicate catalytic site and conserved threonine in activation loop respectively. (Taken from (30))

1.5.1 Eukaryotic-like Ser/Thr kinases in Gram-positive bacteria

eSTKs are observed in both Gram-positive and Gram-negative bacteria. Gram-positive eSTKs generally comprise of three domains: a cytoplasmic domain containing a highly conserved Hanks family kinase; a transmembrane domain that is connected to the cytoplasmic domain via a non-conserved juxta-membrane domain; and an extracellular region that consists of three or four **p**eptidoglycan binding **a**nd **S**er/**T**hr kinase **a**ssociated (PASTA) repeats. The PASTA repeats are commonly found in penicillin binding proteins that participate in peptidoglycan biogenesis and are essential for growth and development (42, 43). The Dworkin lab demonstrated that the PASTA repeats of the *Bacillus subtilis* eSTK PrkC recognize peptidoglycan fragments (muropeptides) providing the first evidence of a possible ligand of a bacterial receptor eSTK (44).

Although most Gram-positive eSTKs regulate essential bacterial processes, they are mostly non-essential with the exception of the *M. tuberculosis* eSTK PknB (45). Gram-positive eSTKs containing PASTA domains have been found to play a role in sensing cell wall homeostasis and cell wall biosynthesis. For example, *B. subtilis* eSTK PrkC is required for sensing muropeptides during spore germination as cells lacking PrkC were unable to germinate suggesting a possible role of PrkC in signaling the spore to germinate (exit dormancy) in response to muropeptides (44). PASTA-containing eSTKs also regulate cell division by directly interacting and modifying cell division proteins involved in septal formation. For example, *Streptococcus pneumoniae* StkP phosphorylates cell division protein DivIVA and regulates the transition from septal to peripheral peptidoglycan synthesis (46). StkP also regulates the stability of the eukaryotic tubulin homolog FtsZ by directly phosphorylating MapZ, a protein responsible for positioning FtsZ rings at the septum (47).

The integral role of PASTA-containing eSTKs in cell division and cell wall homeostasis

suggested that eSTKs could regulate response to cell wall stress inducing antibiotics. Consistently, PASTA-containing eSTKs in *Staphylococcus aureus* (48, 49), *Listeria monocytogenes* (50, 51) and *Enterococci* (52, 53) are important for resistance to β-lactam antibiotics. However, the exact molecular mechanism of how eSTKs mediate β -lactam resistance is still unknown. In addition to role in cell wall biosynthesis and cell division, PASTA containing eSTKs have been implicated in the virulence of multiple pathogens. For example, in *Listeria monocytogenes*, the presence of eSTK PrkA is critical for promoting survival within the host cytoplasm by predominantly regulating basic physiological processes like cell division and morphogenesis (54) and in rare instances by direct regulation of virulence factors (48). PASTA containing eSTKs have also been shown to play an important role in biofilm formation, which in some cases contributes to pathogenesis and disease progression. For example, in *Streptococcus mutans*, deletion of eSTK StkP impairs biofilm formation (55).

1.5.2 Eukaryotic-like Ser/Thr kinases in Gram-negative bacteria

Much less is known about the physiological substrates of eSTKs in Gram-negative bacteria. Although there is no known structure of a Gram-negative eSTK, the predicted structure and features of the kinase domain in Gram-negative eSTKs are homologous to those seen in Gram-positive eSTKs. Unlike Gram-positive eSTKs, eSTKs identified in Gram-negative bacteria lack an extracellular PASTA domain. Although not much is known about the substrates in Gram-negative eSTKs, they have been shown to play an important role in regulating cellular processes including cell development, virulence, biofilm formation and stress response as I will discuss below.

One of the most well studied Gram-negative bacteria with eSTKs is *M. xanthus*. Over 102 putative eSTKs have been identified (unpublished, Monsanto microbial sequence database of *M. xanthus*) of which only 13 eSTKs have been characterized (23, 26, 56-59). Some eSTKs in *M. xanthus* participate in a kinase cascade and regulate fruiting body formation. For example, under nutrient deprived conditions, *M. xanthus* aggregates and forms multicellular fruiting bodies. The *M. xanthus* eSTK Pkn8 phosphorylates and activates another eSTK, Pkn14, which in turn phosphorylates MrpC, a key transcriptional regulator that directly controls expression of genes responsible for fruiting body formation and spore development. Phosphorylation of MrpC inhibits the binding of MrpC to its own promoter resulting in downregulation of genes in involved in fruiting body development. Consistently in *pkn8* and *pkn14* deletion strains, fruiting body development progresses faster as compared to WT strain indicating a fundamental role of eSTK in *Myxococcus* development (25, 60).

Some Gram-negative eSTKs have also been implicated in virulence. For example, the secreted eSTK YpkA is important for virulence of *Yersinia pseudotuberculosis* (61). The *Pseudomonas aeruginosa* eSTK PpkA plays an important role in bacterial virulence in neutropenic mice (62) and activation of Type VI secretion systems (40, 63). A recent study showed that mutations in PpkA also impacts biofilm formation and decreases tolerance to oxidative or osmotic stress (64).

Although Ser/Thr phosphorylation was first reported in *E. coli* in the late 1970s (9, 10) and the whole genome was sequenced in 1997 (65), a gene encoding an eSTK was not identified until ten years later. YeaG is the first and only reported eSTK in *E.coli* (66) which was initially identified in a transcriptomic screen for genes upregulated in response to various stresses including low pH, osmotic stress, entry into stationary phase (67). Sequence analysis of YeaG showed the

presence of an N-terminal ATPase (AAA+) domain and a C-terminal kinase domain. Proteins containing AAA+ domains are often mechanochemical enzymes that convert chemical energy derived from ATP hydrolysis to mechanical force in order to induce conformational change in substrates. The kinase domain of YeaG is similar to that of the *B. subtilis* eSTK PrkA and exhibits distant homology to eukaryotic protein kinases (68). Biochemical analysis of YeaG showed that it is an active kinase which phosphorylates an unknown 65kda cytoplasmic protein (69).

The global nitrogen-sensitive transcription factor NtrC activates *yeaG* expression in response to nitrogen starvation and deletion of *yeaG* led to decreased survival in response to sustained periods of nitrogen starvation (70). Catalytic activity of the YeaG AAA+ and kinase domains were crucial for adaptation to sustained nitrogen starvation (70). More recently, the molecular mechanism of how YeaG is important for adaptation to nitrogen starvation was characterized using transcriptomics and metabolomic approaches (71). Under sustained nitrogen starvation conditions, deletion of *yeaG* resulted in major transcriptome changes specifically the dysregulation of NtrC responsive methionine biosynthesis genes. Aberrant activation of methionine biosynthesis genes resulted in decreased survival of Δ*yeaG* strain under nitrogen starvation conditions (71). Together these results demonstrate that *yeaG* is important for adaptation to nitrogen starvation, however whether or not YeaG kinase activity or its presumed phosphorylation substrates contribute to this adaptation is still unexplored.

1.6 Atypical Ser/Thr kinases in *Escherichia coli*

Although most bacterial Ser/Thr kinases identified thus far belong to the Hanks family of kinases, there are some exceptions. So-called atypical Ser/Thr kinases lack the defined Hanks conserved motifs (72). However, despite the absence of these conserved motifs, these kinases

retained their catalytic activity. Phylogenetic analysis suggested that these atypical Ser/Thr kinases form a separate phyletic group that arose as early as the typical Hanks family of kinases. Classical examples of atypical Ser/Thr kinases in eukaryotic cells are aminoglycoside kinases, choline kinases and phosphatidylinositol 3-kinases (PI3K). Aminoglycoside kinases and choline kinases have distinct structural modifications in the C-terminal lobe while PI3K have a more flat structure with an open active site as compared to Hanks family kinases.

E.coli hipA encodes a Ser/Thr kinase that belongs to the phosphatidylinositol 3/4-kinase (PI3/4K) superfamily (73). Unlike other bacterial eSTKs, HipA does not possess Hanks domains or the absolutely conserved residues that are commonly observed in eSTKs (74). *hipA* was first identified in a genetic screen for genes responsible for increased tolerance to antibiotics. Mutations in *hipA* (notably the *hipA7* allele) resulted in 1000-fold of persisters, cells with a heightened tolerance to antibiotics, as compared to WT strains (75, 76). Subsequently, sequence analysis and biochemical characterization demonstrated that HipA together with HipB is part of a toxin-antitoxin module that dictates multidrug tolerance states. Autophosphorylation of HipA on residue Ser-150 was crucial for multidrug tolerance states (73). Unlike eSTKs, Ser-150 is not present in the activation loop and instead is in the catalytic core in the P-loop. Phosphorylation of Ser-150 stabilizes the HipA molecule in an off state by ejection of P loop thereby inactivating the kinase. Overexpression of *hipA* triggers growth arrest in *E. coli* by activation of stringent response resulting in translational inhibition (77). The exact molecular mechanism of HipA induced bacterial persistence was shown to be mediated via phosphorylation of glutamyl tRNA synthetase (GltX) on a single Ser residue. Phosphorylated GltX failed to aminoacylate tRNA resulting in accumulation of uncharged tRNA at the ribosome and activation of stringent response and bacterial persistence (78, 79). Although HipA phosphorylates GltX on a serine residue, the phosphatase

responsible for reversing this modification is still unknown. In this study, I have identified a novel Ser/Thr phosphatase in *E. coli* but was unable to demonstrate dephosphorylation of either HipA or GltX suggesting that there could be other Ser/Thr phosphatases that are yet to be identified.

E. coli YihE, another atypical Ser/Thr kinase, has structural similarity to choline kinases and aminoglycoside kinases (80). Phenotypic analysis revealed that *yihE* is predominantly expressed in stationary phase in a CpxR dependent manner. CpxR is a response regulator which along with histidine kinase CpxA regulates the response to various cellular stresses including membrane damage, starvation and high osmolarity (81). Subsequent phenotypic analysis of *yihE* showed that in response to antimicrobial stress, YihE regulates programmed cell death in bacteria and protects *E. coli* from antimicrobials by antagonizing the action of MazEF toxin-antitoxin system (82). More recently, the *yihE* gene was shown to be upregulated in low-level quinolone resistant *E. coli* strains suggesting increased protection of resistant *E. coli* strains against programmed cell death (83). However, the mechanistic basis of these phenotypes, specifically, the identity of YihE substrates, remains unknown.

1.7 Eukaryotic-like Ser/Thr phosphatases

The comparatively stable character of Ser/Thr phosphorylation requires a dedicated enzyme to remove the phosphate group in order to facilitate reversible phosphorylation. Protein Ser/Thr phosphatases mediate removal of a phosphate group from Ser/Thr residues. In eukaryotic cells, protein Ser/Thr phosphatases have been broadly classified into three major families depending on their protein structure, substrate specificity and sensitivity to phosphatase inhibitors. These are: aspartate based phosphatase family of phosphatases, phosphoprotein phosphatases (PPP) and metal (Mg^{2+} or Mn^{2+}) dependent protein phosphatases (PPM). Homologs of PPP and PPM

phosphatases have been identified in bacteria

PPP phosphatases are further subdivided into seven subfamilies PP1, PP2A, PP2B, PP4, PP5, PP6 and PP7 that contain both a catalytic subunit and a regulatory subunit that dictates substrate specificity. Although PPP phosphatases are classified as Ser/Thr phosphatases, PPPs exhibit the ability to dephosphorylate phospho His and Tyr residues indicative of broad specificity (84, 85). Unlike PPP phosphatases, PPM phosphatases are more abundantly found in bacteria and are often encoded in the same operon as, and often adjacent to, genes encoding eSTKs suggesting that the function of PPM phosphatases is tightly connected with that of eSTKs. For every bacterial eSTP (PPM) there are one or more eSTKs, suggesting that eSTPs mediate complex regulation of eSTK signal transduction. For example, *M. tuberculosis* has eleven eSTKs and one eSTP (86). Unlike PPP phosphatases, PPM phosphatases do not contain a separate substrate recognition or a regulatory subunit. Therefore, regulation of PPM phosphatase activity and how PPM phosphatases specifically recognize their substrates remains unclear.

1.8 PPM/PP2C phosphatases

1.8.1 PPM/PP2C phosphatases: Structural features

PPM phosphatases are Mg^{2+} or Mn^{2+} dependent Ser/Thr phosphatases that share significant structural and sequence homology to eukaryotic PP2C phosphatases (29, 87, 88). The catalytic domain of PPM/PP2C phosphatases is typically 200-290 amino acids in length with eleven to thirteen signature conserved motifs (89). In addition to these signature motifs, PPM phosphatases contain eight absolutely conserved residues that include four aspartate residues in motif I, II, VII, and XI; a threonine residue in motif IV; and three glycine residues in motif V, VI, and VIII (Fig.1.4A). Together these residues mediate metal coordination, substrate binding, and catalysis.

Bacterial PP2Cs are further subdivided into two groups depending on the presence of signature motifs 5a and 5b (89, 90). Group I PP2C-like phosphatases (eSTPs) contain all the thirteen signature motifs including motif 5a and 5b while Group II PP2Cs lacks motif 5a and 5b (89). The *B. subtilis* sporulation-specific PP2C-like phosphatase SpoIIE (91) and the stress response PP2C-like phosphatases RsbX and RsbU (92, 93) are catalytically active despite the lack of motif 5a and 5b indicating that these motifs are not crucial for activity.

The catalytic core of a PPM phosphatase is buried in the central beta sandwich formed by anti-parallel beta sheets (94). Antiparallel alpha helices surround these sandwiched beta sheets. The metal ions are located in the cleft which is formed by the beta sandwich structure (Fig.1.4B). Metal ion coordination is mediated by conserved aspartate residues and a water molecule. The catalytic activity of PPM phosphatases is dependent on the presence of bivalent metal ions Mg^{2+}/Mn^{2} which bind to a water molecule and initiate a nucleophilic attack on the phosphorous atom while a second water molecule protonates the oxygen on a modified Ser/Thr residue. Structures of several bacterial PP2Cs including *Thermosynechococcus elongatus* tPphA (95), *M. tuberculosis* PstP (96), *Mycobacterium smegmatis* MspP (97) *Streptococcus agalactiae* Stp (98) and *S. aureus* Stp1(99) reveal significant structural homology to human PP2C with all the active sites conserved. The structures of human PP2C (Fig.1.4B) and *T.elongatus* tPphA (Fig.1.4C) illustrate this homology.

Despite the overall similarity, there are however three notable differences in the structure between the bacterial and eukaryotic homologs. First, human PP2C contains a C-terminal domain consisting of three antiparallel alpha helices that are responsible for substrate recognition and specificity but does not impact the catalytic activity (Fig.1.4B). However, this domain is not present in tPphA and other bacterial PP2Cs (Fig.1.4C). Second, structures of the bacterial PP2Cs

show binding to three metal ions instead of two metal ions as seen in human PP2C. In the case of tPphA, two aspartate residues in motif V and VIII respectively mediate metal coordination of third metal ion. Recently, the structure of *S. aureus* eSTP Stp1 revealed the presence of four metal ions suggesting differences in metal co-ordination within bacterial PP2Cs. (99). Third, human PP2Cs contains a flap domain (Fig1.4B, C denoted in red) which is positioned away from the active site to allow substrate access. In bacterial PP2Cs, the flap subdomain is flexible and is positioned closer to the active site. For example, in tPphA, the arginine residue at position 169 acts as a hinge and is responsible for the flexible nature of flap subdomain. Mutation of Arg 169 impairs catalytic activity indicating that the flexible flap domain is essential for substrate binding and catalysis (95).

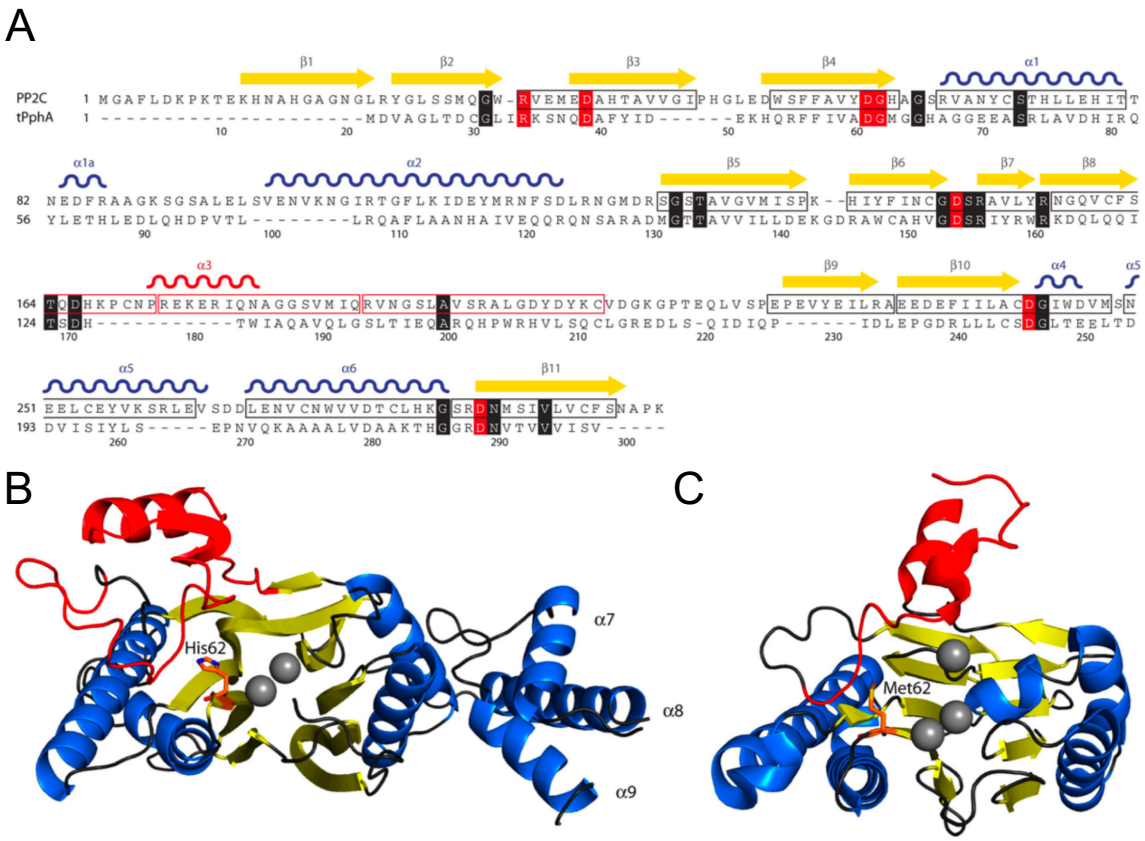

Figure 1.4: Structure of PPM family of Ser/Thr phosphatase
(A)Amino acid sequence alignment of Human PP2C (residues 1-299) and *Thermosynechococcus elongatus* PphA (1-241) catalytic domains. The secondary structure elements are represented on top of the sequence. Conserved motifs 1-5, 5a, 5b and 6-11 as defined as in (89) are shown in boxes. Conserved amino acids are highlighted in black while residues involved in metal binding pocket are shown shaded in red.
(B) Crystal structure of human PP2C structure (PDB ID: 1A6Q). The β sandwich is shown in yellow, α helices in blue, flap subdomain is shown in red while the two manganese ions are shown as gray spheres. His62 (orange) is shown as sticks. The C-terminal domain containing α-helices (α7, α8, α9) are absent in bacterial PP2Cs.
(C) Crystal structure of *Thermosynechococcus elongatus* PPM phosphatase tPphA (PDB ID:2J86). The β sandwich is shown in yellow, α helices in blue, flap subdomain is shown in red while the three manganese ions are shown as gray spheres. Met62 (orange) is shown as sticks and occupies homologous position as His62.(Taken from (30)

1.8.2 Physiological role of Eukaryotic-like Ser/Thr phosphatases (PPM/PP2C)

One important biochemical role of bacterial PP2Cs is to reverse the action of the kinase by directly dephosphorylating activated partner kinase. Examples include the *B. subtilis* eSTP PrpC which dephosphorylates the eSTK PrkC *in vitro* (100), the *S. agalactiae*, eSTP Stp which reverses the action of the eSTK Stk (101) and *M. tuberculosis* PstP which dephosphorylates the eSTKs PknA and PknB *in vitro* (34, 102). Alternatively, bacterial PP2Cs also act by dephosphorylating eSTK substrates. For example, the *S. agalactiae* eSTK/ eSTP pair Stk/Stp reversibly regulates phosphorylation of inorganic pyrophosphatase (101). Other example include *S. pneumoniae*, eSTK/ eSTP pair StkP/PhpP which reversibly regulate phosphorylation of cell division protein DivIVA (103, 104) and the *B. subtilis*, eSTK/ eSTP pair PrkC/PrpC which reversibly regulate phosphorylation of two-component response regulator WalR (105).

As compared to eSTKs, much less is known about the physiological role of bacterial PP2Cs. However, in a few instances, eSTPs have been reported to have opposing roles as eSTK in regulating cellular processes like cell growth, development, antibiotic resistance, and virulence. For example, deletion of the *B. subtilis* eSTP PrpC resulted in an extended stationary phase phenotype which is the exact opposite of a deletion strain of eSTK PrkC that shows a defect in stationary phase (106). In *M. xanthus*, deletion of eSTP Pph1 showed defects in the formation of multicellular fruiting bodies from viable spores under starvation conditions (107). Deletion or point mutations in *S.aureus* eSTP Stp1 results in reduced susceptibility to cell wall antibiotics vancomycin and daptomycin (108, 109). Similarly, mutations in *S. aureus* STP resulted in upregulation of genes that are responsible for cell wall thickening and increase resistance to lysostaphin (49) and downregulation of virulence genes (108). In *Salmonella enterica serovar typhi*, deletion of eSTP/eSTK operon *prpZ/prkY/prkX* resulted in decreased virulence in human

macrophages by promoting phagocytosis (110). Similarly, deletion of both the eSTK and eSTP in *B. anthracis* decreased survival in macrophages (111). However, whether this impact on virulence is due to eSTK or eSTP is still unclear. Although eSTPs impact multiple cellular processes, how eSTPs regulate these processes and the exact mechanism remains poorly understood.

1.9 Identification of phospho substrates using phosphoproteomics

Ser/Thr kinases participate in regulatory networks of eukaryotic cells and initiate signaling cascades by phosphorylating substrate proteins on either a single or multiple Ser/Thr residues (112). Although eSTKs were identified in several bacteria, little was known about specific protein substrates. Mass spectrometry-based phosphoproteomic analysis identified several cellular proteins that are phosphorylated on site-specific Ser/Thr residues (113). For example, ~100 cellular proteins were found to be phosphorylated on Ser/Thr residues in *E. coli* (114) and *B. subtilis* (115) whereas somewhat smaller phosphoproteomes were detected in *Pseudomonas sp.* (116) and *Mycoplasma pneumoniae* (117), each with around 50-60 phosphorylated proteins. One of the largest phosphoproteomes with >300 phosphorylated proteins was detected in *M. tuberculosis* (118) consistent with the presence of eleven eSTKs (86).

In all these studies, a majority of these phosphorylated proteins have a wide array of functions. For example, phosphoproteomes of both Gram-positive and Gram-negative bacteria are overrepresented with enzymes that participate in central carbon metabolism specifically in glycolysis (115, 117, 119-122). In the case of *E. coli* and *B. subtilis*, almost all the enzymes involved in glycolysis are reported to be phosphorylated on Ser/Thr residues hinting at phosphorylation- mediated regulation of glycolysis (115, 120). It should be emphasized, however, that there exists little direct evidence of such regulation.

The metabolic and highly conserved enzyme enolase is reported to be phosphorylated on Ser/Thr/Tyr residues across multiple bacterial genomes. Enolase is a critical glycolytic enzyme that catalyzes the second last step in the glycolytic pathway, the interconversion of 2-phosphoglycerate to phosphoenolpyruvate. In *E. coli (114, 123),* enolase is phosphorylated on Ser-372, Thr-375, Thr-379 while in *B. subtilis* (115) enolase is phosphorylated at Thr-141, Ser 259, Tyr-281, Ser-325. However, the impact of phosphorylation on the regulation of glucose metabolism as well as the kinase/phosphatase responsible for the reversible modification of enolase is not known. In addition to its role in glycolysis, enolase is a vital component of the RNA degradosome complex which includes a major endoribonuclease RNase E, polynucleotide phosphorylase PNPase and an ATP-dependent RNA helicase RhlB (124). The RNA degradosome is responsible for orderly regulation and degradation of transcripts for controlling gene expression (125). A few studies have shed light on the possible role of enolase in the RNA degradosome. Under aerobic conditions, enolase in the RNA degradosome mediates rapid degradation of the glucose transporter *ptsG* mRNA in response to phosphosugar stress (126). More recently, under anaerobic conditions, enolase was reported to be essential for regulation of cell morphology by specifically stabilizing small RNA DicF, a known inhibitor of cell division protein FtsZ (127). However, the exact mechanism of how enolase dictates RNA cleavage depending on environmental conditions, substrate availability or specificity remains unclear. Furthermore, the possible impact of phosphorylation of enolase on RNA degradation is unexplored.

Proteins involved in protein synthesis also have been identified to be phosphorylated on Ser/Thr residues in *E.* coli (114, 128), *B. subtilis* (115)*, M. tuberculosis* (118), *Lactococcus lactis* (129) suggesting that Ser/Thr phosphorylation may regulate translation across bacterial species. For example, the universally conserved GTPase elongation factor Tu (EF-Tu) is phosphorylated

on conserved Ser/Thr residues in different species (130). EF-Tu is an essential translational factor that binds GTP (EF-Tu-GTP) and aminoacylated tRNA (aa-tRNA) to form a ternary complex and delivers the aminoacylated tRNA to the ribosome. Upon a correct codon-anticodon match, the ribosome activates the GTPase activity of EF-Tu thereby allowing accommodation of aa-tRNA into the ribosomal aa-tRNA binding site and release of EF-Tu-GDP from the ribosome (131). A few reports have demonstrated the regulation of EF-Tu function by Ser/Thr phosphorylation. For example, the *M. tuberculosis* eSTK PknB specifically phosphorylates EF-Tu on multiple threonine residues and inhibits its interaction with GTP resulting in decreased protein synthesis (132). Also, the *B. subtilis*, eSTK YabT phosphorylates EF-Tu on a conserved threonine residue in the GTPase active site which in turn inhibits GTPase activity of EF-Tu (133). In *E. coli*, phosphorylation of EF-Tu affects its GTPase activity as well as ternary complex formation (134, 135). However, the kinase responsible for this modification of EF-Tu is still unknown.

Although some of these phosphorylated substrates such as EF-Tu are conserved in phosphoproteomes across several bacteria, the phosphorylation sites are not necessarily conserved. Furthermore, since phosphorylation is a dynamic process, the phosphorylation status of proteins could differ based on environmental conditions used. This was clearly demonstrated by comparative phosphoproteomics in *E. coli* where phosphorylation status was examined under different growth phases (123). Specifically, *E. coli* cells grown in minimal media showed a global increase in phosphorylation levels in late stationary phase, including those of EF-Tu, suggesting that phosphorylation is likely to occur in later phases of growth. Thus, phosphorylation of elongation factors could be (partially) responsible for the diminished rate of protein synthesis during stationary phase.

In order to identify kinase specific substrates, comparative phosphoproteomics have been

carried out by comparing phosphoproteomes of a strain lacking either the eSTK or partner eSTP with the WT strain. This methodology has been utilized previously for identifying phospho substrates of *B. subtilis* PrkC using deletion strains of eSTK PrkC and eSTP PrpC (136). This methodology has also been successfully utilized in *M. pneumoniae*, where 4 out of the 63 phosphorylated proteins were specifically enriched in a deletion strain of novel eSTK PrkC (117). Therefore, phosphoproteomic analysis can serve as a useful tool in identifying phosphorylated proteins.

1.10 *Escherichia coli* as a model organism

Escherichia coli is a Gram-negative bacterium and probably the most widely studied model organism among prokaryotes. Short generation time under laboratory conditions and relatively small genome size has made *E. coli* one of the earliest bacterial genomes to be sequenced and annotated (65). From the physiological context, *E. coli* has been widely used to understand intracellular signal transduction particularly in the context of His/Asp kinases in two- component systems that regulate cellular responses to changing environments. While bacterial signal transduction dependent on Ser/Thr phosphorylation was first identified in *E. coli* in the late 1970s, not much is known regarding the role of Ser/Thr phosphorylation in *E. coli* cell physiology. Despite sequencing the whole genome, eukaryotic-type serine/threonine kinases with conserved Hanks domain features were not identified. It was therefore assumed that *E. coli* may have very few or no eSTKs (137). However, the subsequent identification of >100 Ser/Thr phosphorylated proteins by phosphoproteomic approaches, including essential enzymes involved in glycolysis and protein synthesis (114, 123) indicates the presence of the Hanks-type/eukaryotic-like serine threonine kinases and phosphatases that are responsible for these modifications. Additionally, the functional

consequences of phosphorylation of these key cellular proteins is still an unanswered question.

1.11 Scope of this dissertation

The goal of this dissertation was to understand how Ser/Thr phosphorylation is reversibly regulated in *E. coli* and identify the enzymes that catalyze reversible regulation. Although three Ser/Thr kinases have been identified and biochemically characterized in *E. coli*, a Ser/Thr phosphatase has not been identified. This dissertation includes two main studies. In the first part (Chapter 3), I describe the first PP2C-like Ser/Thr phosphatase in *E. coli.* I used homology-based search with *B. subtilis* PP2C PrpC as a model to identify a PP2C homolog encoded by *yegK* (renamed as *pphC*) in *E. coli*. I used various *in vitro* biochemical assays to understand enzymatic properties of PphC and have identified a putative Ser/Thr kinase (YegI) encoded in the same operon as a physiological substrate for PphC. In the second study (Chapter 4) I show that YegI belongs to a class of well-conserved eukaryotic-like Ser/Thr kinases found in bacteria. Using *in vitro* biochemical assays and gene fusions, I have characterized the enzymatic properties of YegI and identified enolase and elongation factor-Tu (EF-Tu) as potential physiological substrates of YegI kinase.

CHAPTER 2

Materials and Methods

2.1 Bacterial strains and growth conditions

E. coli DH5α cells were used for regular cloning and *E. coli* C43(DE3), BL21(DE3) and LOBSTR (BL21-DE3) strains were used for expression of recombinant proteins. *E. coli* REL606 B strain was used for all the physiology experiments. *E. coli* cells for expression were grown in LB Lennox broth supplemented with ampicillin (100 μg/ml) or carbenicillin (100 μg/ml) at 37 ºC with shaking (220 rpm) unless otherwise specified. Genomic DNA from *E. coli* REL606 and MG1655 was isolated using a Wizard genomic DNA purification kit (Promega) following manufacturer's instructions. Strains used in this study are described in Appendix A. Plasmids used in this study are listed in Appendix B. Oligos used in this study are listed in Appendix C.

2.2 Cloning and expression of YegK (PphC)

The *E. coli yegK (pphC)* gene was PCR amplified using Phusion polymerase (Thermo Scientific) from REL606 genomic DNA using primers (KR38/KR39). Sequence for an N-terminal His_6 tag was included in the primer. The PCR product was digested with *NcoI/PstI* and ligated into similarly digested pBAD24 plasmid backbone. Ligation products were transformed into DH5α cells and selected on LB ampicillin plates. The resulting plasmid generated an N-terminal His_6-tagged YegK (PphC) fusion protein.

For protein expression, all plasmids were transformed into C43(DE3) cells and plated on LB ampicillin (100 μg/ml) agar plates. Single colonies were inoculated into 3 ml LB supplemented with ampicillin (100 μg/ml) for overnight cultures. The next day, 400 ml cultures were diluted 1:250 and grown to an OD_{600} of 0.6-0.8. Recombinant protein was induced by addition of arabinose

(0.2 % w/v) for 3h at 25 ºC. Cells were harvested at 6000 xg for 15 min at 4 ºC. Pellets were washed with ice-cold 50 mM EDTA and centrifuged at 7000 rpm for 15 min at 4 ºC. Washed pellets were saved at -80 ºC until use.

2.3 Oligonucleotide site directed mutagenesis for YegK(PphC) point mutants

Point mutation of aspartic acid residue D46 was generated by two step overlap PCR mutagenesis using primer pairs (KR38/ KR41) and (KR40/ KR39) with Phusion polymerase. A second PCR was performed with primers (KR38/ KR39) using primary PCR products as a template and the subsequent PCR products were digested with *NcoI/PstI* and ligated into pBAD24 to generate an N-terminal His_6 tagged D46N YegK(PphC) fusion protein. Plasmid cloning was subsequently verified by restriction enzyme digest and DNA sequencing (Operon).

Point mutation of serine residue S174 was generated by two step overlap PCR mutagenesis using primer pairs (KR38/KR129) and (KR128/KR39) with Phusion polymerase. A second PCR was performed with primers (KR38/KR39) using primary PCR products as a template and the subsequent PCR products were digested as above and ligated into pBAD24 to generate an N-terminal His_6 tagged S174A YegK(PphC) fusion protein. Plasmid cloning was subsequently verified by restriction enzyme digest and DNA sequencing (Operon).

2.4 Purification of recombinant PphC

Frozen pellets from protein expression were suspended in lysis buffer (20 mM Tris pH 8.0, 250 mM NaCl, 30 mM imidazole, 10 mM β-mercaptoethanol, 0.2 % Triton-X 100, 10 mg/ml lysozyme, 1 mM PMSF) and incubated on ice for 30 min. Initial lysis was carried out by four cycles of freeze/thaw in dry ice/ethanol bath and 37 ºC. Lysate was passed through a 22-gauge

needle and added to pre-chilled 2 mL screw cap tubes with 0.1mm silica beads. Cells were lysed using a FastPrep-24 5G instrument (MP Biomedical) using 2 rounds of 6.5 m/s intensity for 40 secs with 4 min incubation on ice between rounds. Lysates were cleared by centrifugation at 20,000 x g for 30 mins at 4 ºC. Cleared lysates were incubated in Pierce 5ml columns with Ni-NTA agarose beads (Qiagen) at 4 ºC for 1 h. Lysate was allowed to flow through and beads were washed 10 column volumes of wash buffer (20 mM Tris pH 8.0, 250 mM NaCl, 30 mM imidazole, 10 mM β-mercaptoethanol). His_6-tagged protein was eluted using increasing concentrations of imidazole (100-500 mM) in 20 mM Tris pH 8.0, 250 mM NaCl. Elution fractions were analyzed on a 10 % SDS-PAGE gel and fractions containing protein were pooled and dialyzed overnight at 4 ºC using Slide-A-Lyzer mini dialysis device 10K MWCO (Thermo Scientific) in phosphatase storage buffer (20 mM Tris pH 8.0, 50 mM NaCl, 1 mM DTT, 1 mM $MnCl_2$). Dialyzed samples were concentrated in Amicon Ultra 10K centrifugal filters to 1ml and then loaded onto a HiLoad 16/60 superdex 75 prep grade (GE Biosciences) gel filtration column. The column was preequilibrated and run with phosphatase storage buffer. PphC elutes at a retention volume of ~70 ml. Fractions containing PphC were pooled, concentrated and assessed for purity using a 12 % SDS-PAGE gel. The catalytic variant D46N and S174A variant was purified using the same protocol. Proteins were stored at -80 ºC.

2.5 Cloning and expression of HipA

The *E. coli hipA* gene was PCR amplified using Phusion polymerase (Thermo Scientific) from MG1655 genomic DNA using primers (EN5/EN2). Sequence for an N-terminal His_6 tag was included in the primer. The PCR product was digested with *EcoRI/PstI* and ligated into similarly digested pBAD24 plasmid backbone. Ligation products were transformed into DH5α cells and

selected on LB ampicillin plates. The resulting plasmid generated an N-terminal His_6-tagged HipA fusion protein.

For protein expression, plasmid was transformed into C43(DE3) cells and plated on LB ampicillin (100 μg/ml) agar plates. Single colonies were inoculated into 3 ml LB supplemented with ampicillin (100 μg/ml) and grown until OD_{600} ~1. The same day, 500 ml cultures were diluted 1:250 with inoculum culture and grown to an OD_{600} of 0.6-0.8. Recombinant protein was induced by addition of arabinose (0.2 % w/v) for 1h at 37 ºC. Cells were harvested at 6000 x g for 15 min at 4 ºC. Pellets were washed with ice-cold 50 mM EDTA and centrifuged at 7000 rpm for 15 min at 4 ºC. Washed pellets were saved at -80 ºC until use.

2.6 Purification of recombinant HipA

Frozen pellets from protein expression were suspended in lysis buffer (50 mM NaH_2PO_4 pH 8.0, 300mM NaCl, 30mM imidazole, 0.2 % Triton-X 100, 20 mg/ml lysozyme, 1mM PMSF) and incubated on ice for 30 min. Initial lysis was carried out by four cycles of freeze/thaw in dry ice/ethanol bath and 37 ºC. Lysate was passed through a 22-gauge needle and added to pre-chilled 2 mL screw cap tubes with 0.1 mm silica beads. Cells were lysed using a FastPrep-24 5G instrument (MP Biomedical) using 2 rounds of 6.5 m/s intensity for 40 secs with 4 min incubation on ice between rounds. Lysates were cleared by centrifugation at 20,000 x g for 30 mins at 4 ºC. Cleared lysates were incubated in Pierce 5ml columns with Ni-NTA agarose beads (Qiagen) at 4 ºC for 1 h. Lysate was allowed to flow through and beads were washed 10 column volumes of wash buffer (50 mM NaH_2PO_4 pH 8.0, 300 mM NaCl, 30 mM imidazole). His_6-tagged protein was eluted using increasing concentrations of imidazole (100-500 mM) in 50 mM NaH_2PO_4 pH 8.0, 300 mM NaCl . Elution fractions were analyzed on a 10 % SDS-PAGE gel and fractions containing

protein were pooled and dialyzed overnight at 4 ºC using Slide-A-Lyzer mini dialysis device 10 K MWCO (Thermo Scientific) in HipA storage buffer (50 mM Tris pH 8.0, 250 mM NaCl, 5 mM DTT, 10% glycerol). Dialyzed samples were concentrated in Amicon Ultra 10K centrifugal filters and assessed for purity using a 12 % SDS-PAGE gel. Proteins were stored at -80 ºC.

2.7 Cloning and expression of GltX

The *gltX* gene was PCR amplified using Phusion polymerase (Thermo Scientific) from *E. coli* MG1655 genomic DNA using primers (KR23/KR25). Sequence for N-terminal His_6 tag was included in the primer. The PCR product was digested with *NdeI/BamHI* and ligated into similarly digested pET11a plasmid backbone. Ligation products were transformed in DH5α cells and selected on LB/ampicillin plates. The resulting plasmid pKR07 generated an N-terminal His_6-tagged GltX fusion protein. Plasmid cloning was subsequently verified by restriction enzyme digest and DNA sequencing (Operon).

For protein expression, plasmid was transformed into C43(DE3) cells and plated on LB ampicillin (100 μg/ml) agar plates. Single colonies were inoculated into 3 ml LB supplemented with ampicillin (100 μg/ml) for grown overnight. The next day, 200 ml cultures were diluted 1:250 and grown to an OD_{600} of 0.5. Recombinant protein was induced by addition of 1 mM IPTG for 3 h at 25 ºC. Cells were harvested at 6000 x g for 15 min at 4 ºC. Pellets were washed with ice-cold 50 mM EDTA and centrifuged at 7000 rpm for 15 min at 4 ºC. Washed pellets were saved at -80 ºC until use.

2.8 Purification of recombinant GltX

Frozen pellets from protein expression were suspended in lysis buffer (20 mM Tris pH 8.0,

250 mM NaCl, 30mM imidazole, 10 mM β-mercaptoethanol, 0.2 % Triton-X 100, 10 mg/ml lysozyme, 1mM PMSF) and incubated on ice for 30 min. Initial lysis was carried out by four cycles of freeze/ thaw in dry ice/ethanol bath and 37 ºC. Lysate was passed through a 22-gauge needle and added to pre-chilled 2 mL screw cap tubes with 0.1 mm silica beads. Cells were lysed using a FastPrep-24 5G instrument (MP Biomedical) using 2 rounds of 6.5 m/s intensity for 40 secs with 4 min incubation on ice between rounds. Lysates were cleared by centrifugation at 20,000 x g for 30 mins at 4 ºC. Cleared lysates were incubated in Pierce 5ml columns with Ni-NTA agarose beads (Qiagen) at 4 ºC for 1 h. Lysate was allowed to flow through and beads were washed 10 column volumes of wash buffer (20 mM Tris pH 8.0, 250 mM NaCl, 30 mM imidazole, 10 mM β-mercaptoethanol). His_6-tagged protein was eluted using increasing concentrations of imidazole (100-500 mM) in 20 mM Tris pH 8.0, 250 mM NaCl. Elution fractions were analyzed on a 10 % SDS-PAGE gel and fractions containing protein were pooled and dialyzed overnight at 4 ºC using Slide-A-Lyzer mini dialysis device 10 K MWCO (Thermo Scientific) in GltX storage buffer (20 mM Hepes pH 7.5, 10% glycerol , 5 mM β-mercaptoethanol). Dialyzed samples were concentrated using Amicon Ultra 10K centrifugal filters and assessed for purity using a 12 % SDS-PAGE gel. Proteins were stored at -80 ºC.

2.9 Cloning and expression of YegI and YegI-NTD

The *yegI* gene was PCR amplified using Phusion polymerase (Thermo Scientific) from *E. coli* REL606 genomic DNA using primers (KR58/ KR59). Sequence for an N-terminal His_6 tag was included in the primer. The PCR product was digested with *NcoI/SphI* and ligated into similarly digested pBAD24 backbone. Ligation products were transformed in DH5α cells and selected on LB/ampicillin plates. The resulting plasmid pKR31 generated an N-terminal His_6-

tagged YegI fusion protein. Plasmid cloning was subsequently verified by restriction enzyme digest and DNA sequencing (Operon).

The N-terminal domain of *yegI* gene (aa 1-390) was PCR amplified using Phusion polymerase (Thermo Scientific) from *E. coli* REL606 genomic DNA using primers (KR58/KR 60). Sequence for N-terminal His_6 tag was included in the primer. The PCR product was digested with *NcoI/SphI* and ligated into similarly digested pBAD24 plasmid backbone. Ligation products were transformed in DH5α cells and selected on LB/ampicillin plates. The resulting plasmid generated an N-terminal His_6-tagged YegI-NTD fusion protein. Plasmid cloning was subsequently verified by restriction enzyme digest and DNA sequencing (Operon).

The kinase domain of *yegI* gene (aa 1-300) was PCR amplified using Phusion polymerase (Thermo Scientific) from *E. coli* REL606 genomic DNA using primers (KR58/KR61). Sequence for N-terminal His_6 tag was included in the primer. The PCR product was digested with *NcoI/SphI* and ligated into similarly digested pBAD24 plasmid backbone. Ligation products were transformed in DH5α cells and selected on LB/ampicillin plates. The resulting plasmid generated an N-terminal His_6-tagged YegI-KD fusion protein. Plasmid cloning was subsequently verified by restriction enzyme digest and DNA sequencing (Operon).

For protein expression, plasmid was transformed into either C43(DE3) cells or *E. coli* LOBSTR (Kerafast) cells and plated on LB ampicillin (100 μg/ml) agar plates. Single colonies were inoculated into 3 ml LB supplemented with ampicillin (100 μg/ml) for overnight cultures. The next day, a dilution of 1:250 in 500 ml LB was grown to an OD_{600} of 0.6-0.8. YegI recombinant protein was induced by addition of arabinose (0.2% w/v) for 3 h at 18 ºC. YegI-NTD recombinant protein was induced by addition of arabinose (0.2% w/v) for 3 h at 25 ºC. Cells were harvested at 6000 xg for 15 min at 4 ºC. Pellets were washed with ice-cold 50 mM EDTA and centrifuged at

7000 rpm for 15 min at 4 ºC. Washed pellets were saved at -80 ºC until use.

2.10 Oligonucleotide site directed mutagenesis for YegI point mutants

Point mutation of lysine residue K39 was generated by two step overlap PCR mutagenesis using primer pairs (KR58/KR246) and (KR245/59) with Phusion polymerase. A second PCR was performed with primers (KR58/KR59) using primary PCR products as a template and the subsequent PCR products were digested with *Nco1/Sph1* and ligated into similarly digested pBAD24 to generate an N-terminal His_6 tagged K39D YegI fusion protein. Plasmid cloning was subsequently verified by restriction enzyme digest and DNA sequencing (Operon).

Point mutation of aspartic acid residue D141 was generated by two step overlap PCR mutagenesis using primer pairs (KR58/ KR248) and (KR247/KR59) with Phusion polymerase. A second PCR was performed with primers (KR58/KR59) using primary PCR products as a template and the subsequent PCR products were digested with *Nco1/Sph1* and ligated into similarly digested pBAD24 to generate an N-terminal His_6 tagged D141N YegI fusion protein. Plasmid cloning was subsequently verified by restriction enzyme digest and DNA sequencing (Operon). Phosphoablative point mutants used in the study were generated using the same strategy as above and details of plasmid construction are described in Appendix B.

2.11 Purification of recombinant YegI and YegI-NTD

Frozen pellets were suspended in lysis buffer (50 mM Tris pH 8.0, 200 mM NaCl, 10 mM β-mercaptoethanol, 1 mM PMSF and 2% w/v sarkosyl) and incubated at room temperature for overnight lysis. Cells were subsequently lysed using sonication. Lysates were cleared by centrifugation at 15000 x g for 30 min at 4 ºC and incubated in Pierce 5 ml columns with Ni-NTA

agarose beads (Qiagen) at 4 ºC for 1 h. Lysate was allowed to flow through and beads were washed 10 column volumes of wash buffer (50 mM Tris pH 8.0, 200 mM NaCl, 30 mM imidazole, 10 mM β-mercaptoethanol, 0.05% w/v sarkosyl). His tagged protein was eluted using 300 mM imidazole in 50 mM Tris pH 8.0, 200 mM NaCl, 10 mM β-mercaptoethanol and 0.05% w/v sarkosyl. Elution fractions were tested on 12% SDS-PAGE gel and fractions containing protein were pooled and dialyzed overnight at 4 ºC using Snakeskin dialysis tubing 10K MWCO (Thermo Scientific) in kinase storage buffer (20 mM Tris pH 8.0, 125 mM NaCl, 10% glycerol, 1 mM DTT). Dialyzed protein was assessed for purity using 12% SDS-PAGE gel and stored at -80 ºC. YegI variant proteins were purified using the same protocol. Proteins were stored at -80 ºC.

2.12 Phosphatase assays using pNPP as a substrate

The phosphatase activity of PphC (YegK) was determined by measuring hydrolysis of *p*-nitrophenol phosphate (pNPP) to *p*-nitrophenol by spectrophotometry. Assays were performed in triplicate in a 96 well plate. Each well contained 350 nM purified PphC (WT or mutant) in assay buffer (10 mM Tris pH 8.0, 5 mM $MnCl_2$). Reactions were initiated by addition of 5 mM pNPP (NEB) and absorbance measurements were recorded every 10 min at 405 nm for 60 min in a Tecan Infinite M200 plate reader. Amount of phosphate released is represented as nmol pNP/µg of protein and the amount of pNP was calculated using extinction coefficient of 18000 $M^{-1}cm^{-1}$.

Metal dependence was determined by incubating 350 nM purified PphC in assay buffer containing either 5 mM $MgCl_2$, 5 mM $MnCl_2$, 5 mM $CaCl_2$,5 mM $ZnCl_2$, 5 mM $NiCl_2$ or no metal. Absorbance measurements were recorded as above. To determine optimal $MnCl_2$ concentrations, reactions were carried out with 350 nM purified WT PphC in assay buffer with different $MnCl_2$ concentrations (0-10 mM) and absorbance was measured at 405nm.

Sensitivity to phosphatase inhibitors was determined by measuring phosphatase activity of purified PphC in the presence of the following: sodium phosphate (Sigma), sodium fluoride (Sigma), okadaic acid (Cell Signaling), sodium orthovanadate (NEB) or EDTA (Macron Chemicals), sanguinarine chloride (Tocris), aurin tricarboxylic acid (Alfa Aesar) and 5,5' methylene disalycilic acid (Acros Organics). Okadaic acid, sanguinarine chloride, aurin tricarboxylic acid and 5,5' methylene disalycilic acid were diluted in DMSO to get a 1 mM stock. The remaining inhibitors were diluted to stock concentrations in sterile water pH 8. 150 nM of purified WT PphC was incubated in assay buffer containing indicated concentrations of inhibitor or DMSO/water for 5 min. Reactions were initiated by addition of 5 mM pNPP and absorbance was recorded every 5 min for 15 min at 30 ºC in a Tecan Infinite M200 plate reader.

The kinetic parameters of PphC were determined by varying the pNPP concentration (0.1-6.4 mM) in a reaction with 350 nM of purified wild type PphC from either REL606 and MG1655 in assay buffer. Hydrolysis was monitored every 5 min for 30 min in the linear range of the reaction. Initial reaction velocities were calculated for every substrate concentration. To determine K_m and V_{max} values, the data was fit to a Michaelis-Menten curve and Lineweaver-Burke plot was derived using Graphpad Prism 7 software.

Effect of phosphorylation by YegI-NTD on PphC phosphatase activity was assessed using pNPP as a substrate. Firstly, a 175 µL kinase reaction was performed using 89 nM of YegI-NTD and 350 nM of PphC at a kinase: substrate ratio (1:4) in kinase buffer containing 50 mM Tris pH 7.5, 50 mM KCl, 0.5 mM DTT, 10 mM $MgCl_2$, 10 mM $MnCl_2$, 200 µM ATP for 45 mins at 37C to allow transphosphorylation. After 45 mins, phosphatase reactions were initiated by addition of 5 mM pNPP (NEB) and absorbance measurements were recorded every 10 min at 405 nm for 60 min in a Tecan Infinite M200 plate reader.

2.13 Phosphatase assays using synthetic phosphopeptides as substrates

To assess substrate specificity, 200 μM of serine [RRApSVA], threonine [KRpTIRR] or tyrosine [RRLIEDAEpYAARG] phosphopeptides (Millipore) were incubated with 350 nM phosphatase in a 50 μl reaction containing 20 mM Tris pH 8.0 with either 5 mM $MnCl_2$ or 5 mM $MgCl_2$ for 30 min at 37 ºC. Phosphatase reaction was stopped by addition of Biomol Green reagent (Enzo). Reaction was incubated at room temperature for 25 min to allow color development and absorbance at OD_{620} was measured. Phosphate standard (Enzo) was used to calculate the amount of phosphate released.

2.14 Phosphatase assays using β–casein as a substrate

Phosphorylated β–casein (Sigma) was dissolved in 50 mM Tris pH 7.5, 150 mM NaCl to a final concentration of 4 mg/ml. For the phosphatase assay, 4 μg of β–casein was incubated with 1.5 μg PphC (WT/D46N/S174A) in 20 μl of 50 mM Tris pH 8.0 with either 10 mM $MnCl_2$ or 10 mM $MgCl_2$ at 37 ºC for 1 h. Reactions were stopped with 3X SDS loading dye and samples were heat denatured at 95 ºC for 5 min. Samples were loaded on 10% SDS- PAGE gel containing 50 μM Phos-tag acrylamide as per manufacturer's instructions (Wako). Gels were run at constant voltage of 150 V for 75 min at 4 ºC. Proteins were visualized by Coomassie staining.

2.15 Dephosphorylation assays

2.15.1 Dephosphorylation of autophosphorylated HipA

For the dephosphorylation assay, 2 μM of recombinant HipA (60-95% phosphorylated) was incubated with 4 μM PphC (WT/D46N) in 20 μl of 30 mM HEPES pH 7.5 10 mM KCl, 1 mM DTT and 2 mM $MnCl_2$ at 37 ºC for 1 h. Reactions were stopped with 3X SDS loading dye and

samples were heat denatured at 95 ºC for 5 min. Samples were loaded on 10% SDS- PAGE gel containing 50 µM Phos-tag acrylamide as per manufacturer's instructions (Wako). Gels were run at a constant voltage of 150 V for 75 min at 4 ºC. Proteins were visualized by Coomassie staining.

2.15.2 Dephosphorylation of phosphorylated GltX

To obtain phosphorylated GltX, an *in vitro* kinase assay was performed in the presence of 0.2 µM of HipA, 2 µM of GltX in a 100 µL reaction containing 30 mM HEPES pH 7.5, 10 mM KCl, 20 mM $MgCl_2$, 16 µM $ZnSO_4$, 100 mM DTT and 100 µM ATP. Reactions were incubated at 37 ºC for 45 mins and then dialyzed in 500 ml of dialysis buffer (30 mM HEPES pH 7.5, 10mM KCl, 1 mM DTT) overnight at 4ºC using Slide-A-Lyzer mini dialysis device 10K MWCO (Thermo Scientific) to get rid of free unlabeled ATP. For the dephosphorylation assay, 2 mM $MnCl_2$ was added to the dialyzed kinase reaction and was divided into four 20µL reactions. Buffer (HEPES pH 7.5) or 400U of Lambda protein phosphatase or 4 µM PphC-WT or 4 µM PphC-D46N was added to separate 20 µL reactions and reactions were incubated at 37 ºC for 1 h. Reactions were stopped with 3X SDS loading dye and samples were heat denatured at 95 ºC for 5 min. Samples were loaded on 10% SDS- PAGE gel containing 50 µM Phos-tag acrylamide as per manufacturer's instructions (Wako). Gels were run at a constant voltage of 150 V for 75 min at 4 ºC. Proteins were visualized by Coomassie staining.

2.15.3 Dephosphorylation of autophosphorylated YegI

Autophosphorylation of YegI kinase was performed by addition of 5 µCi of [γ-^{32}P] ATP (Perkin Elmer) to 2 µM of purified YegI in 10 µl of reaction buffer containing 50 mM Tris pH 7.5, 50 mM KCl, 0.5 mM DTT, 10 mM $MgCl_2$, 10 mM $MnCl_2$, 200 µM ATP. Phosphatase storage

buffer or PphC or PphC-D46N was added to the above reaction to a final concentration of 4 µM. Reactions were incubated at 37 ºC for 45 mins and were stopped using 3X Laemmli buffer and boiled for 5 min at 95 ºC. Samples were resolved on a 12% SDS-PAGE gel and visualized by staining with Coomassie dye. Radioactive gels were dried for 30 mins at 80 ºC in a gel dryer . Dried gel was exposed to a phosphoscreen and visualized by autoradiography using a Typhoon Scanner (GE Healthcare).

2.16 *In vitro* kinase assay using PphC as a substrate

Transphosphorylation of PphC phosphatase was performed by addition of 5 µCi of [γ-^{32}P] ATP (Perkin Elmer) to 0.5µM of YegI-NTD, 2µM of PphC in a 25µl of kinase reaction buffer containing 50 mM Tris pH 7.5, 50 mM KCl, 1 mM DTT, 10 mM $MgCl_2$, 10 mM $MnCl_2$, 200 µM ATP. Reactions were incubated at 37 ºC and reactions were stopped at different timepoints t=15, 30, 60 mins using 3X Laemmli buffer and boiled for 5 min at 95 ºC. Samples were resolved on a 12% SDS-PAGE gel and visualized by staining with Coomassie dye. Radioactive gels were dried for 30 mins at 80 ºC in a gel dryer . Dried gel was exposed to a phosphoscreen and visualized by autoradiography using a Typhoon Scanner (GE Healthcare).

2.17 *In vitro* kinase assay for phosphopeptide identification

Transphosphorylation of PphC phosphatase for mass spectrometry was performed by addition of 1.33 µM of YegI-NTD and 5.32 µM of PphC in a 30µl of reaction buffer containing 50 mM Tris pH 7.5, 50 mM KCl, 1 mM DTT, 10 mM $MgCl_2$, 10 mM $MnCl_2$, 200 µM ATP. Reactions were incubated at 37 ºC for 1 h and 10 µl of reaction were stopped using 3X Laemmli buffer and boiled for 5 min at 95 ºC. Samples were resolved on a 12% SDS-PAGE gel and visualized by

staining with Coomassie dye . Remainder of sample (20 µl) was submitted for mass spectrometry based phosphopeptide detection.

2.18 Phosphopeptide identification by Mass spectrometry (provided by Dr. Emily Chen)

2.18.1 In-gel protein digestion

In vitro kinase assay samples containing YegI-NTD and PphC were resolved on 4-20% Tris-glycine gradient gel and then stained with GelCode Blue safe Coomassie stain for 2 h followed by de-staining with double distilled water overnight. The resolved proteins were excised and processed at the HICCC Proteomics Shared Resource at Columbia University Medical Center. The excised gel pieces were rehydrated and digested in 80 µl of 12.5 ng/µl Trypsin Gold/50 mM ammonium bicarbonate at 37 °C overnight or 80 µl of 12.5 ng/ul Chymotrypsin/50 mM ammonium bicarbonate at room temperature overnight. After the digestion was complete, condensed evaporated water was collected from tube walls by brief centrifugation using the benchtop microcentrifuge (Eppendorf, Hauppauge, NY). The gel pieces and digestion reaction were mixed with 50 µL 2.5% TFA and rigorously mixed for 15 min. The solution with extracted peptides was transferred into a fresh tube. The remaining peptides were extracted with 80 µl 70% ACN/5% TFA mixture using rigorous mixing for 15 min. The extracts were pooled and dried to completion (1.5–2 h) in SpeedVac. The dried peptides were reconstituted in 30µl 0.1% TFA by mixing for 5 min and stored in ice or at −20°C prior to analysis.

2.18.2 LC-MS/MS analysis

The concentrated peptide mix was reconstituted in a solution of 2 % acetonitrile (ACN), 2 % formic acid (FA) for MS analysis. Peptides were eluted from the column using a Dionex

Ultimate 3000 Nano LC system with a 10-minute gradient from 2% buffer B to 35 % buffer B (100 % acetonitrile, 0.1 % formic acid). The gradient was switched from 35 % to 85 % buffer B over 1 min and held constant for 2 min. Finally, the gradient was changed from 85 % buffer B to 98 % buffer A (100% water, 0.1% formic acid) over 1 min, and then held constant at 98 % buffer A for 5 more minutes. The application of a 2.0 kV distal voltage electro sprayed the eluting peptides directly into the Thermo Fusion Tribrid mass spectrometer equipped with an EASY-Spray source (Thermo Scientific). Mass spectrometer-scanning functions and HPLC gradients were controlled by the Xcalibur data system (Thermo Scientific).

2.18.3 Database search and interpretation of MS/MS data

Tandem mass spectra from raw files extracted and transformed to mzXML format with MS convert within ProteoWizard (138). The spectra were searched against an *E. coli* protein database containing the sequences of his-tagged YegK (PphC), YegI, EF-Tu using Inspect (139) (proteomics.ucsd.edu). The program was instructed to look for variable phosphorylation modifications on Ser, Thr and Tyr, as well as variable modification for acetylation on Lys, oxidation on Met and fixed modification of carbamidomethylation on Cys. Instrument was set as FT-hybrid, with either trypsin or chymotrypsin as protease. Putative phosphorylated peptides (with a p-value < 0.1) were manually matched to their respective spectra to determine likelihood of match. If a match was able to be verified, a new experiment was conducted to target these specific peptides. The instrument was setup to only make MS/MS on the specific parent masses for these peptides. After the experiment, data was again manually verified to make sure that the peptides were phosphorylated. Elution traces for the specific peptides, tracing specific fragments for the peptides, were created within QualBrowser (Thermo Scientific).

2.19 Autophosphorylation assays

2.19.1 Autophosphorylation assay using different bivalent cations

Autophosphorylation of YegI or YegI-NTD was performed by addition of 5 µCi of [γ-^{32}P] ATP (Perkin Elmer) to 1 µM of purified YegI or YegI-NTD in 10 µl of reaction buffer containing 50 mM Tris pH 7.5, 50 mM KCl, 0.5 mM DTT, 200 µM ATP. $MgCl_2$ or $MnCl_2$ or $CaCl_2$ or $NiCl_2$ was added to a final concentration of 10 mM. Reactions were incubated at 37 ºC for 30 mins and were stopped using 3X Laemmli buffer and boiled for 5 min at 95 ºC. Samples were resolved on a 12% SDS-PAGE gel and visualized by staining with Coomassie dye. Radioactive gels were dried for 30 mins at 80 ºC in a gel dryer, exposed to a phosphoscreen and visualized by autoradiography using a Typhoon Scanner (GE Healthcare).

2.19.2 Autophosphorylation assay using YegI point mutants

Autophosphorylation of YegI and point mutants was performed by addition of 5 µCi of [γ-^{32}P] ATP (Perkin Elmer) to 1 µM of purified YegI or YegI point mutants in 10 µl of reaction buffer containing 50 mM Tris pH 7.5, 50 mM KCl, 0.5 mM DTT, 200 µM ATP, 10mM $MgCl_2$ and 10mM $MnCl_2$. Reactions were incubated at 37 ºC for 30 mins and were stopped using 3X Laemmli buffer and boiled for 5 min at 95 ºC. Samples were resolved on a 12% SDS-PAGE gel and visualized by staining with Coomassie dye. Radioactive gels were dried for 30 mins at 80 ºC in a gel dryer, exposed to a phosphoscreen and visualized by autoradiography using a Typhoon Scanner (GE Healthcare).

2.19.3 Inhibition of autophosphorylation by staurosporine

Staurosporine sensitivity experiments were performed using 1μM of YegI in 10 μl of reaction buffer containing 50 mM Tris pH 7.5, 50 mM KCl, 0.5 mM DTT, 10 mM $MgCl_2$ and 10 mM $MnCl_2$. Staurosporine (Calbiochem) was dissolved in DMSO to a obtain a stock concentration of 10 mM. Staurosporine stock (10 mM) was diluted in DMSO and added to the above kinase reaction to obtain final concentrations in the range of 12.5-100 μM. DMSO was added to the no inhibitor control. Reactions were incubated at 25 ºC for 10mins followed by addition of 5 μCi of [γ-^{32}P] ATP (Perkin Elmer). Reactions were incubated for additional 30 mins at 37 ºC and were stopped using 3X Laemmli buffer. Samples were boiled for 5 min at 95 ºC and resolved on a 12% SDS-PAGE gel. Gel was visualized by staining with Coomassie dye. Radioactive dried gel was exposed and visualized by autoradiography using a Typhoon Scanner (GE Healthcare).

2.20 Membrane topology analysis

2.20.1 Construction of YegI PhoA-lacZα fusion and derivatives

To study the membrane topology of YegI, I first constructed plasmid pKR72 that encodes a dual *pho-lac* reporter which is in-frame to full length YegI. The YegI-PhoA-lacZα was constructed by a PCR-mediated overlap extension (140). First, the *yegI* gene fragment encoding aa 2-646 was PCR amplified using Phusion polymerase (Thermo Scientific) from *E. coli* REL606 genomic DNA using primers (KR223/KR224). Alkaline phosphatase PhoA fragment (aa 21-471) and the alpha fragment of beta galactosidase LacZ (aa 5-60) was PCR amplified from *E. coli* MG1655 genomic DNA using primers (KR225/KR226) for *phoA* and (KR227/KR228) for *lacZα* respectively. Eighteen nucleotides encoding a GSGSGS linker along with eighteen nucleotides from the *phoA* DNA was introduced in the reverse primer KR224 to generate an overlapping region between *yegI*

and *phoA*. Similarly, eighteen nucleotides from the *lacZ* DNA was introduced in the reverse primer KR226 to generate an overlapping region between *phoA* and *lacZ*. The *yegI* and *phoA* PCR products were purified and used as templates for a second PCR to create a fused *yegI-linker-pho* DNA that was amplified using primers (KR229/KR226). Sequence for N-terminal His_6 tag was included in the primer KR229. Purified PCR products *yegI-linker-phoA* DNA and *lacZ* DNA were used a templates for third and final round of PCR to create a fused *yegI-linker-pho-lac* fusion that was amplified using primers (KR229/KR228). The PCR product was digested with *Nhe1/Kpn1* and ligated into similarly digested pBAD24 plasmid backbone. Ligation products were transformed into DH5α cells and selected on LB/ampicillin plates. The resulting plasmid pKR72 generated an N-terminal His_6-tagged YegI-PhoA-lacZα fusion protein. Plasmid cloning was subsequently verified by restriction enzyme digest and DNA sequencing (Operon).

Plasmid derivatives of pKR72 with pho-lac fusions were constructed in frame with different codons of YegI using the Q5 Site-Directed mutagenesis kit (NEB). Primers used to generate pho-lac fusions in frame to different codons E439 (KR230/KR231), T432 (KR230/KR232), R414 (KR230/KR233), E390 (KR230/KR234), E340 (KR230/KR235) were designed using NEBaseChanger. Primers were designed such that the 5' ends were annealing back-to-back following manufacturer's instructions. PCR amplification was performed using Q5 hotstart high fidelity master mix with respective primers and 2 ng of Plasmid pKR72 as template DNA. The PCR product was subsequently treated with Kinase/Ligase/Dpn1 mix for 5 mins and transformed in NEB5alpha competent *E. coli* cells (C2987). This method generated plasmids with in-frame *pho-lac* fusions to different codons of YegI at positions E439 (pKR73), T432 (pKR74), R414 (pKR75), E390 (pKR76), E340 (pKR77). pKR78, a derivative of pKR72 lacking yegI was used as a control plasmid and was constructed using the same method using primers KR230/KR240.

Plasmid cloning was subsequently verified by colony PCR and DNA sequencing (Operon).

2.20.2 Membrane topology assay

To assess membrane topology *in vivo*, *E. coli* DH5α cells were transformed with the resulting pho-lac fusion plasmids and streaked on dual indicator plates containing LB agar with 5-bromo-4-chloro-3-indolyl phosphate disodium salt (X-Phos) (Sigma) at a final concentration of 80µg/ml and 6-chloro-3-indolyl-β-D-galactoside (Red-Gal) (Sigma) at a final concentration of 100 µg/ml as indicators. L-arabinose at a final concentration of 0.1% was added as an inducer for reporter expression. 100µg/ml of ampicillin was added for plasmid selection. Plates were incubated at 25^{o} C for 24 h and scanned using EPSON image scanner.

2.21 Generation of in-frame deletion of *yegI* in *E. coli* REL606

λ red recombination system (141) was used for generation of in-frame deletions of *yegI* in *E. coli* REL606. pKD13 (141), which encodes kanamycin resistance, was used as the template plasmid in PCR reactions. FRT-Kan-FRT cassette of pKD13 was amplified with primers (KR176/KR177) containing 20 bases of homology to pKD13 sequence and 40 bases of homology upstream and downstream of *yegI* chromosomal sequence. Primers were designed such that PCR product recombines at two ends of *yegI* locus replacing *yegI* ORF from aa 9-624 with FRT-Kan-FRT cassette. The PCR product was transformed by electroporation into strain KR103 (REL606/pKD46) as in (141) and the deletion was verified by colony PCR and sequencing, resulting in strain KR154 (Δ*yegI*::[FRT-kan-FRT]).

The kanamycin marker was excised via Flp mediated recombination by transforming Flp helper plasmid pCP20 into KR154 by electroporation as in (141). Colonies were selected on

ampicillin plates at 30 ºC. Loss of kanamycin marker was confirmed by patching on kanamycin plates. The kanamycin sensitive colonies contained a single FRT scar at the desired *yegI* chromosomal site along with helper plasmid pCP20 resulting in KR156 (Δ*yegI*::FRT/ pcp20). Flp helper plasmid pCP20 has a temperature sensitive origin of replication. Therefore, to cure the strain of helper plasmid , strain KR156 was incubated at 42 ºC resulting in KR160 (Δ*yegI*).

2.22 Generation of *yegI*-FRT-*lacZ* fusion in *E. coli* REL606

KR156 (Δ*yegI*::FRT/ pcp20) was utilized for generation of *yegI*-FRT-*lacZ* fusion using pCE40 as in (142). pCE40 has been used previously to convert an FRT site to translational lacZ fusion by site specific FLP mediated recombination event. pCE40 is a translational fusion vector with a single FRT site followed by *lacZ* sequence that lacks a translational start site. pCE40 was transformed by electroporation into strain KR156 and transformants were selected on kanamycin plates at 37 ºC . Integration of pCE40 at FRT site in correct orientation resulted in fusion of 9th codon of YegI in-frame with FRT scar and LacZ sequence at the C terminus. The *lacZ* fusion was verified by colony PCR and sequencing, resulting in strain KR168 (Δ*yegI* ::[FRT-*lacZY* kan]).

To avoid endogenous beta-galactosidase activity, the gene *lacZ* from amino acid 10-1011 was replaced with FRT-Kan-FRT cassette amplified from pKD4 using primers (KR185/KR186) as described in (141). The PCR product was transformed by electroporation into KR103 (REL606/pKD46) as in (141) and the deletion was verified by colony PCR and sequencing, resulting in strain KR178 (Δ*lacZ*::[FRT-kan-FRT]). The kanamycin marker was excised by transformation of pCP20 into KR178 by electroporation resulting in strain KR181 (Δ*lacZ*::FRT). KR181 was confirmed for loss of β-galactosidase activity by patching on LB+ 50 µg/ml Xgal (GoldBio) plates and sequencing. KR181 was used a control strain for β-galactosidase assays. The

chromosomally integrated *yegI*-FRT-*lacZY-kan* was moved from strain KR168 to strain KR181 by P1 transduction as in (143) and selecting for kanamycin resistance. This strain was named KR188 (Δ*lacZ* Δ*yegI* ::[FRT-*lacZY* kan]).

2.23 β-galactosidase assay

Assay for β-galactosidase activity was conducted as described (144). Briefly, strains KR181 and KR188 were grown in LB lennox broth at 37 ºC until OD_{600}~0.6 or OD_{600}~3. 2 ml of cultures were chilled on ice until the desired OD was attained. 2 ml cultures pellets were resuspended in 640µl of Z buffer (60 mM Na_2HPO_4 $7H_20$, 40mM NaH_2PO_4, 10 mM KCl, 1 mM $MgSO_4$ $7H_20$, 50 mM β-mercaptoethanol). Cells were lysed using 160µl of lysozyme (2.5 mg/ml in Z buffer) followed by incubation at 37 ºC for 5 mins. Samples were returned to ice and 8 µl of 10 % Triton-X-100 was added to each of the samples. Each tube was vortexed for 10 s and samples were transferred to a 30 ºC water bath for 5 mins. The reaction was initiated by addition of 200 µl of ONPG (o-Nitrophenyl β -D-galactopyranoside) (4 mg/ml in Z buffer; Sigma) at 10 s intervals to each of the tubes. When yellow color develops, 400 µL of 1M Na_2CO_3 was added to stop the reaction. Time taken to develop yellow color was recorded. 1ml of reaction mixture was transferred to microcentrifuge tubes and centrifuged at 16000 X g for 1 min to get rid of cell debris. 150µl of supernatant from reaction mixture was transferred to 96 clear well Nunclon Delta surface plates (Thermo Scientific) and the optical density was recorded at 420 nm and 550 nm. Enzyme units of β-galactosidase was calculated as follows:

$$\mathbf{1000 \times (OD_{420} - 1.75 \times OD_{550}) / t \times v \times OD_{600} = \text{units of } \beta\text{-galactosidase}}$$

Where, OD_{420} and OD_{550} are optical density measurements from the reaction mixture; OD_{600} represents the cell density of cultures before the assay; t is the time of reaction in minutes and v is the volume of culture used in reaction mixture.

2.24 Examining growth in minimal media

Cultures for indicated strains were grown overnight in minimal A medium (144) containing 0.4 % w/v glucose or 0.4 % v/v glycerol as a carbon source. Cultures were then diluted 1:500 into 150 µL of the same media in each well in clear-bottom, polystyrene 96-well plate (Thermo scientific 167008). Cultures were incubated at 37 C with continuous shaking at medium speed in a Tecan infinite M200 plate reader. Growth was measured by taking optical density readings at 600 nM every 10 mins for 20-22 h.

2.25 Generation of in-frame deletion of *yegI* in *E. coli* MG1655

In-frame deletion of *yegI* (JW2055-4) in *E. coli* BW25113 was obtained from the Keio collection stock center (145). P1 virion was made from JW2055-4 and transduced into recipient strain *E. coli* MG1655 and the transductants were selected on kanamycin. P1 transduction into recipient strain was confirmed by colony PCR resulting in strain KR60. The kanamycin marker was excised via FLP mediated recombination by transforming Flp helper plasmid pCP20 into strain KR60 by electroporation as in (141). Colonies were selected on ampicillin plates at 30 ºC. Loss of kanamycin marker was confirmed by patching on kanamycin plates. Strain was incubated at 42 ºC to cure Flp helper plasmid pCP20 resulting in strain KR257 (MG1655 Δ*yegI*).

2.26 Antibiotic sensitivity assays

2.26.1 MIC determination using microtiter broth dilution method

Antibiotics used for MIC determination by microtiter broth dilution method were as follows: Cefotaxime (Mpbio, 50 mg/ml in water), Ceftriaxone (Sigma, 20 mg/ml in water) , Cefoxitin (Sigma, 10.5 mg/ml in water), Cefipime (Sigma, 16.9 mg/ml in phosphate buffer pH 8.0), Fosfomycin (Sigma, 50 mg/ml in water), Kanamycin (Fisher Scientific, 50 mg/ml in water), Chloramphenicol (Sigma, 5 mg/ml in ethanol), Tetracycline (Sigma, 10 mg/ml in 50% ethanol), Ciprofloxacin (Enzo, 30 mg/ml in water), Gentamycin (Gibco, 50 mg/ml in water). Antibiotics were dissolved in respective solvents and diluted in sterile BBL Mueller Hinton II (MHII) broth (Bector Dickinson) to 2X the highest concentration desired in the test. Serial dilutions were prepared in MHII broth and 100 µl of 2X antibiotic solutions are added to sterile clear 96-well Nunclon Delta surface plates (Thermo Scientific). Bacterial colonies from a freshly streaked plate were suspended into 3 ml of sterile 1X phosphate buffered saline (PBS) to yield a final density of 10^8 cfu/ml roughly equivalent to 0.5 Macfarland's unit. This suspension was diluted 1:100 in MHII media and 100 µl is added to 96 well plates containing 100 µL of 2X antibiotic. Plates were sealed with parafilm and incubated without shaking at 37 ºC for 24h. Plates were scanned by eye or read spectrophotometrically at 600 nm to determine the minimum inhibitory concentration.

2.26.2 MIC determination using Etest strips

To determine MIC by Etest strips, I used Mueller Hinton II (MHII) agar plates prepared using manufacturer's instructions. Inoculation of cultures was done by swabbing the MHII agar plates in all directions with a swab soaked in bacterial suspension equivalent to 0.5 Macfarland's unit. Cefotaxime Etest strips (Biomerieux) (0.0002- 32 µg/ml) was placed on inoculated plates using sterile forceps. Plates were incubated at 37 ºC for 20 h and scanned using image scanner.

2.26.3 Antibiotic sensitivity

Antibiotic sensitivity was assessed by back-diluting overnight cultures of indicated strains in LB to OD_{600} ~1. Aliquots of cultures were serially diluted 10-fold and 4 µl volumes of each of the dilutions were spotted on the surface of LB agar plates supplemented with antibiotics (Cefotaxime, 0.125 µg/ml) or (Nalidixic acid, 1 µg/ml). Plates were incubated at 37 ºC for 20-24h and scanned using image scanner.

2.27 Complementation assays

2.27.1 Plasmid construction for complementation assay

Plasmids used for complementation assay were constructed using the Q5 Site-Directed mutagenesis kit (NEB) by using pKR31 as a template. Primers used to generate in frame deletions of *yegI* from aa 2-300 (KR274/KR275), aa 2-436 (KR276/KR275), aa 2-535 (KR287/KR288), aa 2-565 (KR289/KR290) were designed using NEBaseChanger. Primers were designed such that the 5' ends annealed back-to-back following manufacturer's instructions. PCR amplification was performed using Q5 hotstart high fidelity master mix with respective primers and 2 ng of Plasmid pKR31 as template DNA. The PCR product was subsequently treated with Kinase/Ligase/Dpn1 mix for 5 mins and transformed into NEB5alpha competent *E. coli* cells (C2987). This method generated plasmids with different truncations of *yegI* in frame with N terminal His_6 tag as follows: Δ2-300 (pKR93), Δ2-436 (pKR92), Δ2-536 (pKR95), Δ2-566 (pKR96). pBAD24 was used as a control plasmid for complementation assays. Plasmid cloning was subsequently verified by colony PCR and DNA sequencing (Operon). Plasmids were transformed in strain KR160 for complementation assays and selected on LB ampicillin plates.

2.27.2 Complementation assay

Overnight cultures of indicated strains were grown in LB carbenicillin and were back-diluted in fresh LB to OD_{600} ~1. Aliquots of cultures were serially diluted 10-fold and 4 µl volumes of each of the dilutions were spotted on the surface of LB agar plates supplemented with antibiotics. Wherever indicated, arabinose (0.2% w/v) and carbenicillin (100 µg/ml) were added for induction of protein expression and maintenance of plasmid respectively.

2.28 UV sensitivity assay

Overnight cultures of indicated strains were grown in LB and were back-diluted in fresh LB to OD_{600} ~1. Aliquots of cultures were serially diluted 10-fold and 4 µl volumes of each of the dilutions were spotted on the surface of LB agar plates. Spotted plates were exposed to different doses of UV (0, 5, 10, 20, 40, 60 J/m^2) using UV crosslinker (Stratagene). Plates were covered in aluminum foil, incubated at 37 ºC for 20-24h and scanned using image scanner.

2.29 Generation of in-frame deletion of *tolC* in *E. coli* REL606

λ red recombination system (141) was used for generation of in-frame deletions of *tolC* in *E. coli* REL606. pKD13, which encodes kanamycin resistance was used as the template plasmid in PCR reactions (141). FRT-Kan-FRT cassette of pKD13 was amplified with primers (KR299/KR300) containing 20 bases of homology to pKD13 sequence and 40 bases of homology upstream and downstream of the *tolC* chromosomal sequence. Primers were designed such that PCR product recombines at two ends of *tolC* locus replacing *tolC* ORF from aa 10-475 with FRT-Kan-FRT cassette. The PCR product was transformed by electroporation into strain KR103 (REL606/pKD46) as in (141) and the deletion was verified by colony PCR and sequencing,

resulting in strain KR329 (Δ*tolC*::[FRT-kan-FRT]). The kanamycin marker was excised via FLP mediated recombination by transforming Flp helper plasmid pCP20 by electroporation as in (141). Colonies were selected on ampicillin plates at 30 ºC. Loss of kanamycin marker was confirmed by patching on kanamycin plates. Strain was incubated at 42 ºC to cure Flp helper plasmid pCP20 resulting in strain KR337 (REL606 Δ*tolC*).

To generate Δ*tolC* in Δ*yegI* background, P1 virion was made from KR329 (Δ*tolC*::[FRT-kan-FRT]) and transduced into recipient strain KR160 (Δ*yegI*), selecting on kanamycin. P1 transduction into recipient strain was confirmed by colony PCR resulting in strain KR336 ((Δ*tolC*::[FRT-kan-FRT] Δ*yegI*). The kanamycin marker was excised using pCP20 by electroporation as in (141). Colonies were selected on ampicillin plates at 30 ºC. Loss of kanamycin marker was confirmed by patching on kanamycin plates. Strain was incubated at 42 ºC to cure Flp helper plasmid pCP20 resulting in strain KR338 (REL606 Δ*yegI* Δ*tolC*).

2.30 Comparative phosphoproteomics (In collaboration with Dr. Ljiljana Pasa-Tolic)

2.30.1 Growth conditions

E. coli REL606 (JDE2735) and REL606 Δ*yegI* (KR160) were grown overnight at 37 ºC in minimal A medium (144) containing 0.4 % w/v glucose as a carbon source. Cultures were grown in triplicates and then diluted 1:500 into 1 L of the same media in Erlenmeyer flasks . Cultures were incubated at 37 ºC with continuous shaking and cells were harvested by centrifugation at OD_{600} of 0.8 (log phase) and OD_{600} of 2.5 (stationary phase). Cell pellets were washed with 100 mM ammonium bicarbonate pH 8.0 and shipped to our collaborator Dr. Ljiljana Pasa-Tolic at PNNL, WA. Protein extraction, phosphopeptide enrichment and data analysis were performed by Dr. Jared Shaw (Pasa-Tolic Lab).

2.30.2 Protein extraction and digestion (Provided by Dr. Jared Shaw)

Each cell pellet was diluted in 2-5 mL of 8 M urea in 100 mM ammonium bicarbonate, pH 8. 1 mL was transferred to 2 mL snap-cap centrifuge tubes (Eppendorf) with 0.1 mm zirconia beads and bead beat in a bullet Blender (Next Advance) at speed 8 for 3 minutes at 4°C. After bead beating, the lysate was spun into a 15 mL Falcon tube at 2000 xg for 10 minutes at 4°C. The supernatant (200 µl) was removed to a clean tube and a bicinchoninic acid (BCA) assay (Thermo Scientific) was performed to determine protein concentration. Following the assay, 10 mM dithiothreitol (DTT) was added to the samples and incubated at 60°C for 30 minutes with constant shaking at 800 rpm followed by the addition of 40 mM iodoacetamide (IAA) with 30 minutes of room temperature incubation in the dark. Samples were then diluted 8-fold for preparation for digestion with 100 mM NH_4HCO_3, 1 mM $CaCl_2$ and sequencing-grade modified porcine trypsin (Promega, Madison, WI) was added to all protein samples at a 1:50 (w/w) trypsin-to-protein ratio for 3 h at 37˚C. Digested samples were desalted using a 4-probe positive pressure Gilson GX-274 ASPEC™ system (Gilson Inc.) with Discovery C18 100 mg/1 mL solid phase extraction tubes (Supelco), using the following protocol: 3 mL of methanol was added for conditioning followed by 2 mL of 0.1 % trifluoroacetic acid (TFA) in H_2O. The samples were then loaded onto each column followed by 4 mL of 95:5:H_2O:Acetonitrile , 0.1% TFA. Samples were eluted with 1mL acetonitrile 80:20 Acetonitrile :H_2O, 0.1% TFA. The samples were concentrated down to ~100 µL using a Speed Vac and a final BCA was performed to determine the peptide concentration. The sample volumes were calculated to contain 500 µg each and aliquoted into new low-protein binding 1.5 mL centrifuge tubes. For the pooled channel, 83 µg of each sample within each set were combined to make 500 µg. All the volumes were brought up using 0.5M triethylammonium bicarbonate (TEAB) to 75 µl. The pH of each sample was measured and brought to over pH 8

using 1M TEAB. Each vial of 8-plex iTRAQ reagent (AB Sciex) was brought to room temperature. The reagents were pulse spun to ensure the contents were collected at the bottom and 60 µl of isopropanol was added to each reagent vial. The reagents were thoroughly vortexed, spun down and 5 vials of each reagent were added to the appropriate 500 µg sample. Each sample was vortexed and spun down to incubate at room temperature for 2 hours at which time 100µl of nanopure water was added to hydrolyze the sample and incubated for an additional 30 minutes. The samples were partially dried down in a speed vac to remove the organic solvent and then pooled together to obtain 3 samples each containing all 7 of the iTRAQ labels and C18 cleaned again as described above followed by another BCA assay to determine the final peptide mass for phosphopeptide enrichment. Peptides were brought up to a concentration of 0.5 µg/µL in 80:20 Acetonitrile :H_2O, 0.1% TFA and used for phosphopeptide enrichment.

2.30.3 Phosphopeptide enrichment using IMAC and phosphopeptide desalting

Immobilized metal affinity chromatography (IMAC) columns by prepared by first prepared by pretreating Ni-NTA superflow agarose beads with 100 mM EDTA to strip beads of the nickel. Beads were washed with HPLC water and then activated with 10 mM iron (III) chloride aqueous solution for 30 mins at RT. Beads were then treated with 1:1:1 acetonitrile:methanol:0.01% acetic acid to make a slurry of 1:1:1 beads: acetonitrile :methanol:0.01% acetic acid. IMAC beads were then incubated with prepared peptide solution and incubated for 30 mins at RT on a shaker at 1000 rpm. Beads/peptide solution was spun to remove supernatant and then brought up to 200 µL volume in 80:20 Acetonitrile :H_2O, 0.1% TFA to get phosphoenriched beads. For desalting step, 2-plug C18 stage tips were prepared using Empore C18 extraction disks. Stage tips were conditioned with methanol and centrifuged at 3000Xg for 3 mins to discard any liquid from the

collection vial. Stage tips were washed with 50 % acetonitrile in 0.1% formic acid twice and then equilibrated in 1% formic acid. The phosphoenriched beads loaded onto the stage tip and centrifuged at 3000Xg for 3 mins to discard any liquid from the collection vial. Beads were subsequently washed with 80:20 Acetonitrile :H_2O, 0.1% TFA twice followed by wash with 1% formic acid. Peptides were eluted off the beads and onto the C18 plugs using 500 mM potassium phosphate buffer (1M monobasic + 1M dibasic potassium phosphate). C18 plugs were washed with 1 % formic acid and then peptides were eluted off C18 plugs with 50 % acetonitrile in 0.1% formic acid. Eluate was transferred to an HPLC vial, freeze dried, reconstituted in 2% acetonitrile/0.1 % formic acid and analyzed by LC-MS/MS as described (146).

2.31 Cloning and expression of *E. coli* enolase

The *E. coli eno* gene encoding enolase was PCR amplified using Phusion polymerase (Thermo Scientific) from REL606 genomic DNA using primers (KR211/KR212). The PCR product was digested with *Nde1/BamHI* and ligated into similarly digested pETPhos plasmid backbone (147). Ligation products were transformed into DH5α cells and selected on LB ampicillin plates. The resulting plasmid pKR71 generated an N-terminal His_6-tagged Eno fusion protein.

Point mutation of serine residue S400 was generated by two step overlap PCR mutagenesis using primer pairs (KR211/KR250) and (KR249/KR212) with Phusion polymerase. A second PCR was performed with primers (KR211/KR212) using primary PCR products as a template and the subsequent PCR products were digested with *Nde1/BamHI* and ligated into similarly digested pETphos to generate plasmid pKR85 expressing an N-terminal His_6 tagged S400A enolase fusion protein. Plasmid cloning was subsequently verified by restriction enzyme digest and DNA

sequencing (Operon).

For protein expression, plasmid pKR85 was transformed into BL21(DE3) cells and plated on LB ampicillin (100 μg/ml) agar plates. Single colonies were inoculated into 3 ml LB supplemented with ampicillin (100 μg/ml) for overnight cultures. The next day, 400 ml cultures were diluted 1:200 and grown to an OD_{600} of 0.6-0.8. Recombinant protein was induced by addition of IPTG (1mM) for 3h at 25 ºC. Cells were harvested at 6000 x g for 15 min at 4 ºC. Pellets were washed with ice-cold 50 mM EDTA and centrifuged at 7000 rpm for 15 min at 4 ºC. Washed pellets were saved at -80 ºC until use.

2.32 Purification of recombinant enolase

Frozen pellets from protein expression were suspended in lysis buffer (20 mM Tris pH 7.5, 300 mM NaCl, 30mM imidazole, 10 mM β-mercaptoethanol, 0.2 % Triton-X 100, 10 mg/ml lysozyme, 1mM PMSF) and incubated on ice for 30 min. Initial lysis was carried out by four cycles of freeze/ thaw in dry ice/ethanol bath and 37 ºC. Lysate was passed through a 22-gauge needle and added to pre-chilled 2 mL screw cap tubes with 0.1mm silica beads. Cells were lysed using a FastPrep-24 5G instrument (MP Biomedical) using 2 rounds of 6.5 m/s intensity for 40 secs with 4 min incubation on ice between rounds. Lysates were cleared by centrifugation at 20,000 xg for 30 mins at 4 ºC. Cleared lysates were incubated in Pierce 5ml columns with Ni-NTA Agarose beads (Qiagen) at 4 ºC for 1 hr. Lysate was allowed to flow through and beads were washed 10 column volumes of wash buffer (20 mM Tris pH 7.5, 300 mM NaCl, 30 mM imidazole, 10 mM β-mercaptoethanol). His_6-tagged protein was eluted using 300 mM imidazole in 20 mM Tris pH 7.5, 300 mM NaCl. Elution fractions were analyzed on a 12 % SDS-PAGE gel and fractions containing protein were pooled and dialyzed overnight at 4 ºC using Snakeskin dialysis tubing

10K MWCO (Thermo Scientific) in enolase storage buffer (20 mM Tris pH 7.5, 50 mM NaCl, 100 mM KCl, 10 % glycerol 1 mM DTT, 1 mM $MgSO_4$). Dialyzed samples were concentrated and assessed for purity using a 12 % SDS-PAGE gel. The S400A variant was purified using the same protocol. Proteins were stored at -80 ºC.

2.33 *In vitro* kinase assay using enolase as a substrate

Transphosphorylation of His-Eno was performed by addition of 5 µCi of [γ-^{32}P] ATP (Perkin Elmer) to 0.5 µM of YegI-NTD, 2 µM of His-Eno in a 25µl of kinase reaction buffer containing 50 mM Tris pH 7.5, 50 mM KCl, 1 mM DTT, 10 mM $MgCl_2$, 10 mM $MnCl_2$, 200 µM ATP. Reactions were incubated at 37 ºC for 1h and stopped using 3X Laemmli buffer and boiled for 5 min at 95 ºC. Samples were resolved on a 12% SDS-PAGE gel and visualized by staining with Coomassie dye. Radioactive gels were dried for 30 mins at 80 ºC in a gel dryer. Dried gel was exposed to a phosphoscreen and visualized by autoradiography using a Typhoon Scanner (GE Healthcare).

2.34 Cloning and expression of *E. coli* elongation factor-Tu (EF-Tu)

The *E. coli tufB* gene encoding Elongation factor-Tu (EF-Tu) was PCR amplified using Phusion polymerase (Thermo Scientific) from MG1655 genomic DNA using primers (KR145/KR146). The PCR product was digested with *BamHI/Xho1* and ligated into similarly digested pGEX-6p1 plasmid backbone. Ligation products were transformed into DH5α cells and selected on LB ampicillin plates. The resulting plasmid pKR61 generated an N-terminal GST-tagged EF-Tu fusion protein.

For protein expression, plasmid was transformed into BL21(DE3) cells and plated on LB

ampicillin (100 μg/ml) agar plates. Single colonies were inoculated into 3 ml LB supplemented with ampicillin (100 μg/ml) for overnight cultures. The next day, 250 ml cultures were diluted 1:125 and grown to an OD_{600} of 0.6-0.8. Recombinant protein was induced by addition of IPTG (1mM) for 3h at 25 ºC. Cells were harvested at 6000 x g for 15 min at 4 ºC. Pellets were washed with ice-cold 50 mM Tris pH 7.5, 150 mM NaCl, 1 mM DTT and centrifuged at 7000 rpm for 15 min at 4 ºC. Washed pellets were saved at -80 ºC until use.

2.35 Purification of recombinant EF-Tu

Purification of GST-EF-Tu was adapted from (148). Briefly, frozen pellets were suspended in lysis buffer (50 mM Tris pH 7.5, 100 mM NaCl, 2 mM β-mercaptoethanol, 1 mM PMSF, 0.5 mM $MgCl_2$, 0.2 mM GDP, 1% v/v Triton-X-100) and incubated on ice for 15 mins. Cells were subsequently lysed using sonication. Lysates were cleared by centrifugation at 15000 x g for 30 min at 4 ºC and incubated in Pierce 5 ml columns with prepared immobilized glutathione beads (Pierce) at 4 ºC for 1 h. Immobilized glutathione beads were prepared by washing five times with five column volumes of lysis buffer. Lysate was allowed to flow through and beads were washed 10 column volumes of wash buffer (50 mM Tris pH 7.5, 100 mM NaCl, 2 mM β-mercaptoethanol, 0.5 mM $MgCl_2$, 0.2 mM GDP). GST-tagged protein was eluted using 10 mM reduced glutathione (Calbiochem) prepared in wash buffer. Elution Fractions were tested on 12% SDS-PAGE gel and fractions containing protein were pooled and dialyzed overnight at 4 ºC using Snakeskin dialysis tubing 10K MWCO (Thermo Scientific) in 2X translation factor storage buffer (20 mM Tris pH 7.5, 100 mM KCl, 1 mM $MgCl_2$,10 mM β-mercaptoethanol, 0.4 mM GDP). Dialyzed protein was assessed for purity using 12% SDS-PAGE gel, glycerol was added to a final concentration of 50 % and stored at -80 ºC.

2.36 *In vitro* kinase assay using EF-Tu as a substrate

Transphosphorylation of GST-EF-Tu was performed by addition of 5 μCi of [γ-^{32}P] ATP (Perkin Elmer) to 2 μM of YegI-NTD, 2 μM of GST or GST-EF-Tu in a 25μl of kinase reaction buffer containing 50 mM Tris pH 7.5, 50 mM KCl, 0.5 mM DTT, 10 mM $MgCl_2$, 10 mM $MnCl_2$, 200 μM ATP. Reactions were incubated at 37 ºC for 45 mins and stopped using 3X Laemmli buffer and incubated for 5 min at 95 ºC. Samples were resolved on a 12% SDS-PAGE gel and visualized by staining with Coomassie dye. Radioactive gels were dried for 30 mins at 80 ºC in a gel, exposed to a phosphoscreen and visualized by autoradiography using a Typhoon Scanner (GE Healthcare).

2.37 Phosphorylation of EF-Tu *in vivo*

2.37.1 Construction of pETDuet-1 co-expressing EF-Tu and tagless YegI-NTD.

E. coli EF-Tu was phosphorylated in vivo by co-expression of tagless YegI N-terminal domain (YegI-NTD) and His_6-tagged EF-Tu from a pETDuet-1 derived plasmid. The *E. coli tufB* gene encoding EF-Tu was first PCR amplified using Phusion polymerase (Thermo Scientific) from MG1655 genomic DNA using primers (KR293/KR294). The PCR product was digested with BamHI/Not1 and ligated into multiple cloning site (MCS-1) of similarly digested pETDuet-1 plasmid backbone. Ligation products were transformed into DH5α cells and selected on LB ampicillin plates. The resulting plasmid pKR103 generated an N-terminal His_6-tagged EF-Tu fusion protein with no co-expressing kinase.

Derivative of pKR103 co-expressing a tagless YegI-NTD was constructed by PCR amplifying YegI-NTD (aa 1-390) using Phusion polymerase (Thermo Scientific) from REL606 genomic DNA using primers (KR62/KR64). The PCR product was digested with BglII/Xho1 and ligated into multiple cloning site (MCS-2) of similarly digested pKR103 plasmid backbone.

Ligation products were transformed into DH5α cells and selected on LB ampicillin plates. The resulting plasmid pKR105 generated an N-terminal His_6-tagged EF-Tu fusion protein co-expressed with tagless YegI-NTD.

2.37.2 Expression and purification of phosphorylated EF-Tu

For protein expression, plasmids (pKR103 or pKR105) were transformed into BL21(DE3) cells and plated on LB ampicillin (100 μg/ml) agar plates. Single colonies were inoculated into 3 ml LB supplemented with ampicillin (100 μg/ml) for overnight cultures. The next day, 200 ml cultures were diluted 1:100 and grown to an OD_{600} of 0.6-0.8. Recombinant protein was induced by addition of IPTG (1 mM) for 3h at 25 ºC for plasmids pKR103 and pKR105 whereas for pKR104 recombinant protein was induced by addition of IPTG (1 mM) for 3h at 18 ºC. Cells were harvested at 6000 x g for 15 min at 4 ºC. Pellets were washed with ice-cold 50 mM EDTA and centrifuged at 7000 rpm for 15 min at 4 ºC. Washed pellets were saved at -80 ºC until use.

Frozen pellets were suspended in lysis buffer (50 mM Tris pH 7.5, 300 mM NaCl, 10 mM β-mercaptoethanol, 10 mM imidazole, 2 mM PMSF, 0.5 mM $MgCl_2$, 0.2 mM GDP, 1 mg/ml lysozyme, Halt phosphatase inhibitor cocktail (Thermo scientific) and incubated on ice for 5 mins. Cells were lysed using a FastPrep-24 5G instrument (MP Biomedical) using 2 rounds of 6.5 m/s intensity for 40 secs with 4 min incubation on ice between rounds. Lysates were cleared by centrifugation at 15000 x g for 30 min at 4 ºC . Cleared lysates were incubated in Pierce 5ml columns with Ni-NTA Agarose beads (Qiagen) at 4 ºC for 1 hr. Lysate was allowed to flow through and beads were washed 10 column volumes of wash buffer (50 mM Tris pH 7.5, 300 mM NaCl, 10 mM β-mercaptoethanol, 30 mM imidazole, 0.5 mM $MgCl_2$, 0.2 mM GDP, Halt phosphatase inhibitor cocktail (Thermo scientific). His_6-tagged protein was eluted using 300 mM of imidazole

in 50 mM Tris pH 7.5, 300 mM NaCl, 0.5 mM $MgCl_2$, 0.2 mM GDP. Elution fractions were analyzed on a 12 % SDS-PAGE gel and fractions containing protein were pooled and dialyzed overnight at 4 ºC using Snakeskin dialysis tubing 10K MWCO (Thermo Scientific) in translation factor storage buffer (10 mM Tris pH 7.5, 50 mM KCl, 5 mM β-mercaptoethanol, 0.5 mM $MgCl_2$, 0.2 mM GDP). Dialyzed protein was assessed for purity using 12% SDS-PAGE gel and glycerol was added to a final concentration of 10 %. Protein was concentrated to 2 µg/µl using Amicon Ultra 10K centrifugal filters and stored at -80 ºC.

2.38 *In vitro* translation of CotE-FLAG

In vitro translation assay was carried out using a modified PURExpress system (New England Biolabs) following manufacturer's instructions to transcribe and translate a C-terminal flag tagged CotE protein. A plasmid expressing a ~21kda CotE-FLAG protein has been previously used as a template for *in vitro* translation assay (133). The modified PURExpress system contains all the necessary components for synthesis of CotE-FLAG except elongation factor Tu (EF-Tu). 170 ng of CotE-FLAG expressing plasmid (pSFP234) was added to a 5µl reaction (2.4 µl of Solution A + 1.56 µl of Solution B (-EF-Tu) + 0.7µl of sterile water). Translation reaction was initiated by addition of unphosphorylated or phosphorylated EF-Tu to a final concentration of 2 µg. Reaction was incubated at 37 ºC for 10 mins and reactions were stopped using 30 µl of 3X Laemmli buffer and boiled for 5 min at 95 ºC. Samples were resolved on a 12% SDS-PAGE gel and transferred to a PVDF membrane at 4 ºC at 300 mA for 90 mins. PVDF membrane was subsequently blocked with 3 % BSA in PBS-T for 1h at room temperature. After blocking, membrane was probed with α-FLAG-HRP antibody (Sigma, 1:25000) and then detected using Super signal West Pico PLUS chemiluminescent substrate (Thermo Scientific).

CHAPTER 3

Identification and biochemical characterization of a novel PP2C-like Ser/Thr phosphatase in *Escherichia coli*

This chapter is adapted from:

Rajagopalan K, Dworkin J (2018). Identification and biochemical characterization of a novel PP2C-like Ser/Thr phosphatase in *Escherichia coli*. *Journal of Bacteriology*, JB.00225-18.

This study was initiated to identify PP2C-like serine/threonine phosphatases in *E. coli*. I contributed to all the figures in the paper. I designed and performed all the experiments for the biochemical characterization of the phosphatase. I wrote the first draft of the manuscript and participated in the subsequent rounds of editing.

3.1 Introduction

Reversible protein phosphorylation is an important regulatory mechanism in eukaryotes and prokaryotes (149). In eukaryotes, signaling phosphorylation typically occurs on serine, threonine or tyrosine residues and is mediated by the combined action of kinases and phosphatases. In prokaryotes, signaling phosphorylation has been thought to occur largely on histidine and aspartate residues mediated by histidine kinases of two-component systems (14). However, mass spectrometry based-phosphoproteomic analyses over the past decades have identified numerous Ser/Thr/Tyr phosphorylated proteins in many bacteria (30, 113, 150), including *Escherichia coli* (114, 119, 123, 146). Some of these phosphoproteins and the specific phosphosites are conserved in divergent species (114) suggesting that this regulation may be physiologically relevant.

Ser/Thr kinases from phylogenetically diverse bacteria have been described (30). For example, in *E. coli*, YeaG plays a role in nitrogen starvation (70), YihE is involved in the Cpx stress response (80) and cell death pathways (82) and HipA regulates bacterial persister formation by phosphorylating a tRNA synthetase (78, 79). However, both the authentic *in vivo* substrates of these kinases and/or their proximal activating stimuli are largely uncharacterized, complicating

efforts to understand their precise physiological role.

Phosphorylation on serine or threonine residues is more stable than phosphorylation on histidine or aspartate residues and is subject to additional regulation by Ser/Thr phosphatases. Analysis of phylogenetically diverse bacterial genomes revealed the presence of genes encoding proteins (88, 89, 151) which bear significant resemblance to eukaryotic Ser/Thr PP2C phosphatases (89, 137) hence they are referred to as eukaryotic-like Ser/Thr phosphatases (eSTPs). Some of these proteins have been characterized biochemically and structurally, with these studies confirming their general similarity to their eukaryotic counterparts. Eukaryotic Ser/Thr protein phosphatases are divided into two classes, either phosphoprotein phosphatases (PPP) or metal-dependent protein phosphatases (PPM), according to structure, presence of signature motifs, metal ion dependence and sensitivity to inhibitors (152). PPM phosphatases require Mg^{2+}/Mn^{2+} to mediate dephosphorylation of phospho-serine or phospho-threonine residues. A well-studied member of the PPM phosphatase family is human protein phosphatase 2C (PP2C) (94) which bears a striking resemblance to bacterial PPM phosphatases. PPM/PP2C phosphatases are characterized by the presence of 11 signature motifs with 8 absolutely conserved residues (89, 152).

While several bacterial PPM-type phosphatases have been biochemically characterized (100, 101, 107, 153-157), PPM-type phosphatases have not been identified in *E. coli* despite strong evidence of Ser/Thr phosphorylation. Here, I characterize a previously undescribed ORF, *yegK,* that is present in both *E. coli* B and K strains. This ORF encodes a ~28 kDa protein which bears sequence similarity to PP2C-type phosphatases. We designate this gene *pphC* and its protein product as PphC. Recombinant PphC was purified and its enzymatic properties characterized. Despite some differences in sequence conservation as compared to other bacterial eSTPs, PphC resembles PP2C-type phosphatases in various biochemical assays. Furthermore, we show that

PphC dephosphorylates autophosphorylated YegI (a previously undescribed Ser/Thr kinase) which is encoded in the same operon as *pphC*. To our knowledge, this is the first report of the identification and biochemical characterization of an *E. coli* PP2C-like phosphatase.

3.2 Results

3.2.1 YegK is an atypical PP2C-like phosphatase

To identify PP2C-like phosphatases in *E. coli*, I performed a homology-based BLAST search using *Bacillus subtilis* PrpC, a well-characterized PP2C-like phosphatase (100), as the query. This analysis revealed a previously uncharacterized 762 bp ORF, *yegK,* which encodes a putative 253 amino acid polypeptide. Sequence analysis and domain prediction of YegK revealed that amino acids 11-232 have homology to a PP2C domain (Fig.3.1A). PP2C phosphatases include 11 conserved signature motifs (29, 89). Multiple sequence alignment of YegK with known PP2C phosphatases from other Gram-negative bacteria shows presence of these 11 motifs but with low overall sequence similarity. However, unlike other bacterial PP2C homologs (107, 154, 155, 157, 158), YegK contains only six of the eight absolutely conserved residues that are involved in metal binding, coordination and catalysis (Fig.3.1B). In particular, the amino acid sequence alignment clearly shows that YegK lacks the conserved glycine residue in motif VI and the aspartic acid residue in motif VIII (Fig. 3.1B).

A

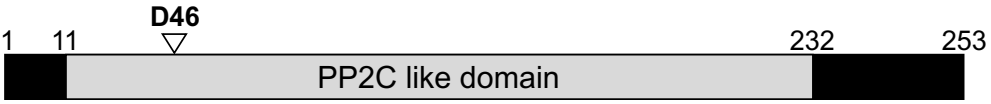

B

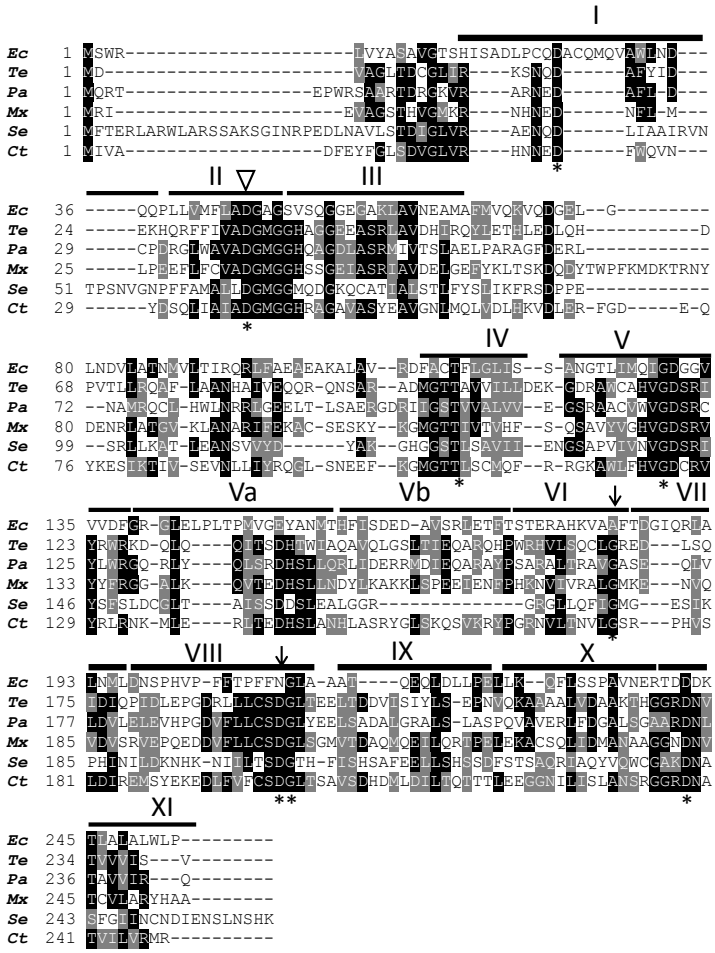

Figure 3.1 YegK is an atypical PP2C-like phosphatase.
(A) **Domain architecture of YegK.** Metal binding site D46 is highlighted in black. (B) **Amino acid sequence alignment of YegK with bacterial PP2C-like phosphatases**. YegK (*Ec: Escherichia coli*) was aligned to PP2C homologs from Gram-negative bacteria using T-coffee (159) and Boxshade. Identical residues are shaded in black and similar residues are shaded in gray. The eight absolutely conserved residues found in bacterial PP2Cs are depicted with asterisks. The conserved residues absent in YegK are indicated by arrows. Signature motifs seen in most bacterial PP2Cs are denoted as roman numerals based on Shi et al. (89). The aspartic acid residue involved in metal binding is depicted with open triangle. *Te: Thermosynechococcus elongatus* tPphA; *Pa: Pseudomonas aeruginosa* Stp1; *Mx: Myxococcus xanthus* Pph1; *Se: Salmonella enterica* serovar Typhi PrpZ (aa 1-260); *Ct: Chlamydia trachomatis* CTL0511 (Cpp1).

A predicted structure of YegK using Phyre2 algorithm (Fig. 3.2B) closely resembles the published structure of the bacterial PP2C-like phosphatase PphA (Fig.3.2A) from *Thermosynechococcus elongatus* (95) consisting of β-sheets and a catalytic core in the center surrounded by exterior alpha helices. In addition, *yegK* is located immediately upstream of *yegI*, an ORF which encodes a protein with homology to eukaryotic-like Ser/Thr kinases, consistent with the observation that bacterial Ser/Thr kinases and phosphatases are often located in operons (30). Taken together, these observations suggest that, despite the absence of two highly conserved residues, *yegK* likely encodes a PP2C-like phosphatase.

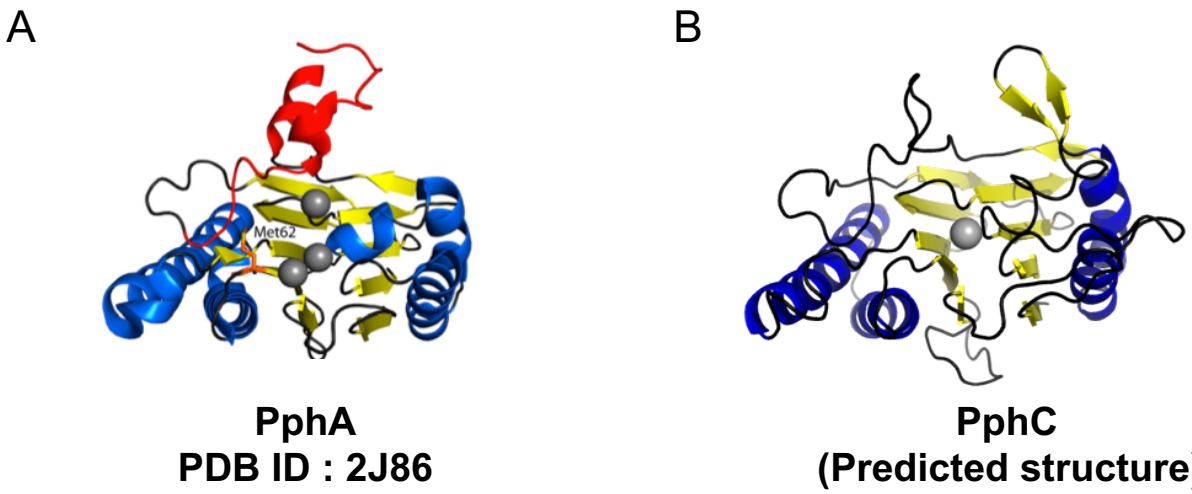

Figure 3.2 Predicted structure of YegK (PphC) resembles crystal structure of eSTP *Thermosynechococcus elongatus* PphA.
(A) Crystal structure of *Thermosynechococcus elongatus* PphA (PDB ID 2J86) (95). (B) Predicted structure of *E. coli* YegK (PphC). The Phyre2 algorithm (160) was used to predict structural model of YegK (PphC).

3.2.2 Biochemical characterization of YegK

To demonstrate that *yegK* encodes a functional protein phosphatase, the 762 bp fragment was cloned in frame with an N-terminal six-histidine tag into the pBAD24 vector (161). The plasmid was transformed into *E. coli* C43 (DE3) and following protein expression, the cell lysate was subjected to affinity purification using Ni^{2+}-NTA resin and subsequent analysis by SDS-PAGE. The protein migrated at an apparent molecular mass of ~25 kDa, similar to the calculated molecular mass of 28.18 kDa (Fig 3.3A). The phosphatase activity of purified YegK was determined using an absorbance-based assay which measures the hydrolysis of *p*-nitrophenyl phosphate to *p*-nitrophenol. Formation of *p*-nitrophenol detected at an absorbance of 405 nm is directly proportional to the phosphatase activity which is expressed as nmol of pNP formed/µg protein. Consistent with the alignment (Fig. 3.1B), YegK displayed a time-dependent increase in phosphatase activity (Fig. 3.3B) suggesting that it is an active protein phosphatase. We have therefore renamed YegK as PphC (**P**rotein **ph**osphatase C) following the nomenclature of two previously characterized *E. coli* protein phosphatases PphA and PphB (162) and the bacterial PP2C-like phosphatase PphA from *T. elongatus* (95)

To further confirm the bioinformatic identification of PphC as a PP2C-like phosphatase, the aspartic acid residue (D46) in motif II was mutated to asparagine. A similar approach was used in the analysis of the PP2C-like phosphatase Cpp1 from *Chlamydia trachomatis* (154). The mutant protein (PphC-D46N) was purified as above and phosphatase activity was compared to wild-type PphC. PphC-D46N displays no hydrolysis of pNPP suggesting that the aspartic acid residue is essential for catalytic activity (Fig. 3.3B). To ensure that the loss of activity of PphC-D46N was not a consequence of improper folding, PphC and PphC-D46N were subjected to size exclusion chromatography. The gel filtration elution profile shows that PphC-D46N eluted as a single peak

and at the same retention volume as PphC indicating that the loss of phosphatase activity observed with the PphC-D46N mutant is most likely due to a loss of catalytic activity (Fig. 3.3C).

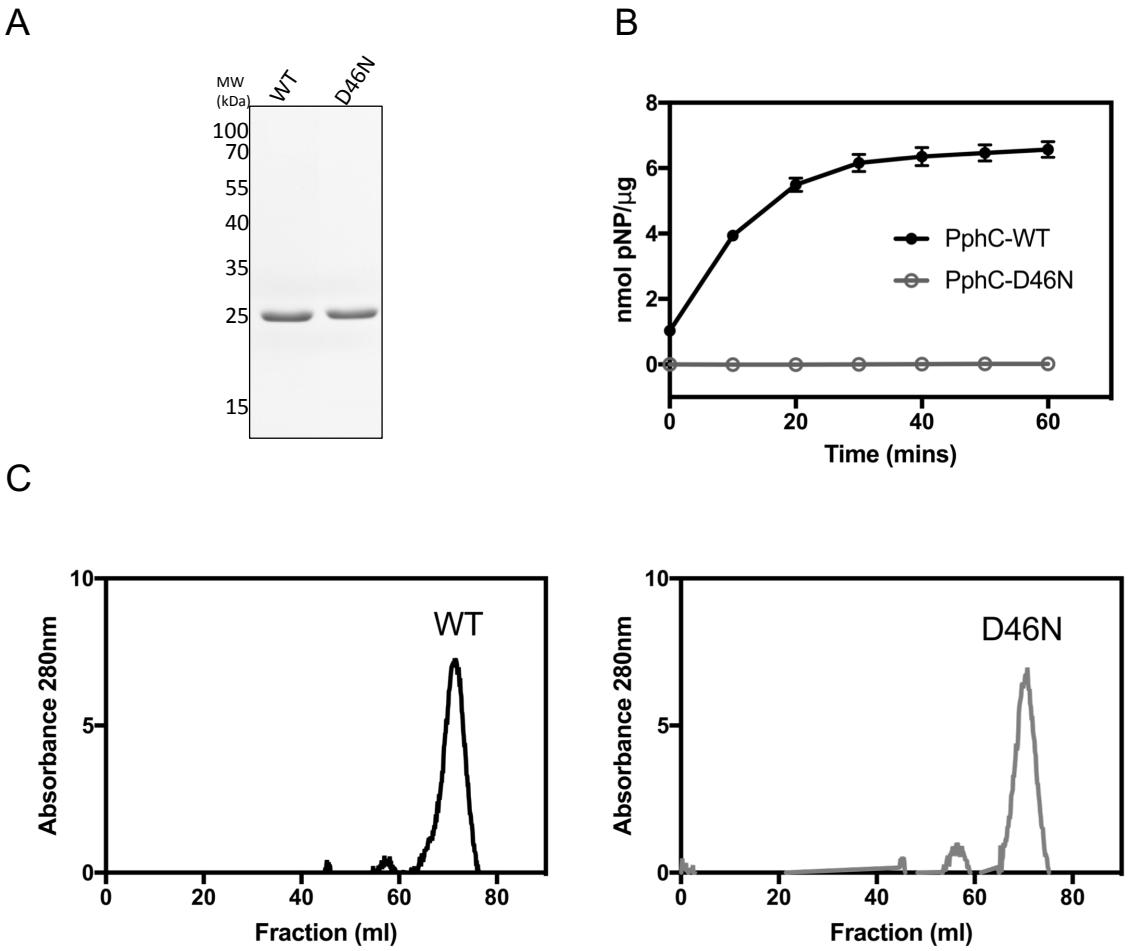

Figure 3.3 YegK is an active phosphatase.
(A) Coomassie brilliant blue stained 10% SDS-PAGE gel. Purified WT and D46N PphC (2 µg) migrate at an apparent molecular mass of ~25Kda. (B) **Assessment of phosphatase activity of YegK using pNPP as substrate.** Reactions were performed at 37 ºC for 60 mins with 350 nm of phosphatase (WT/D46N mutant), 5mM pNPP substrate in phosphatase assay buffer (20mM Tris pH 8.0 and 5mM $MnCl_2$). (C) **Size exclusion chromatography profile of WT and D46N YegK**. His_6-tagged protein (10nmol) was loaded on a Superdex 75 size exclusion column and eluted in 20 mM Tris pH 8.0, 50 mM NaCl, 1 mM DTT, 1 mM $MnCl_2$.

PP2C phosphatases belong to the PPM family of metal-dependent Ser/Thr phosphatases that require either Mg^{2+} or Mn^{2+} for activity (29, 152). The requirement for a divalent cation for PphC phosphatase activity was assessed by measuring hydrolysis of pNPP in the presence of either $MgCl_2$/$MnCl_2$/$CaCl_2$/$ZnCl_2$/$NiCl_2$. Since pNPP hydrolysis was only observed in the presence of $MnCl_2$ but not $MgCl_2$,$CaCl_2$, $ZnCl_2$, $NiCl_2$, PphC is a Mn^{2+} dependent phosphatase (Fig. 3.4A,B). This result is consistent with the requirement for Mn^{2+} ion for previously characterized bacterial PP2Cs (101, 153-157). The concentration dependence of PphC phosphatase activity on Mn^{2+} was measured and the optimal $MnCl_2$ concentration was determined to be between 1-2 mM (Fig. 3.4C)

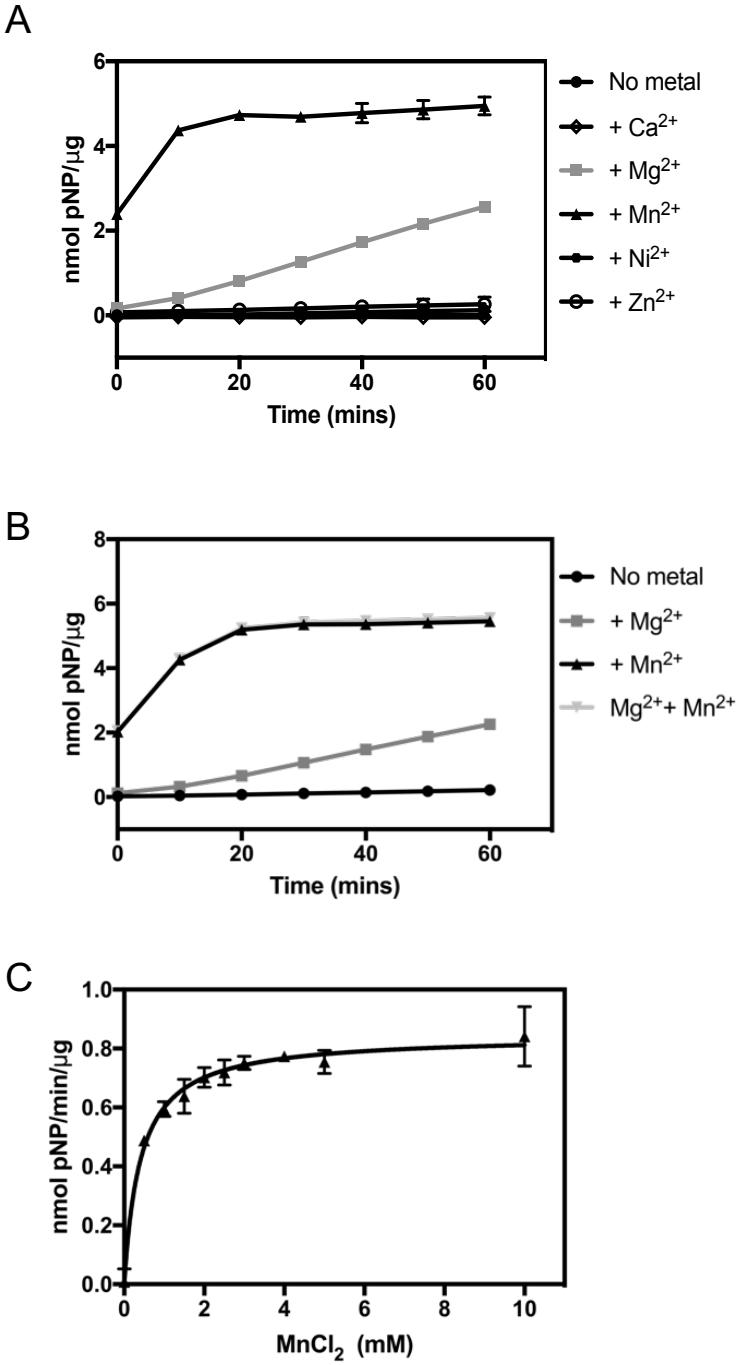

Figure 3.4 PphC (YegK) is a Manganese dependent PP2C-like phosphatase.
Metal dependency of PphC phosphatase was tested using pNPP as a substrate. (A) Reactions were carried out at 37 ºC for 60 min in buffer containing 350 nM phosphatase, 5 mM pNPP substrate with either 5 mM $MgCl_2$/ $MnCl_2$/$CaCl_2$/$NiCl_2$/$ZnCl_2$. (B) Reactions were carried out at 37 ºC for 60 min in buffer containing 350 nM phosphatase, either 5mM $MgCl_2$ or 5mM $MnCl_2$, or both, with 5mM pNPP substrate. (C) **Effect of Mn^{2+} concentration on PphC catalytic activity using pNPP as a substrate**. Reactions were carried out at 37 ºC for 30 min in assay buffer containing 350 nM phosphatase, 5 mM pNPP substrate and different concentrations of $MnCl_2$.

The effect of different classes of protein phosphatase inhibitors on PphC phosphatase activity was tested using pNPP as a substrate (Table 3.1). PphC activity dramatically decreased in the presence of general protein phosphatase inhibitor sodium phosphate and was slightly affected by sodium fluoride (~30% decrease at 100 mM). Okadaic acid, a known inhibitor of PP1 family of phosphatases (163), did not inhibit PphC activity. PphC activity was also unaffected by sodium orthovanadate, a known tyrosine phosphatase inhibitor. Aurin tricarboxylic acid and 5,5' Methylene disalycilic acid which were previously reported to inhibit *Staphylococcus aureus* Stp1 (99, 164) had little effect on PphC phosphatase activity. Similarly, sanguinarine chloride an inhibitor of Human PP2Cα (165) did not affect phosphatase activity. However, a ~60% decrease in activity was detected in the presence of bivalent metal chelator EDTA confirming that PphC is a metal dependent phosphatase. Together, these data are consistent with the characterization of PphC as a PP2C-like phosphatase.

Table 3.1. Effect of inhibitors on PphC activity[a].

Sr.No.	Inhibitors (Concentration)	% Relative activity[b]
1	No inhibitor	100
2	Sodium phosphate (5 mM)	13
	Sodium phosphate (10 mM)	6
3	Sodium fluoride (10 mM)	81
	Sodium fluoride (100 mM)	70
4	Sodium orthovanadate (5 μM)	87
	Sodium orthovanadate (50 μM)	95
5	Okadaic acid (0.1 μM)	91
	Okadaic acid (1 μM)	88
6	EDTA (1 mM)	63
	EDTA (2 mM)	38
7	Aurin tricarboxylic acid (25 μM)	82
	Aurin tricarboxylic acid (50 μM)	66
	Aurin tricarboxylic acid (100 μM)	52
8	5,5' Methylene disalycilic acid (25 μM)	100
	5,5' Methylene disalycilic acid (100 μM)	87
9	Sanguinarine chloride (50 μM)	98

[a] Reactions were carried out at 30 ºC for 15 min in buffer containing 150 nM phosphatase with 5 mM pNPP in the presence or absence of inhibitors.

[b] Relative activity was calculated as a percentage of phosphatase activity in the presence of inhibitor versus activity in absence of inhibitor.

3.2.3 PphC phosphatase activity is different in closely related *E.coli* strains.

I identified striking differences in the genetic architecture surrounding the *pphC* (*yegK*) locus in *E. coli* K and B strains. Specifically, in the *E. coli* B strain REL606, *pphC* (*yegK*) is immediately upstream *of yegI*, an ORF encoding a putative Ser/Thr kinase, whereas in the *E. coli* K strain MG1655, *yegJ*, a putative ORF, is located between the *pphC* (*yegK*) and *yegI* genes facing the opposite direction (Fig. 3.5A). This different genomic organization is conserved in other K and B strains, suggesting that it pre-dates the divergence of these lineages (166). A reasonable prediction is that *pphC* and/or *yegI* expression would be affected by the presence of the divergently oriented *yegJ*, but as I have not identified conditions under which we can robustly detect *pphC* expression, it has not been possible to evaluate this prediction.

In addition to this difference in the genetic architecture around the *pphC* locus, multiple sequence alignment of *pphC* from a K strain (MG1655) and a B strain (REL606) revealed that only ~92 % of the PphC sequence is conserved (Fig. 3.5B). This is in contrast to the extremely high degree of sequence identity typically observed for the *E. coli* proteome: more than half the proteins in MG1655 have 100 % sequence identity with the corresponding protein in REL606 (166).

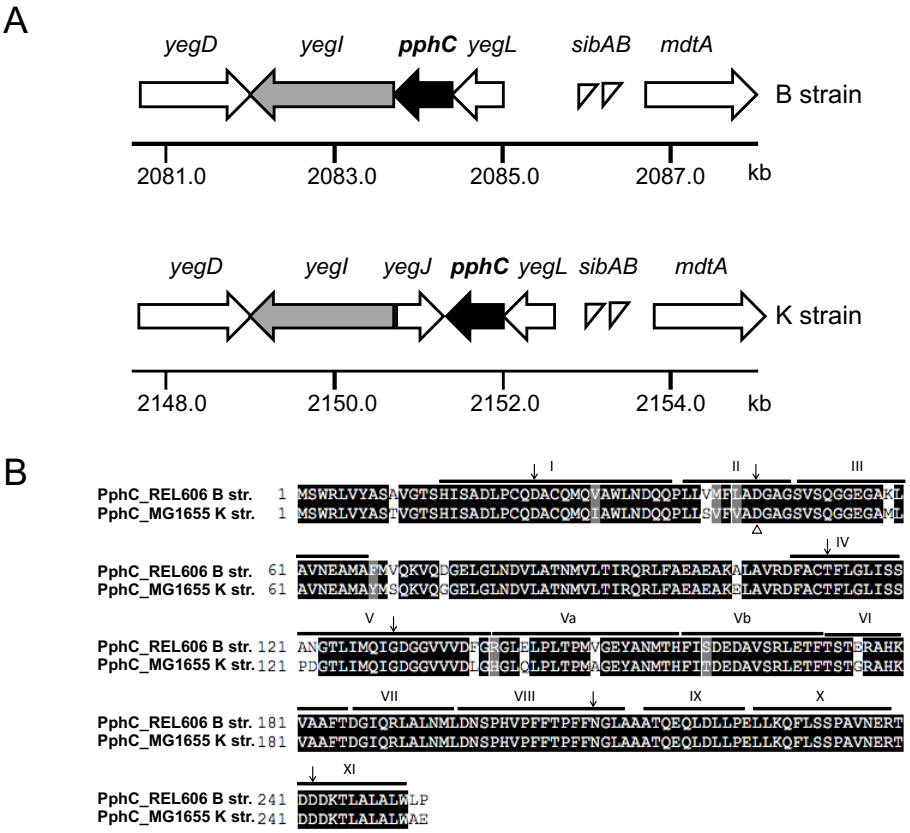

Figure 3.5 PphC locus and amino acid sequence differs in closely related *E. coli* strains.
(A) **Genetic map of *yegK/yegI* operon from *E. coli* B strain REL606 and K strain MG1655**: Thick arrows denote ORFs. The genes *yegL*, *yegK* and *yegI* encode a von Willebrand factor type A, a PP2C-like phosphatase and an eukaryotic-like Ser-Thr kinase respectively. The gene *mdtA* encodes a subunit of a multidrug efflux pump and *yegD* encodes an actin family protein. The *yegJ* gene encodes a protein of unknown function. (B) **Amino acid sequence alignment of PphC from *E. coli* B strain REL606 and K strain MG1655**. Identical residues are shaded in black and similar residues are shaded in gray. Signature motifs seen in bacterial PP2C phosphatases are depicted as Roman numerals based on (89). The aspartic acid residue involved in metal binding is conserved and indicated by open triangle. The conserved residues found in bacterial PP2Cs are depicted with arrows.

To determine whether these differences in amino acid sequence affect phosphatase activity, the gene product of *yegK* from *E. coli* MG1655 was over-expressed and purified by the same method used to purify REL606 PphC. The enzyme kinetics of the two proteins was compared using the pNPP assay (Fig. 3.6A). Phosphatase activity (pmol pNP/min/μg) was determined with increasing concentrations of pNPP and K_m and V_{max} values were calculated (Fig. 3.6B). Since the K_m and V_{max} of Rel606 PphC is lower than those of MG1655 PphC (Fig. 3.6C), it reaches a maximum velocity at a lower substrate concentration. Similarly, the K_{cat} values were calculated to be 0.2089 s^{-1} and 0.093s^{-1} for REL606 and MG1655 PphC, respectively. Previously reported kinetic values for known bacterial PP2Cs range from 0.35 mM to 5.7 mM pNPP for Km, 0.1-4.5μmole/min/mg for Vmax and 0.1 to 7.4 s^{-1} for K_{cat} (96, 100, 101, 154-156, 167-170), indicating that PphC has relatively low phosphatase activity *in vitro* as compared to previously characterized bacterial PP2C-like phosphatases.

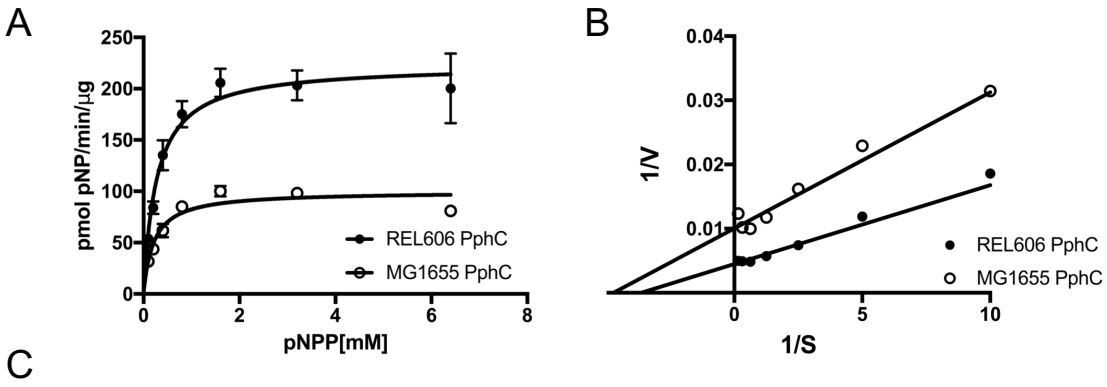

C

Parameters	REL606 PphC [B strain]	MG1655 PphC [K strain]
Km	0.2750 ± 0.04009mM	0.2119 ± 0.03647mM
Vmax	223.3± 7.896 pmol/min/µg	99.85± 3.833 pmol/min/µg
Kcat	0.2089 s^{-1}	0.093s^{-1}
Kcat/Km	0.759*10^3 $M^{-1}s^{-1}$	0.440*10^3 $M^{-1}s^{-1}$

Figure 3.6 PphC phosphatase activity differs in closely related *E. coli* strains. (**A and B**) **Enzyme kinetics of PphC from REL606 and MG1655 strains.** Substrate-dependent activity was assessed using different concentrations of pNPP (0.1-6.4 mM) in assay buffer containing 350 nm phosphatase and 5 mM $MnCl_2$. Data were fitted to a Michaelis-Menten curve **(A)** and a Lineweaver-Burk plot **(B)**. The Lineweaver-Burk plot was used to determine K_m, V_{max} and K_{cat} values **(C)**.

3.2.4 Substrate specificity of PphC

The results of the pNPP assay suggested that PphC has phosphatase activity. Therefore, I investigated whether PphC is capable of dephosphorylating a protein substrate. β-casein is phosphorylated on five serine residues at the N-terminus (171) and was used as a model protein in our assay. Using Mn^{2+}-Phos-tag/SDS-PAGE to monitor phosphorylation state (172), untreated β-casein migrated at an apparent molecular mass of 30 kDa (Fig. 3.7A, lane 1), but β-casein that had been pre-incubated with PphC in $MnCl_2$ buffer exhibited a mobility shift (Fig. 3.7A, lane 2). Since such a change is indicative of a loss in phosphorylation, PphC likely dephosphorylated the serine residues of β -casein. Further, this mobility shift was not detected following incubation of β-casein with the catalytic mutant PphC-D46N (Fig. 3.7A, lane 4). Dephosphorylation of β-casein by PphC and not PphC-D46N was also observed in $MgCl_2$ buffer (Fig.3.7B). However, the extent of dephosphorylation was 2-fold lower in comparison to $MnCl_2$ buffer. These results indicate that PphC is capable of acting as a serine phosphatase in a Mn^{2+} or a Mg^{2+} dependent manner.

The substrate specificity of PphC was further examined using commercially available phosphopeptides. Previously characterized PP2Cs have demonstrated preferential specificity to phosphoserine/threonine peptides over phosphotyrosine peptides (154, 155, 158, 167). Phosphatase assays were performed with phosphoserine RRA(pS)VA, phosphothreonine KR(pT)IRR and phosphotyrosine RRLIEDAE(pY)AARG peptide substrates (Fig. 3.7C). In $MnCl_2$ buffer, PphC released two-fold and six-fold more phosphate in the presence of the phosphotyrosine peptide as compared to the phosphothreonine peptide and phosphoserine peptide, respectively. In comparison to $MnCl_2$ buffer, PphC activity in $MgCl_2$ buffer towards all phosphopeptides was substantially lower further confirming that PphC is a Mn^{2+} dependent phosphatase. To confirm that the phosphopeptides are capable of being dephosphorylated, I used

a known PP2C-like phosphatase (*B. subtilis* PrpC) as a positive control. As expected, PrpC dephosphorylated both serine and threonine residues and had minimal activity to tyrosine (Fig. 3.7D). Thus, since PphC had overall minimal activity on phosphopeptides in comparison to PrpC, they may not be ideal substrates for PphC.

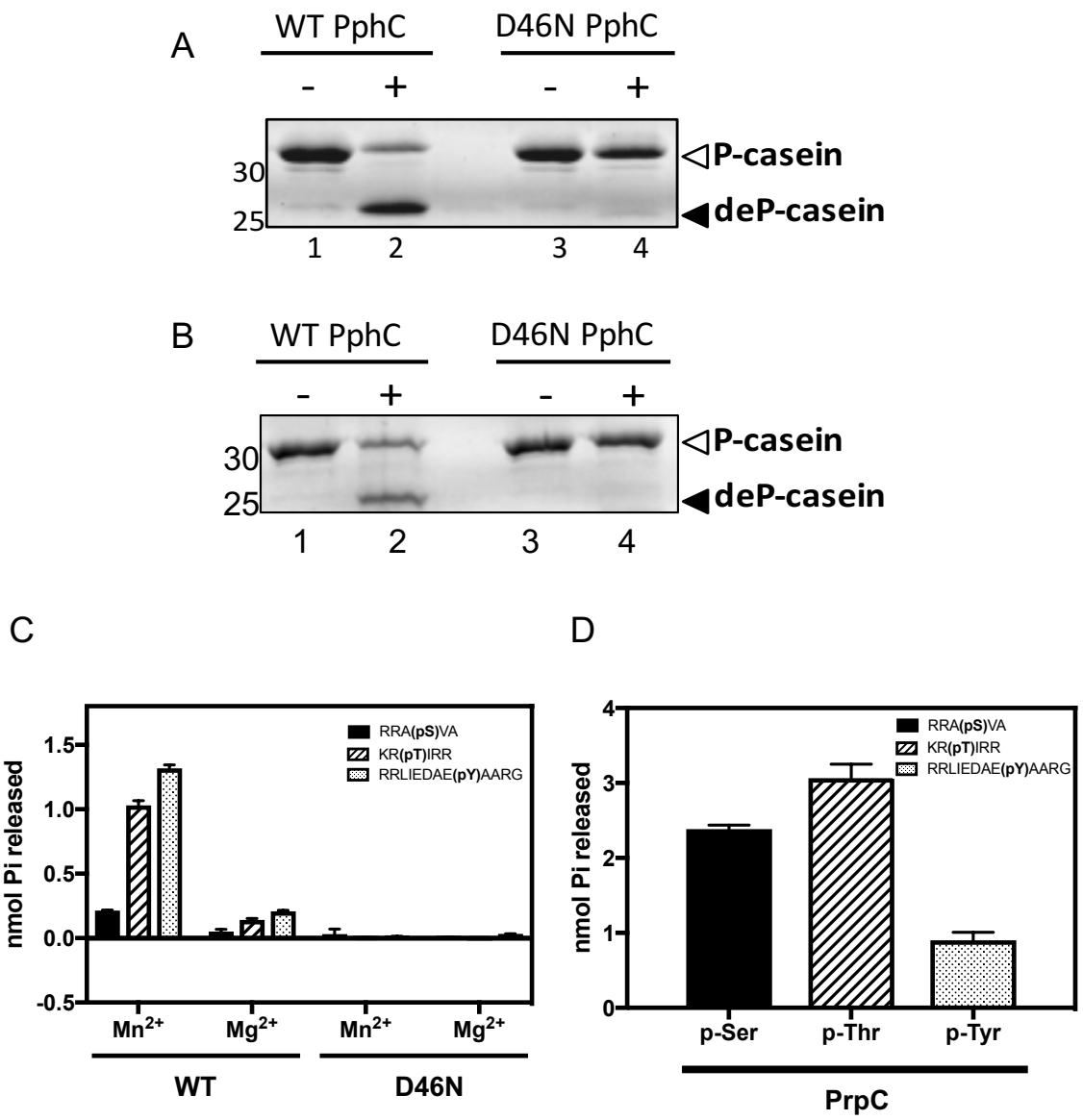

Figure 3.7 Effect of bivalent cations on PphC phosphatase activity using β-casein and phosphopeptides as substrates. Dephosphorylation reactions were carried out at 37 ºC for 60 min in buffer containing 50 mM Tris pH 8, 4 µg phosphorylated β-casein, 1.5 µg (9 µM) phosphatase in the presence of 10 mM $MnCl_2$ (A) or 10 mM $MgCl_2$ (B) and examined on Mn^{2+} Phostag/SDS-PAGE **(C) Comparison of synthetic phosphopeptide specificity of *E. coli* PphC (WT and D46N) in $MgCl_2$ or $MnCl_2$ buffer.** Dephosphorylation reactions were carried out at 37 ºC for 30 min in assay buffer containing 350 nM PphC phosphatase and 200 µM phosphopeptide. Amount of free phosphate was measured using malachite green assay. **(D) Synthetic phosphopeptide specificity of *B. subtilis* PrpC phosphatase.** Dephosphorylation reactions were carried out at 37 ºC for 30 min in assay buffer containing 350 nM PrpC phosphatase and 200µM phosphopeptide. Amount of free phosphate was measured using malachite green assay. *B. subtilis* PP2C-like phosphatase PrpC was purified as previously described (105).

3.2.5 Identification of a PphC substrate

Ser/Thr phosphatases can regulate reversible phosphorylation by dephosphorylating a Ser/Thr kinase or by dephosphorylating a substrate protein. Three genes encoding Ser/Thr kinases *yihE, hipA* and *yeaG* have been identified in *E.coli,* but their physiological substrates are largely unknown. The exception is HipA, an atypical Ser/Thr kinase that has similarity to the phosphatidylinositol-3/4 kinase family. HipA overexpression results in cell growth arrest and autophosphorylation of Ser-150 is crucial for this arrest in cell growth suggesting that kinase activity plays an important role in maintaining cell growth arrest (73). *hipA* was first identified for its role in bacterial persistence, a non-inherited epigenetic state which allows a subpopulation of slow growing cells to survive in the presence of antibiotics (75, 76). More recently, the molecular mechanism by which HipA mediates bacterial persistence has been characterized (78, 79). HipA phosphorylates glutamyl tRNA synthetase (GltX) at Ser-239 and thereby inhibits GltX function. Since phosphorylated GltX is unable to aminoacylate tRNA, uncharged tRNAs accumulate at the ribosome and this accumulation results in the activation of the stringent response and subsequent cell growth arrest. This growth arrest is thought to be essential for persister cell formation since non-growing cells are phenotypically tolerant to many antibiotics. However, the advantages gained by this state would be lost if the cells are unable to re-initiate growth at some future time. Thus, how is HipA or GltX phosphorylation reversed? Since phosphorylation on Ser/Thr residues is a stable modification, a dedicated phosphatase is required to reverse this modification. Therefore, I hypothesized that PphC is the Ser/Thr phosphatase responsible for dephosphorylation of HipA and/or GltX.

To test if HipA is a PphC substrate, I first expressed and purified N-terminal His_6-tagged HipA recombinant protein from BL21(DE3) cells using Ni^2-NTA chromatography. It has been previously reported that recombinant HipA when purified from *E.coli*, is about 65-90% phosphorylated on Ser150 (73, 173). Using Mn^{2+}-Phos-tag/SDS-PAGE to monitor phosphorylation state (172), purified untreated HipA migrated ~55kda (Fig. 3.8A, lane 1) but HipA that had been preincubated with a non-specific lambda protein phosphatase in $MnCl_2$ displayed a mobility shift (Fig. 3.8A, lane 2). Since faster mobility on Phos-tag containing SDS-PAGE is indicative of loss of phosphorylation, this confirmed previous observations that HipA is phosphorylated during purification. However, when HipA was preincubated with PphC-WT (Fig. 3.8A, lane 3) or with PphC-D46N (Fig. 3.8A, lane 4), there was no difference in mobility as compared to untreated HipA suggesting that HipA is not a PphC substrate.

To test if phosphorylated GltX is a substrate for PphC, I first expressed and purified N-terminal His_6-tagged GltX recombinant protein from BL21(DE3) cells using Ni^{2+}-NTA chromatography. Following an *in vitro* kinase reaction with HipA and GltX in the presence of cold ATP , I examined GltX phosphorylation state using Mn^{2+}-Phos-tag/SDS-PAGE. Consistent with previous reports (78, 79), I was able to detect the phosphorylated form of GltX that migrated ~60kDa, as compared to unphosphorylated form (~50kda) (Fig. 3.8B, lane 1). Although HipA migrates close to ~50kDa, I was unable to visualize HipA due to the low concentrations used in the reaction (~0.2 μM). After the kinase reaction, I dialyzed the samples to remove free unlabeled ATP. I observed a mobility shift when phosphorylated GltX was preincubated with the non-specific Lambda protein phosphatase (Fig. 3.8B, lane 2), but I was unable to see any mobility shift when preincubated with PphC-WT(Fig. 3.8B, lane 3), or with PphC-D46N(Fig. 3.8B, lane 4). Taken together, these results suggest that neither HipA nor GltX is a substrate for PphC.

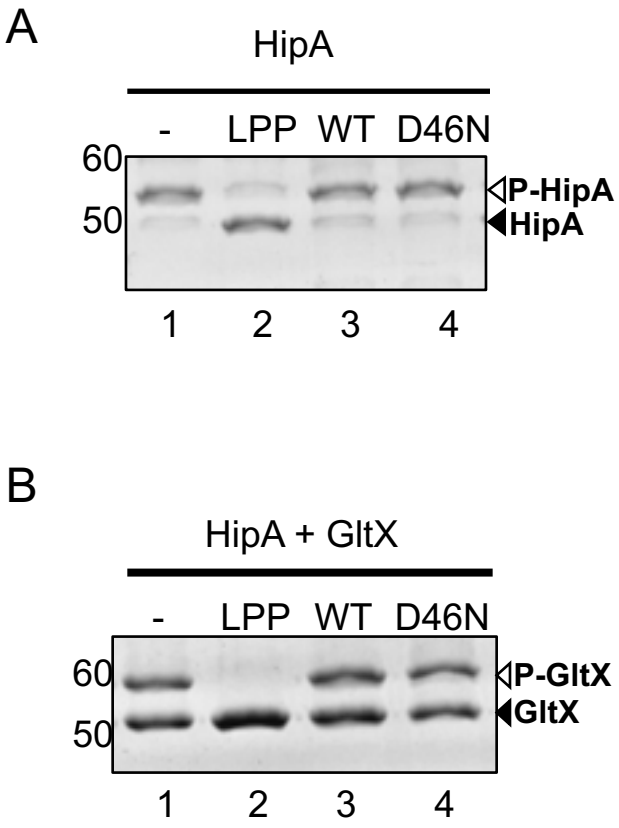

Figure 3.8 Effect of PphC on HipA kinase and phosphorylated GltX
(A) Effect of PphC on HipA kinase. Dephosphorylation reactions contained 2 µM of phosphorylated HipA and 4 µM PphC (WT or D46N) in reaction buffer as described in materials and methods. For control reaction, 400 U of Lambda protein phosphatase (LPP) was used in reaction buffer. Reactions were stopped at t=1 h and analyzed on Mn^{2+}-Phostag/SDS-PAGE. Molecular weights are denoted on the right as kDa.
(B) Effect of PphC on phosphorylated GltX. Kinase reactions contained 0.2 µM HipA and 2 µM GltX in reaction buffer for 45 mins. Dialyzed kinase reactions were used to setup dephosphorylation reactions at 37 ºC with either 400 U of LPP or 4 µM PphC-WT or 4µM of PphC-D46N. Dephosphorylation reactions were stopped at t=1 h and analyzed on Mn^{2+}-Phostag/SDS-PAGE. Molecular weights are denoted on the right as kDa.

Bacterial PP2C-like phosphatases are often present in the same operon as a Ser/Thr kinase (30) and the kinase is often itself a substrate of the phosphatase (100-102, 157). As noted above, *pphC(yegK)* is located immediately adjacent to *yegI*, a 1947 bp ORF encoding a 648 amino acid protein with homology to eukaryotic-like Ser/Thr kinases (Fig. 3.5A). (30). Thus, to examine if YegI could serve as a substrate for PphC, autophosphorylated YegI kinase (Fig. 3.9, lane 1) was incubated in the presence of wild type or D46N mutant PphC and assayed for loss of phosphorylation. While wild type PphC dephosphorylates YegI kinase, as indicated by the loss of the radiolabeled band (Fig. 3.9, lane 2), this effect is not seen following incubation with the catalytic mutant PphC-D46N (Fig. 3.9, lane 3). Interestingly, while PphC-D46N is phosphorylated, phosphorylation of wild type PphC is not observed (Fig. 3.9, lane 2), suggesting that either PphC can dephosphorylate itself or that inactivation of the YegI kinase by PphC could result in decreased phosphorylation of PphC-WT.

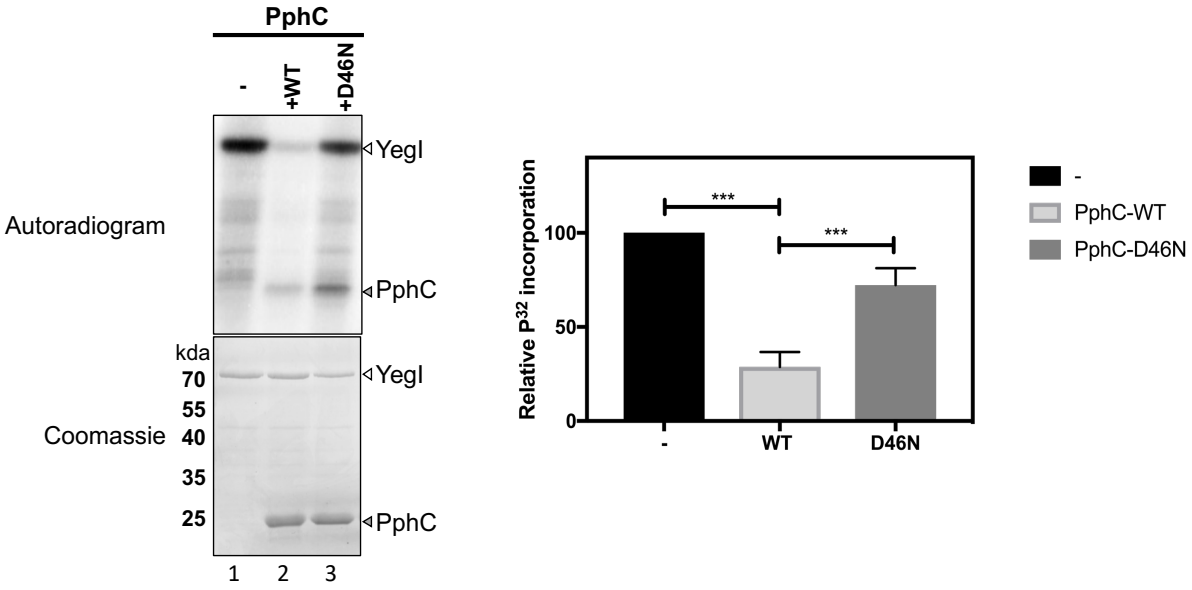

Figure 3.9 Effect of PphC on YegI kinase.
(Left panel) Effect of PphC on YegI kinase. Dephosphorylation reactions were carried out at 37 ºC with 2 µM of phosphorylated YegI and 4 µM PphC in reaction buffer as described in materials and methods. Reactions were stopped at t=45mins and run on 12% SDS-PAGE followed by autoradiography. Molecular weights are denoted as kDa. (Right panel) Percent relative ^{32}P incorporation was calculated by densitometry analysis using FIJI software. Data represents the mean +/- SE of five independent experiments. Statistical analysis used unpaired T-test (*** P value<0.0001).

3.2.6 Phosphorylation of PphC by co-encoded kinase

In these assays, a weak phosphorylation product of ~25kDa corresponding to PphC-D46N was observed (Fig. 3.9, lane 3), suggesting that YegI could transphosphorylate PphC. Low levels of phosphorylation of PphC could be due to weak transphosphorylation potential of YegI. In order to obtain more robust phosphorylation of PphC, we expressed and purified the N-terminal region of YegI (aa 1-390) which includes the predicted kinase domain (aa1-300). The purified protein is annotated as YegI-NTD. Firstly, I tested if PphC serves as a substrate for YegI-NTD. Using radioactive kinase assay, I observed autophosphorylation of YegI-NTD (Fig. 3.10, lane 1) suggesting that the purified N-terminal domain of YegI is an active kinase. Furthermore, I observed of robust phosphorylation of PphC by YegI-NTD in a time dependent manner (Fig. 3.10, lane 3-5) validating PphC as a potential substrate for YegI-NTD.

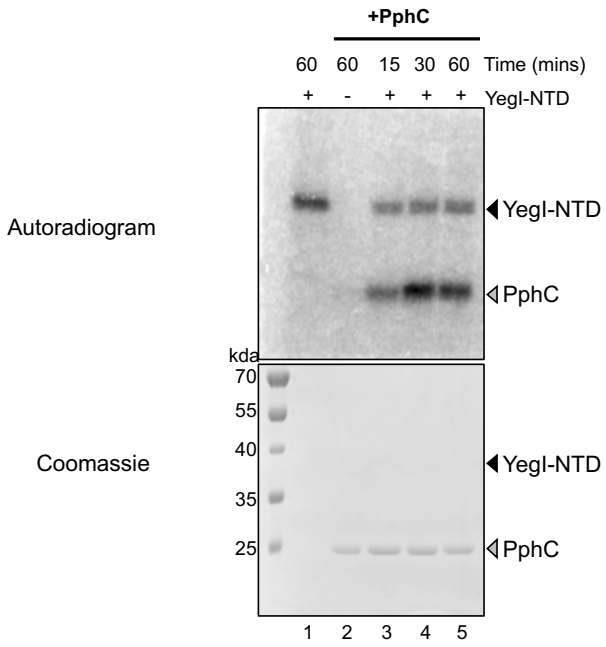

Figure 3.10 Phosphorylation of PphC by YegI-NTD.
Phosphorylation reactions were carried out at 37 ºC with 0.5 µM of YegI-NTD alone (lane 1) or 2 µM PphC alone (lane 2) or both (lane 3-5) in kinase assay reaction buffer as described in materials and methods. Reactions were stopped after addition of [γ-^{32P}]ATP at indicated times and run on 12% SDS-PAGE followed by autoradiography. Molecular weights are denoted as kDa.

Since PphC phosphorylation was more robust with YegI-NTD as compared to YegI, subsequent phosphopeptide detection using mass spectrometry was performed using *in vitro* kinase assay sample of PphC that has been incubated with/without YegI-NTD (Fig. 3.11A). Samples were submitted to the Columbia University Medical Center Herbert Irving Cancer Center Proteomics Center. To identify the phosphorylation site(s) of PphC, Dr. Emily Chen performed mass spectrometry analysis. She identified one phosphopeptide corresponding to serine residue at position 174 (Fig. 3.11B, C).

A

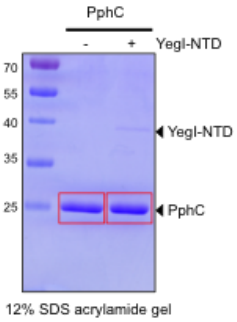

12% SDS acrylamide gel

B

His-PphC
355 peptides, 4423 spectra, 98.5% coverage

```
  1 MAHHHHHHSW RLVYASAVGT SHISADLPCQ DACQMQVAWL NDQQPLLVMF
 51 LADGAGSVSQ GGEGAKLAVN EAMAFMVQKV QDGELGLNDV LATNMVLTIR
101 QRLFAEAEAK ALAVRDFACT FLGLISSANG TLIMQIGDGG VVVDFGRGLE
151 LPLTPMVGEY ANMTHFISDE DAVSRLETFT STERAHKVAA FTDGIQRLAL
201 NMLDNSPHVP FFTPFFNGLA AATQEQLDLL PELLKQFLSS PAVNERTDDD
251 KTLALALWLP
```

C

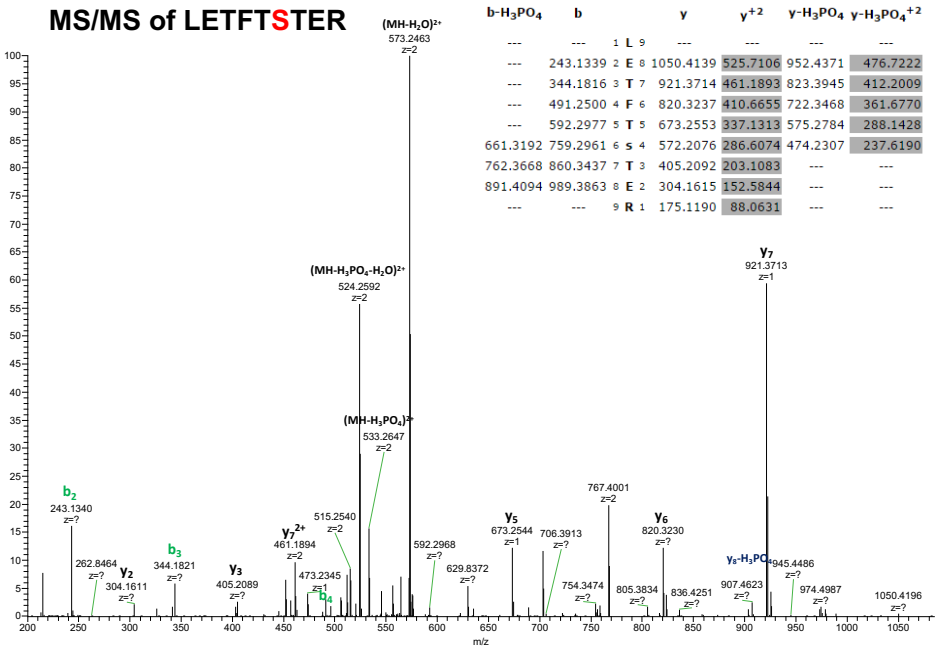

$b\text{-}H_3PO_4$	b			y	y^{+2}	$y\text{-}H_3PO_4$	$y\text{-}H_3PO_4{}^{+2}$
---	---	1	L	9 ---	---	---	---
---	243.1339	2	E	8 1050.4139	525.7106	952.4371	476.7222
---	344.1816	3	T	7 921.3714	461.1893	823.3945	412.2009
---	491.2500	4	F	6 820.3237	410.6655	722.3468	361.6770
---	592.2977	5	T	5 673.2553	337.1313	575.2784	288.1428
661.3192	759.2961	6	S	4 572.2076	286.6074	474.2307	237.6190
762.3668	860.3437	7	T	3 405.2092	203.1083	---	---
891.4094	989.3863	8	E	2 304.1615	152.5844	---	---
---	---	9	R	1 175.1190	88.0631	---	---

Figure 3.11 YegI-NTD phosphorylates PphC on Ser-174.
(A) Phosphorylation reactions were carried out at 37 ºC with 5.32 µM of PphC alone (lane 1) or 5.32 µM PphC in the presence of 1.33µM of YegI-NTD (lane 2) in kinase assay reaction buffer for mass spectrometry as described in materials and methods. 10µl of sample was run on 12% SDS-PAGE to verify sample homogeneity. (B) Amino acid sequence of PphC. Residues will full coverage are shown in black color and residues with no coverage are indicated in gray color. Phosphorylated residue Ser-174 is indicated by red circle. N-terminal his tag used for purification of PphC is underlined. (C) Representative MS/MS spectra of phosphopeptide obtained after trypsin digestion of PphC.

To examine if PphC phosphorylation on serine 174 has any impact on phosphatase activity *in vitro*, I purified a mutant protein where I replaced the serine residue at position 174 to an alanine residue (PphC-S174A). Although I observed robust phosphorylation of PphC on Ser-174 using mass spectrometry data, I was unable to demonstrate any effect of this modification on PphC activity *in vitro* (Fig.3.12). Using β-casein as a substrate, PphC-S174A dephosphorylated β-casein similarly to PphC-WT (Fig. 3.12A). While a slight difference in the rate of dephosphorylation as compared to the wildtype was observed, this difference was not statistically significant suggesting that Ser174 residue may be not be important for phosphatase activity, at least *in vitro*. To test if phosphorylation of PphC affects phosphatase activity, I modified the pNPP assay by first performing an *in vitro* kinase reaction of PphC (WT or S174A) and YegI-NTD to obtain P~PphC followed by addition of pNPP. Using pNPP as a substrate, I observed no difference in phosphatase activity between unphosphorylated PphC and phosphorylated PphC (P~PphC) (Fig.3.12B). Similar to the β-casein result, I observed a slight decrease in phosphatase activity of PphC-S174A as compared to PphC-WT; however, this difference was also not statistically significant. Together, these results show that phosphorylation of PphC at Ser-174 has no significant impact on phosphatase activity *in vitro*.

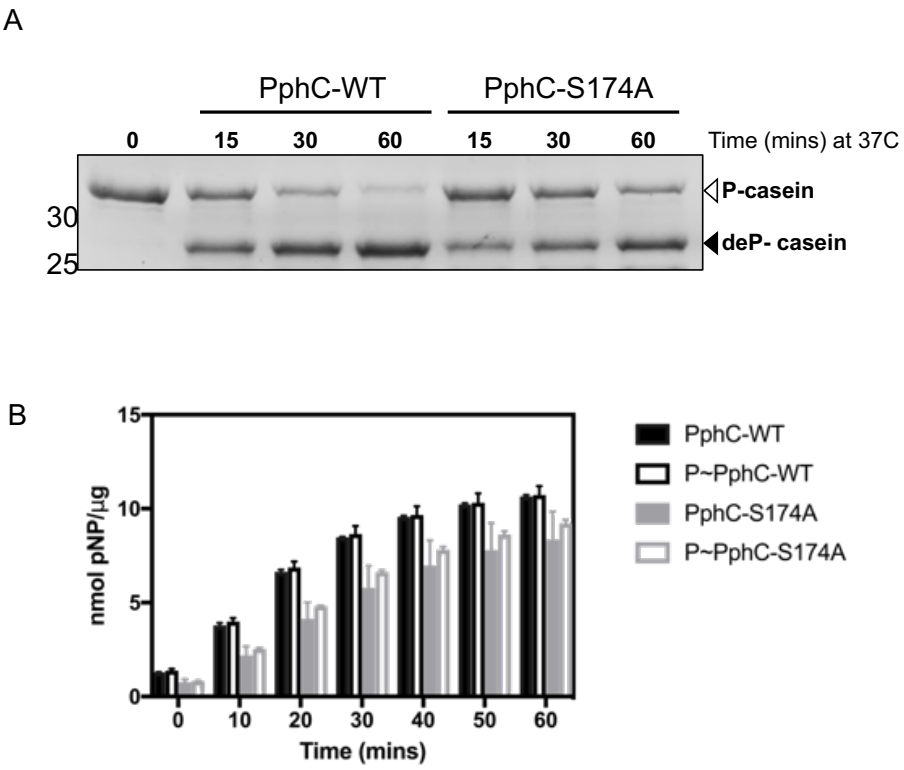

Figure 3.12 S174A mutation of PphC does not impact phosphatase activity .
(A) β-casein as a substrate: Dephosphorylation reactions were carried out at 37 ºC for indicated timepoints in buffer containing 50 mM Tris pH 8, 4 µg phosphorylated β-casein, 1.5 µg (9 µM) phosphatase in the presence of 10 mM $MnCl_2$. (B) Effect of phosphorylation on phosphatase activity of PphC using pNPP as substrate. In vitro kinase reactions were performed with 350nM of phosphatase (WT/S174A mutant) in the presence or absence of 89 nM YegI-NTD for 45 mins at 37 ºC in reaction buffer as described in materials and methods. 5 mM pNPP was added and absorbance at 405nM was recorded for 60 mins.

3.3 Discussion

Mass spectrometry-based phosphoproteomic analysis has revealed that many Ser/Thr/Tyr residues undergo phosphorylation in phylogenetically diverse species. In most cases, the kinases and phosphatases responsible for these modifications have not been identified, although the presence of homologs of eukaryotic Ser/Thr kinases and phosphatases in most (if not all) bacterial species suggest that they could play a role. These so-called eukaryotic-like Ser/Thr kinases and their partner PP2C-like Ser/Thr phosphatases have extensive structural and biochemical similarity with their eukaryotic counterparts (30). In *E. coli*, extensive Ser/Thr phosphorylation has been observed, with several studies reporting >75 phosphorylated proteins (114, 119, 123, 146). However, the kinases and phosphatases responsible for making or removing these modifications are not known. Here, I have described biochemical analysis of PphC, a protein product of a previously undescribed *E. coli* ORF, *yegK*, that encodes the first reported PP2C-like Ser/Thr phosphatase in *E. coli.*

PphC contains all of the 11 conserved motifs present in PPM/PP2C phosphatases (29, 89, 151, 152). However, unlike bacterial PP2C-like phosphatases from other Gram-negative bacteria, PphC has only 6 out of the 8 absolutely conserved residues involved in metal co-ordination and catalysis (95, 96, 98). Specifically, PphC lacks a conserved glycine residue in motif VI and a conserved aspartate residue in motif VIII (Fig. 3.1B). The aspartate residue in motif VIII is important for metal ion co-ordination in bacterial PP2C-like phosphatases (95, 96, 98). Despite these differences in amino acid sequence, PphC effectively hydrolyzed the chromogenic substrate pNPP, suggesting that the requirement of all 8 residues as a criterion for assessing the likelihood that an ORF encodes a PP2C-like phosphatase may be too stringent.

The regulation of PP2C-like phosphatases has been studied in a number of contexts including

Mycobacterium tuberculosis PstP whose activity is stimulated by phosphorylation on multiple Thr residues by two eukaryotic-like Ser/Thr kinases (174). Although I observed that PphC is phosphorylated at residue Ser 174 by its partner Ser/Thr kinase YegI (Fig. 3.11), I was unable to detect any effect of on PphC activity using phosphoablative mutant (Fig. 3.12). Another regulatory mechanism occurs in the *B. subtilis* SpoIIE protein, a PP2C-like phosphatase that plays an essential role during sporulation. A single residue in SpoIIE (Val-697) mediates an alpha-helical switch that changes the coordination of a metal ion in the active site and thereby activates the phosphatase (175). However, since this residue is not conserved in PphC, a similar regulatory mechanism is probably not operating in the context of PphC function.

Bacterial PP2C-like phosphatases are known to dephosphorylate pSer/pThr containing peptides (154-156). PphC was initially identified using a homology search using *B. subtilis* PrpC but unlike PrpC (Fig. 3.7D), PphC displayed low preference for pSer/pThr/pTyr peptides (Fig. 3.7C). This minimal activity against phosphopeptides is in contrast to the ability of PphC to dephosphorylate the pSer containing protein substrate β-casein. A possible explanation could be that PphC may require additional residues for substrate recognition and/or binding that are not present in the phosphopeptides. However, this is not likely to be a sufficient explanation as β-casein is a generic substrate that would not be expected to contain specificity determinants for PphC. Alternatively, this result suggests that there may be limits to using phosphopeptide dephosphorylation as an accurate assay of PP2C-like phosphatase function.

Bacterial eukaryotic-like Ser/Thr kinases and PP2C-like phosphatases are often encoded in the same operon and in many cases the kinase is a substrate for the phosphatase (100, 101, 153, 157). Similarly, in the *E. coli* B strain REL606, the ORF *yegI* encodes a putative eukaryotic-like Ser/Thr kinase and is located immediately downstream of *pphC.* My data demonstrate that YegI is

a substrate of PphC (Fig. 3.8). However, in *E. coli* K strain MG1655, there is a putative intervening ORF, *yegJ*, located between the *yegI* and *pphC* genes and that is transcribed divergently (Fig. 3.5A), suggesting potential regulatory differences between the two strains. I have been unable to observe transcription of the *pphC* locus under any conditions, so we do not know if *yegJ* has an effect on expression of this locus. Interestingly, mutations in *yegI*, the gene encoding the partner kinase of PphC, repeatedly emerge in long-term evolution experiments (176), suggesting that this kinase/phosphatase pair may have significant fitness effects. Consistently, the presence of the potentially disruptive *yegJ* locus in the K lineage may be also reflect these effects. However, at present, in the absence of a deeper understanding of the physiological role of YegI/PphC pair, these effects remain mysterious.

In addition to the differences in the genome organization around *pphC* in the *E. coli* B and K lineages, the amino acid sequence of PphC differs between the two strains, with several non-conservative substitutions. This observation is intriguing given that half of the proteome is identical between these two strains (166). Although these differences are not in residues that are absolutely conserved among bacterial PP2C-like phosphatases (95, 96, 98), they may have functional consequences since the two proteins exhibited modest differences in enzyme kinetics (Fig. 3.6). Future work will be aimed at identifying the impact of specific substitutions in the residues that differ on the relative activity of the different PphC alleles.

Finally, PP2C phosphatases play important roles in cellular regulation in more complex systems including mammals (152). One issue in investigating PP2C function in these *in vivo* contexts is that specific chemical inhibitors do not exist. Thus, the bacterial homologs such as PphC may be useful in identifying cell-permeable inhibitors, both because of the technical tractability of the organism as well as the presence of only a single PP2C-phosphatase gene in the

genome.

In summary, this study provides the first evidence for the existence of a PP2C-like phosphatase in *E. coli*. Despite some differences in sequence conservation as compared to other PP2Cs, PphC is an active PP2C-like phosphatase, albeit with lower K_m and V_{max} values than other bacterial PP2Cs. Future studies will be required to identify physiological substrates of PphC and to ascertain its physiological role *in vivo*. I expect that further characterization of PphC's partner kinase, YegI (see Chapter 4), will greatly facilitate these efforts.

CHAPTER 4

Characterization of a novel membrane Ser/Thr kinase in *Escherichia coli*

4.1 Introduction

Protein phosphorylation on Ser/Thr residues was widely assumed to be present only in eukaryotes and absent in prokaryotes. This assumption was challenged by phosphoproteomic analysis of phylogenetically diverse bacterial species that identified numerous proteins to be phosphorylated on Ser/Thr residues. For example, phosphoproteomic studies of the Gram-negative bacterium *Escherichia coli* identified ~100 proteins modified on Ser/Thr residues (114). However, the enzymes responsible for this phosphorylation in *E. coli* have not been identified to date.

Bacterial Ser/Thr kinases can be divided into two classes based on their structure and sequence homology: eukaryotic-like Ser/Thr kinases (eSTKs) and atypical Ser/Thr kinases. eSTKs bear striking resemblance in structure and function to Hanks family Ser/Thr kinases from eukaryotes (30). Unlike eSTKs, atypical Ser/Thr kinases lack any sequence homology to eukaryotic kinases. So far, three genes (*hipA, yeaG, yihE*) encoding Ser/Thr kinases have been reported in *E.coli* of which HipA and YihE are atypical Ser/Thr kinases while YeaG is an eSTK.

HipA resembles a eukaryotic phosphatidyl inositol 3/4-kinase and was found to be involved in bacterial persistence (73). Bacterial persistence is an epigenetic state exhibited by a subpopulation of slow growing cells that display enhanced survival in the presence of antibiotics. This state is temporary and can be readily reversed by removal of antibiotic treatment. HipA regulates bacterial persistence by phosphorylating a substrate protein glutamyl tRNA synthetase (GltX) on a single serine residue. Phosphorylated GltX can no longer aminoacylate tRNA, leading to accumulation of uncharged tRNAs at the ribosome which in turn inhibits translation, induces the stringent response and thereby results in persistence. (78, 79).

YihE was identified as an atypical Ser/Thr kinase that shares significant structural homology to eukaryotic choline kinases but lacks several of the absolutely conserved residues in the catalytic loop (80). While the transphosphorylation of YihE has not been shown with physiological substrates, it transphosphorylates the generic protein substrate myelin basic protein (MBP) (82). YihE was shown to play a role in regulating stress response leading to programmed cell death in *E. coli* (82) although little mechanistic insight is available. YeaG was the first eSTK to be reported in *E. coli* (66). YeaG functions in modulating transcription of methionine biosynthetic genes, facilitating adaptation of cells to sustained nitrogen stress (70, 71).

Although these Ser/Thr kinases have been shown to be active in the cell and participate in regulating various cellular physiological processes, the substrates for these kinases have not been characterized *in vitro* except in the case of HipA. Similarly the Ser/Thr kinases/phosphatases responsible for the Ser/Thr phosphorylation of proteins reported in *E.coli* phosphoproteomics studies are not known(114, 119, 177).

I recently reported the identification and characterization of a PP2C-like Ser/Thr phosphatase PphC in *E.coli* (178) (Chapter 3). PphC is the first PP2C-like phosphatase to be characterized in *E.coli.* In our efforts to identify a substrate for PphC, we noted an adjacent gene, *yegI,* that encodes a putative Ser/Thr kinase. In this chapter, I describe the biochemical characterization of YegI, an integral membrane Ser/Thr kinase with two Helix-hairpin-Helix (HhH) motifs in the C-terminal domain. Additionally, I show that a strain carrying a deletion of *yegI* exhibited decreased susceptibility of cells to the β-lactam antibiotic cefotaxime and to the DNA damage inducing agent nalidixic acid.

Using comparative phosphoproteomics and an *in vitro* kinase assay, I identify the glycolytic enzyme enolase as a substrate for YegI. Finally, I demonstrate that elongation factor Tu (EF-Tu)

is a target for YegI *in vitro* and this phosphorylation inhibits the function of EF-Tu in protein synthesis.

4.2 YegI is a novel eukaryotic-like Ser/Thr kinase

Analysis of the genome of *E. coli* strain REL606 revealed the presence of a 1941bp orf *yegI* which encodes a 646 amino acid protein YegI predicted to be a Ser/Thr kinase. *In E. coli* REL606 and in several pathogenic strains such as *E. coli* O157:H7 EDL933, *yegI* occurs in the same putative operon as a PP2C-like phosphatase *pphC (yegK)* with a four nucleotide overlap (ATGA) at the 5' end suggesting that the genes could be cotranscribed. Alternatively, in *E. coli* K strains (*e.g*., MG1655/W3110), the *yegI-pphC* operon is disrupted by *yegJ,* encoding a protein of unknown function (Fig. 4.1A). Amino acid sequence analysis and alignment of YegI with bacterial eSTKs (Fig. 4.1B) revealed the presence of Hanks signature motifs (I-XI) suggesting that YegI is an authentic eukaryotic-like Ser/Thr kinase (eSTK) (13). Although YegI contains all the Hanks signature motifs, it contains only seven out of the ten absolutely conserved residues that are commonly found in eSTKs. For example, in motif III, YegI has an aspartic acid residue instead of the conserved glutamic acid (Fig.4.1B). The conserved glutamic acid residue which contacts Lys-39 in Motif II for stable binding of α and β phosphates of ATP (35). YegI also lacks the conserved asparagine (replaced by serine) in motif VI that together with catalytic site Asp-141 and Asp-159 is important for stability of Mg^{2+} ion binding (35). Lastly, YegI lacks a conserved arginine (replaced by glycine) in motif XI that is important for stabilizing the substrate-protein interactions (Fig.4.1B).

In order to identify how these sequence changes affect the structure, I created a homology model of the YegI kinase domain (aa1-300) with the crystal structure of *M. tuberculosis* eSTK

PknB (PDB 1MRU) as a template using Swiss-model (179). Despite the absence of three conserved residues, the predicted structure of the YegI kinase domain shows all the structural features seen in *M. tuberculosis* eSTK PknB (Fig.4.1C) suggesting that YegI is an eSTK. Specifically, YegI adopts the canonical bilobed structure seen in eSTKs. The N-terminal lobe of the YegI kinase domain contains the ATP binding P-loop and the helix C structure (See Fig.4.1B, C) which is responsible for proper orientation of active site with substrate protein. The C-terminal lobe includes the catalytic loop which contains all the residues required for catalysis and an activation loop which is important for kinase activation by autophosphorylation. Although overall the YegI sequence is only ~20% identical to PknB (Fig.4.1B), the predicted structure of YegI is very similar to solved structure of PknB (Fig.4.1D), strongly suggesting that YegI is an eukaryotic-like Ser/Thr kinase.

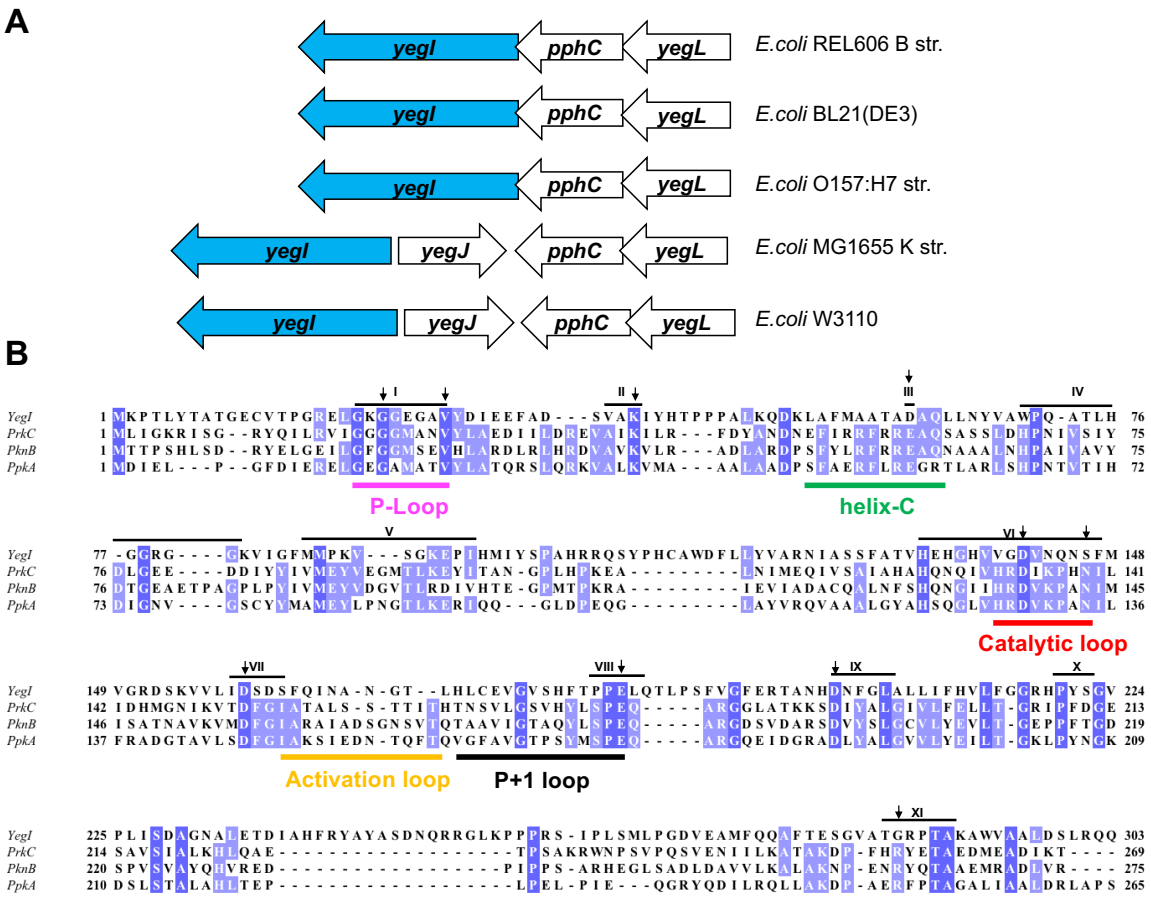
A
yegI
pphC
yegL
E.coli REL606 B str.
yegI
pphC
yegL
E.coli BL21(DE3)
yegI
pphC
yegL
E.coli O157:H7 str.
yegI
yegJ
pphC
yegL
E.coli MG1655 K str.
yegI
yegJ
pphC
yegL
E.coli W3110
B
P-Loop
helix-C
Catalytic loop
Activation loop
P+1 loop
C
D

Figure 4.1 YegI is a novel eukaryotic-like ser/thr kinase
(A)**Genome organization of *yeg* operon in different *E. coli* strain backgrounds**. Thick arrows denote orfs. Genes *yegL, pphC, yegI* encode a predicted Von Willebrand factor, a PP2C-like phosphatase and an eukaryotic-like Ser/Thr kinase respectively. The *yegJ* gene encodes a protein of unknown function. *E. coli* strain backgrounds are indicated on the right.
(B) **Amino acid sequence alignment of YegI with bacterial eSTKs**. YegI (*Escherichia coli*) was aligned to bacterial eSTKs PrkC (*Bacillus subtilis),* PknB *(Mycobacterium tuberculosis)* and PpkA (*Pseudomonas aeruginosa)* using T-coffee (159). Alignment was visualized using Jalview. Absolutely conserved residues are shaded in dark blue whereas residues conserved in three out of the four kinases are shaded in light blue. The ten absolutely conserved residues found in bacterial eSTKs are depicted with arrows. Hanks conserved domains are depicted on top of the sequence as roman numerals (I-XI). YegI (aa 1- 303), PrkC (aa 1-269), PknB (aa 1-275) and PpkA (aa 1-265) which includes the kinase domain was used for alignment. Structurally and functionally important motifs are indicated below the sequence.
(C) **Predicted structure of YegI kinase domain (aa 1-302)**. The Phyre2 algorithm (160) was used to predict structural model of YegI kinase domain. Structurally important motifs such as P-loop (pink), Helix C (green), Catalytic loop (red), activation loop(yellow) and P+1 loop (black) are indicated in structure. Corresponding amino acid sequences are depicted in (B).
(D) Structural overlay of predicted structure of YegI kinase domain (blue) and *Mycobacterium tuberculosis* eSTK PknB (pink) (Protein data bank PDB:1MRU). Mg^{2+} ion is represented as a grey sphere.

4.3 Biochemical properties of YegI

4.3.1 Expression and Purification of YegI

Although the predicted structure of YegI revealed striking similarities to the structure of *M. tuberculosis* eSTK PknB, three of the ten absolutely conserved residues of the Hanks family STKs were absent raising the question of whether YegI is an active kinase. Domain prediction of YegI revealed the presence of a Ser/Thr catalytic domain (aa 13-300), two transmembrane domains (aa 391-411, 414-436) and a C-terminal domain (aa 436-646). To directly test if YegI exhibits kinase activity, I first expressed and purified either recombinant His_6-tagged YegI or a His_6-tagged fragment of YegI that includes the entire N-terminal fragment encompassing the Ser/Thr kinase domain and 90 residues of the linker to the transmembrane helix (YegI-NTD) (Fig. 4.2A). Plasmids expressing YegI and YegI-NTD were transformed in C43(DE3) cells and expression was confirmed by western blot analysis with an α-his antibody (Fig.4.2B). I detected a 72 kDa and a 43.5 kDa band, likely corresponding to YegI and YegI-NTD respectively post induction with arabinose confirming that both proteins were expressed. Since YegI has two predicted transmembrane domains, lysis and purification was carried out in the presence of anionic detergent

N-lauryl sarcosine to facilitate solubilization and purification. N-lauryl sarcosine has been shown to help with cell lysis as well as protein solubility of membrane bound proteins (180). Using N-lauryl sarcosine, I was able to successfully purify both the full length form (Fig.4.2C) and the N-terminal domain of YegI (Fig.4.2D). However, SDS-PAGE analysis showed the presence of an equally abundant protein at 25 kDa. This co-purifying protein could be one of two possibilities: a potential interacting protein which forms a complex with YegI or a his-tag affinity purification contaminant. To examine these possibilities, purified protein samples were submitted to the Columbia University Medical Center Herbert Irving Cancer Center Proteomics Center. Dr. Emily Chen performed MALDI Peptide Mass Fingerprinting of the 25kDa gel band. She identified that the 25kDa protein was indeed a common his-tag affinity purification contaminant, peptidyl-prolyl cis/trans-isomerase (SlyD), thus ruling out the possibility of co-purification of an interacting partner. To avoid co-purification of SlyD, YegI and YegI-NTD were expressed in a SlyD mutant strain LOBSTR (181) which lacks the histidine-rich region of SlyD thereby preventing SlyD from binding to Ni^{2+}-NTA beads. As expected, expression of YegI and YegI-NTD in the LOBSTR strain eliminated the 25kDa contaminating SlyD to yield pure protein (Fig. 4.2E,F).

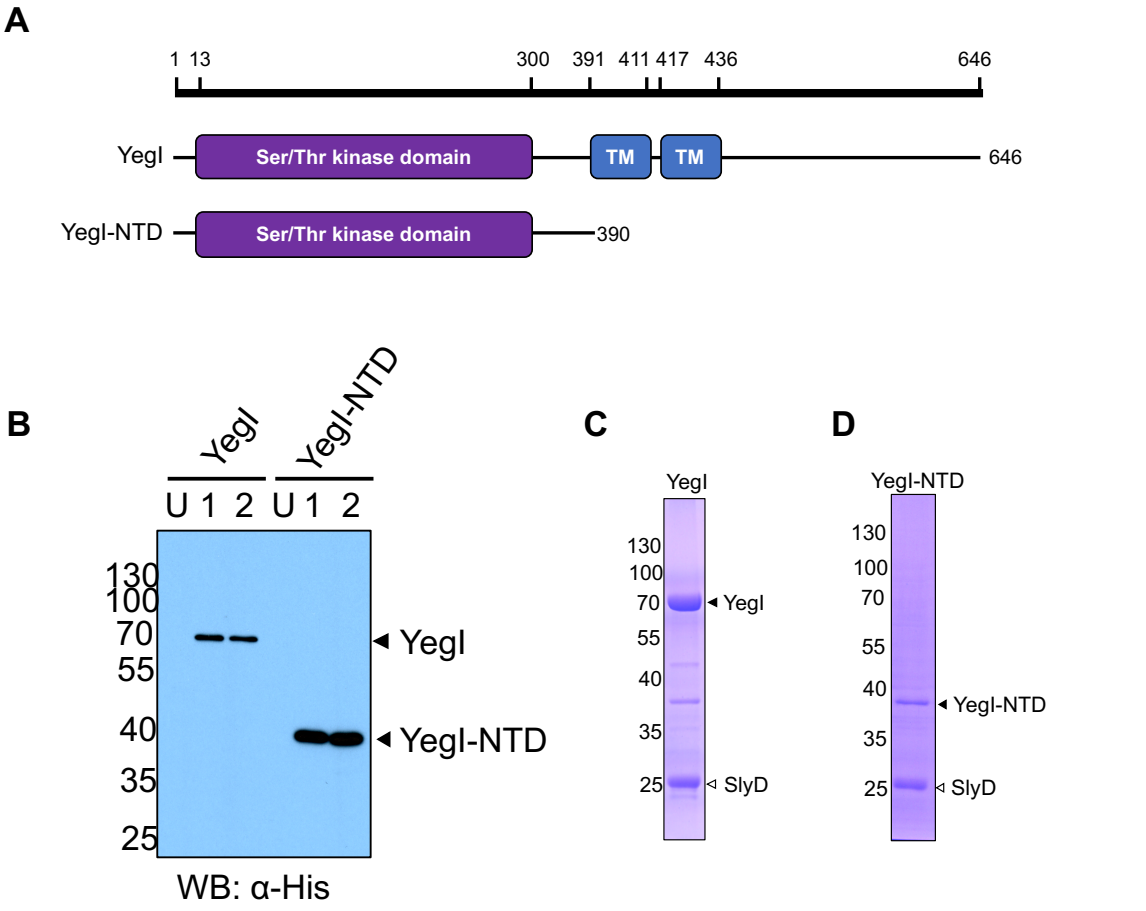
A
1 13
300
391
411 417
436
646
YegI
Ser/Thr kinase domain
TM
TM
646
YegI-NTD
Ser/Thr kinase domain
390
B
YegI
YegI-NTD
U 1 2 U 1 2
130
100
70
55
40
35
25
YegI
YegI-NTD
WB: α-His
C
YegI
130
100
70
55
40
35
25
YegI
SlyD
D
YegI-NTD
130
100
70
55
40
35
25
YegI-NTD
SlyD
E
Elutions
U I TL SF 1 2 3 4 5
170
130
100
70
55
40
35
25
YegI
F
Elutions
U I TL SF FT 1 2 3 4 5
170
130
100
70
55
40
35
25
15
YegI-NTD

Figure 4.2 Expression and purification of His-YegI and His-YegI-NTD
(A) **Graphical representation of domain architecture of YegI**. Amino acids corresponding to different domains are indicated at the top. TM: Transmembrane domain. Amino acid boundaries for YegI (aa 1-646) and YegI-N terminal domain YegI-NTD (1-390) are indicated.
(B) **Western blot analysis using α-HIS antibody to confirm expression of His-YegI and His-YegI-NTD**. Molecular weights (kDa) are indicated on the left. U represents Uninduced culture at OD_{600}:0.8. 1 and 2 represents samples taken at 1h and 2h post induction with 0.2% arabinose respectively.
(C) **Purification of YegI from C43(DE3) using Ni-NTA resin**. Sample after elution from Nickel beads was verified by gel electrophoresis. A 25kDa band corresponding to Peptidyl-prolyl cis/trans-isomerase (SlyD), a common his contaminant that co-purifies with YegI is indicated.
(D) **Purification of Yeg-NTD from C43(DE3) using Ni^{2+}-NTA resin**. Sample after elution from Nickel beads was verified by gel electrophoresis.
(E) **Purification of YegI from LOBSTR using Ni^{2+}-NTA resin**. U: Uninduced sample, I: Induced fraction, TL: Total lysate after sonication and overnight lysis with 2% sarkosyl, SF: Soluble fraction, FT: Flow through after Ni-NTA binding , 1-5: Elutions with 300mM imidazole.
(F) **Purification of YegI-NTD from LOBSTR using Ni^{2+}-NTA resin**: same as in (E)

4.3.2 YegI is an active kinase

Despite the absence of three of the ten absolutely conserved residues (Fig. 4.1B), I demonstrated that His-YegI is indeed an active kinase capable of autophosphorylation (Chapter 3, Fig.3.9) (178). YegI contains a conserved lysine at position 39 and a conserved aspartic acid site at position 141, both of which are known to play a crucial role in ATP binding and catalysis respectively (28). To confirm that the kinase activity depends on both these residues, I generated lysine to aspartic acid (K39D), lysine to alanine (K39A) and aspartic acid to asparagine (D141N) mutations in YegI. Single point mutants were expressed and purified in the same manner as the WT YegI. Kinase activity was demonstrated using an *in vitro* radioactive kinase assay using radiolabeled $\boldsymbol{\gamma}$-[^{32}P] ATP. Mutation of either Lys-39 or Asp-141 resulted in complete loss of autophosphorylation activity of YegI as compared to WT indicating that both residues are essential for kinase activity (Fig.4.3A).

Staurosporine is widely used as a small molecule inhibitor for Ser/Thr kinases (182) . Eukaryotic Ser/Thr protein kinases are sensitive to staurosporine with IC_{50} in the nM range (183). Sensitivity of the YegI kinase to staurosporine was assessed by incubating YegI with increasing μM concentrations of staurosporine. In comparison to eukaryotic protein kinases, YegI shows an

IC_{50} of 50 μM (Fig.4.3B). This is comparable to the *Enterococcus faecalis* eSTK IreK which has an IC_{50} of 150 μM (53) and the *Staphylococcus epidermis* eSTK Stk which has as IC_{50} of 320 μM (184).

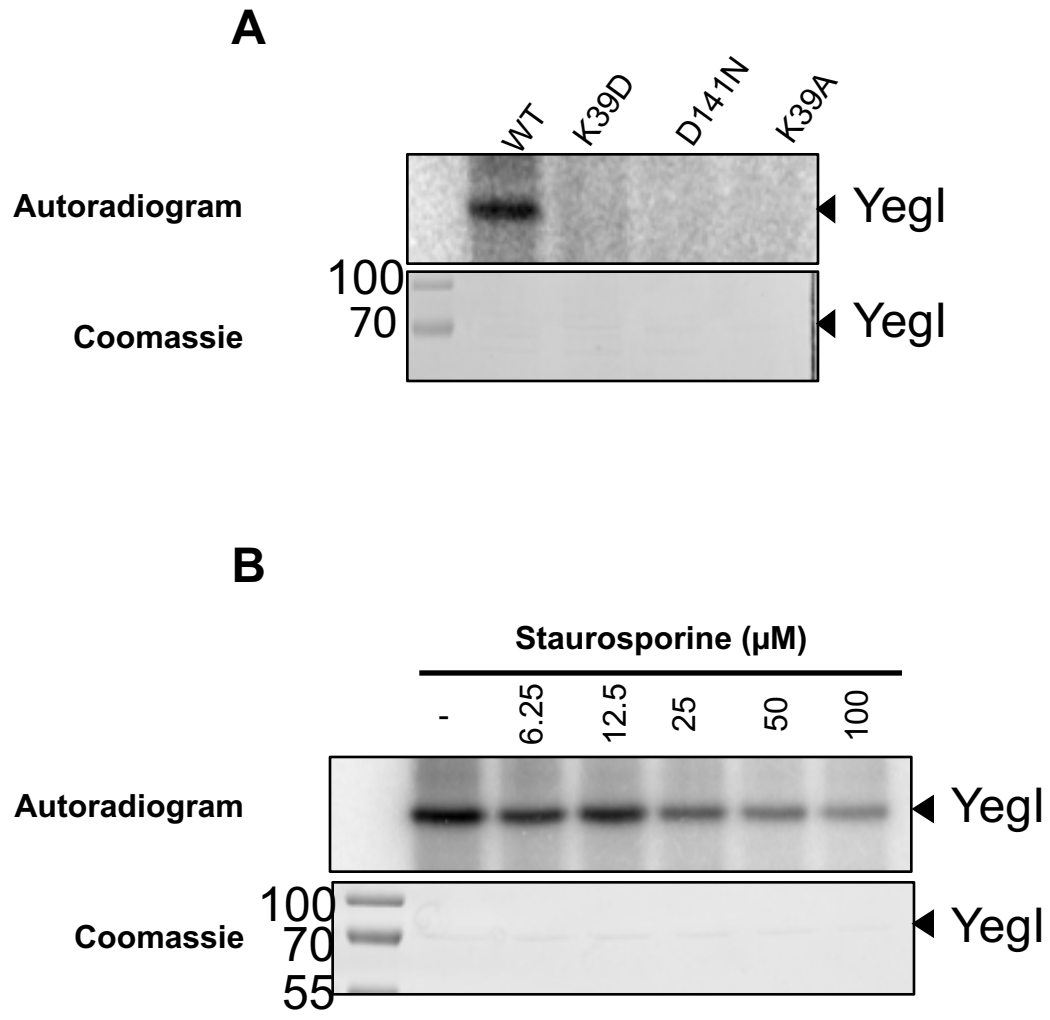

Figure 4.3 YegI is an active kinase

(A) **Kinase activity of YegI**: Autophosphorylation reactions were carried out at 37 ºC with 0.2 μM of YegI (WT or K39D, D141N or K39A) in kinase buffer (50 mM Tris pH 7.5, 50 mM KCl, 1 mM DTT, 10 mM $MgCl_2$, 10 mM $MnCl_2$, 200 μM cold ATP and 5 μCi γ-[^{32}P]ATP. Reactions were stopped at t=30 mins and run on 12 % SDS-PAGE followed by autoradiography. Molecular weights (kDa) are indicated on the right of the gel.

(B) **Sensitivity to staurosporine:** Autophosphorylation reactions were carried out at 37 ºC with 1 μM of YegI (WT) in kinase buffer without cold ATP. Different concentrations of staurosporine (μM) was added to the reaction at indicated concentrations. Reactions were stopped at t=30 mins and run on 12% SDS-PAGE followed by autoradiography. Molecular weights are indicated on the right of the gel.

4.3.3 Metal ion requirement of YegI

Bacterial eSTKs require the presence of bivalent cations for activity (34, 101, 153, 185). To test the effect of different bivalent cations on YegI activity, radioactive kinase assays were performed in the presence of either $MgCl_2$/$MnCl_2$/$CaCl_2$/$NiCl_2$. Similar to many eSTKs, YegI and YegI-NTD catalyzed autophosphorylation only in the presence of $MgCl_2$ and $MnCl_2$, albeit to different levels. Both YegI (Fig.4.4A) and YegI-NTD (Fig.4.4B) displayed much higher autophosphorylation in the presence of Mn^{2+} ion than Mg^{2+} ion suggesting that YegI is a Mn^{2+} dependent kinase.

The structures of eukaryotic kinases indicate that the DFG motif present in domain VII coordinates Mg^{2+} ion binding (33, 186). However, YegI does not contain the DFG sequence which is instead replaced by the residues DSD (Fig.4.1B). To examine if addition of the DFG motif to YegI alters preference to $MgCl_2$, I generated point mutations to replace the DSD motif with DFG: serine to phenylalanine at position 160 and aspartic acid to glycine at position 161 (S160F, D161G). Point mutants were expressed and purified in the same manner as the WT YegI and kinase activity in the presence of $MgCl_2$/$MnCl_2$ was assessed. Surprisingly, replacement of DSD to DFG completely inactivated the kinase (Fig.4.4C) indicating that the DSD motif is indispensable for YegI autophosphorylation.

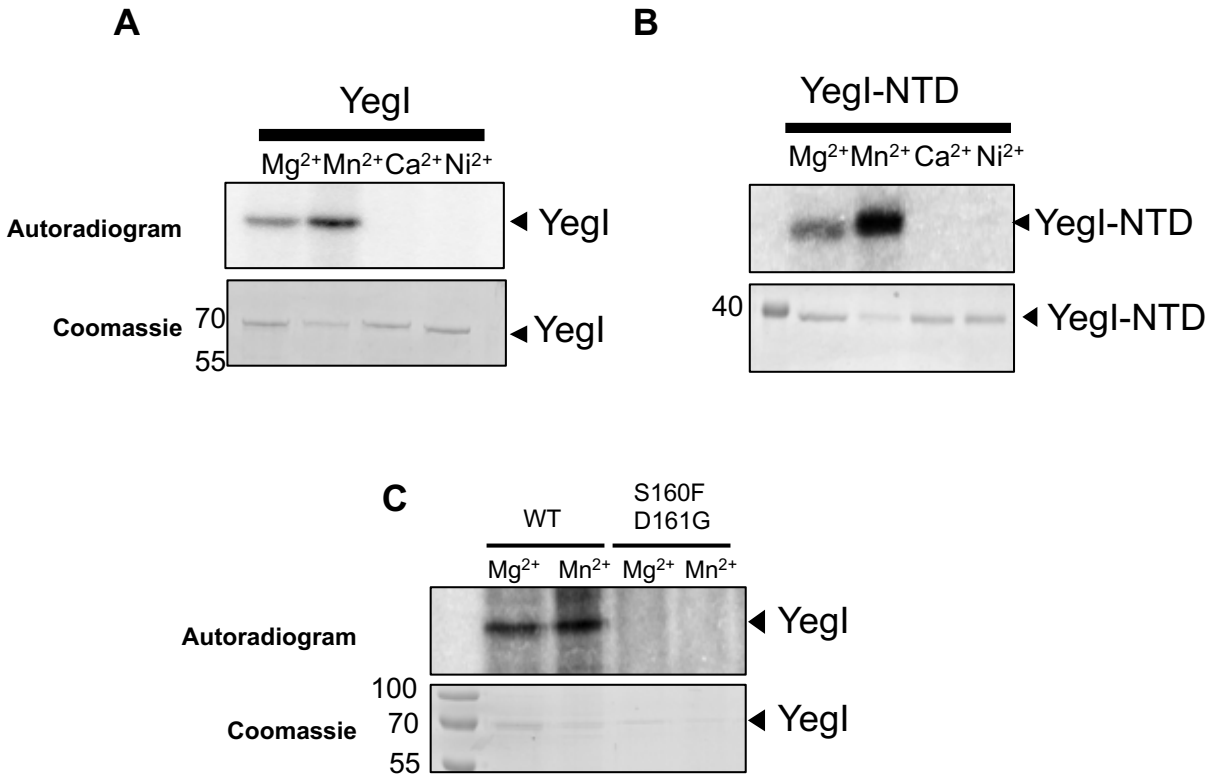

Figure 4.4 YegI is Mn^{2+} ion dependent kinase
(A) **Requirement of bivalent cations**: Autophosphorylation reactions were carried out at 37 ºC with 1 µM of YegI (WT) in kinase buffer with either 10 mM of $MgCl_2$/ $MnCl_2$, $CaCl_2$/ $NiCl_2$. Reactions were stopped at t=30 mins and run on 12% SDS-PAGE followed by autoradiography
(B) **Requirement of bivalent cations**: Autophosphorylation reactions were carried out at 37 ºC with 1 µM of YegI-NTD (WT) in kinase buffer as described in (A)
(C) **Requirement of DFG motif**: Autophosphorylation reactions were carried out at 37 ºC with 0.2 µM of YegI (WT or S160FD161G or D161G) in kinase buffer with either 10 mM of $MgCl_2$/ $MnCl_2$ as described in (A)

4.3.4 Autophosphorylation of YegI

Autophosphorylation is a common model for activation of eukaryotic kinases (33), therefore identifying the sites of autophosphorylation can provide insight into how these kinases are activated. To map the sites of autophosphorylation, phosphopeptide detection using mass spectrometry was performed using His-YegI that had been subjected to an *in vitro* kinase reaction. Samples were submitted to the Columbia University Medical Center Herbert Irving Cancer Center Proteomics Center. To identify the autophosphorylation site(s) of YegI, Dr. Emily Chen performed mass spectrometry analysis and identified two phosphopeptides that each included a serine residue: at position 602 and 644 at the C-terminus of YegI (Fig. 4.5A). To confirm the sites of autophosphorylation, I mutated both serine residues to alanine (S602AS644A). The mutant protein was expressed and purified in the same manner as WT and assessed for loss of autophosphorylation using a radioactive kinase assay. I observed that mutation of both Ser-602 and Ser-644 led to a decrease in autophosphorylation but not a complete loss suggesting that there are additional sites of autophosphorylation (Fig.4.5B).

Since eSTKs have previously been shown to undergo autophosphorylation on serine or threonine residues particularly in the activation loop of the kinase domain (41, 111, 187, 188), the lack of observable autophosphorylation in this region of YegI was surprising. Therefore, we repeated the mass spectrometry analysis using *in vitro* phosphorylation samples with the His-YegI-NTD protein instead to identify phosphorylation sites primarily in the kinase domain. Dr. Emily Chen identified three phosphopeptides corresponding to serine residues at position 153, 160 and 162 in the kinase domain (Fig.4.5A). Ser-153, Ser-160 and Ser-162 are located between Motif VI and VII in close proximity to the catalytic loop and activation loop and therefore I hypothesized that these residues could be important for kinase activity.

To characterize the functional role of the autophosphorylation sites of YegI-NTD, I mutated all three serine residues to alanine (S153A, S160A, S162A). The triple mutant protein was expressed and purified in the same manner as the WT and assessed for loss of autophosphorylation. In contrast to full-length YegI, I observed that mutating all three residues (S153A, S160A, S162A) in YegI-NTD lead to complete loss of autophosphorylation (Fig. 4.5C), suggesting that phosphorylation of Ser-153, Ser-160 and Ser-162 residues could be play an important role in activation of YegI kinase. The impact of individual phosphoablative mutants on YegI activation is yet to be assessed.

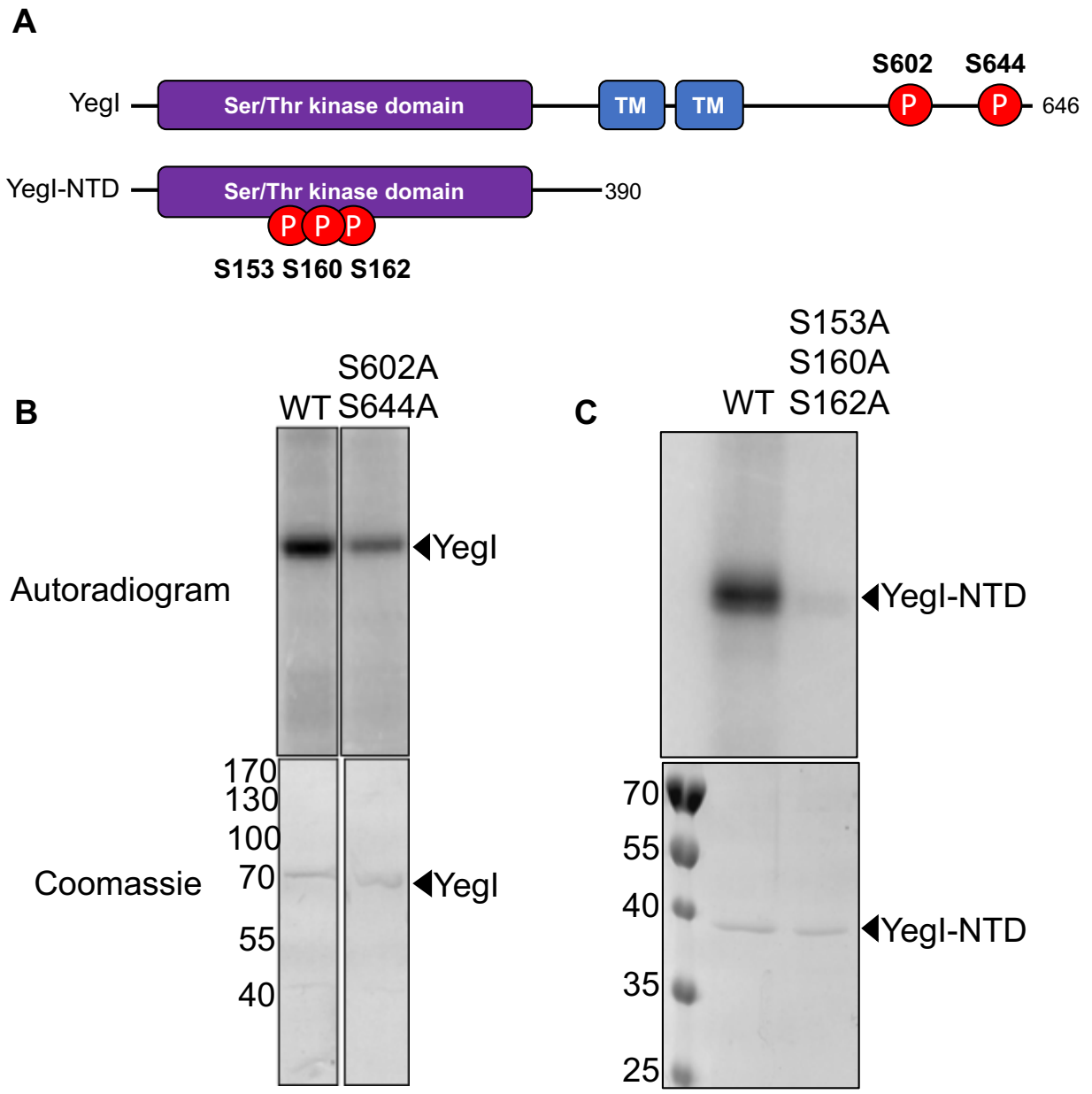

Figure 4.5 YegI autophosphorylation occurs on Ser residues in the catalytic loop and at the C-terminus

(A)**Graphical representation of YegI and YegI-NTD:** Domain structure depicting phosphorylation sites following mass spectrometry analysis of autophosphorylation. Phosphorylated residues are indicated by red circles.

(B) **Sites of autophosphorylation on YegI**: Reactions were carried out at 37 ºC with 1 µM of YegI (WT or S602AS644A) in kinase buffer. Reactions were stopped at t=30 mins and run on 12 % SDS-PAGE followed by autoradiography. Molecular weights (kda) are indicated on the right of the gel.

(C) **Sites of autophosphorylation on YegI-NTD**: Reactions were carried out at 37 ºC with 1 µM of YegI-NTD (WT or S153AS160AS162A) in kinase buffer. Reactions were stopped at t=30 mins and run on 12 % SDS-PAGE followed by autoradiography. Molecular weights (kDa) are indicated on the right of the gel.

4.4 Topology and domain organization of YegI

4.4.1 YegI is an inner membrane protein

Recombinant protein purification of YegI required the presence of the anionic detergent N-lauryl sarcosine suggesting that YegI could be a membrane protein. Additionally, examination of the protein sequence using the domain prediction algorithm Phobius (189) predicted that YegI protein has two transmembrane domains joined by a short periplasmic loop and with both the N- and the C-terminus of the protein in the cytosol (Fig. 4.6A).

To test if YegI is a membrane bound protein, I utilized the PhoAlacZα dual reporter system to experimentally validate the predicted topology of YegI. The PhoAlacZα dual reporter system has been widely used to examine the topology of membrane proteins (190-193). Specifically, a reporter with mature alkaline phosphatase (PhoA, aa 21-471) lacking the periplasmic localization signal is fused in frame with the α-fragment of *E. coli* β-galactosidase (LacZα, aa 5-60). PhoA is active only in the bacterial periplasm whereas LacZ is only active in the cytoplasm. Therefore when the protein of interest fused with PhoAlacZα is targeted to the periplasm or to the membrane, the reporter fusion displays high phosphatase activity but no β-galactosidase activity. On the contrary, if the protein of interest fused with PhoAlacZα is targeted to the cytoplasm, then reporter fusion displays high β-galactosidase activity with no phosphatase activity. PhoAlacZα reporter fusions can be assessed using dual indicator plates with PhoA or LacZ specific chromogenic substrates that allow identification of periplasmic or cytoplasmic fusions (192). Cells expressing PhoAlacZα protein fusions with high levels of phosphatase activity are able to process the X-phos (5-bromo-4-chloro-3-indolyl phosphate) substrate resulting in blue colored colonies, while cells expressing PhoAlacZα protein fusions with high levels of β-galactosidase activity enzymatically process the Red-gal (6-chloro-3-indolyl-β-D-galactoside) substrate to yield red colored colonies.

I constructed in-frame C-terminal pho-lac fusions expressing *E. coli* alkaline phosphatase fragment (PhoA, aa 21-471) in frame with the α-fragment of *E. coli* lacZ (aa 5-60) in an arabinose inducible pBAD24 plasmid. C-terminal pho-lac fusions were made to YegI at amino acid positions 340, 390, 414, 432, 439 and 646 (Fig. 4.6A). *E. coli* DH5α cells have low endogenous phosphatase activity (Δ*phoA*) and are capable of β-galactosidase α-complementation (*E. coli* LacZΔM15), therefore DH5α cells were used for the expression of pho-lac fusions. DH5α cells expressing just the empty backbone vector pBAD24 (shown as (C) in Fig.4.6.B) was used as a negative control, while DH5α cells expressing phoAlacZα without YegI (shown as phoAlacZα in Fig.4.6.B) was used as a positive control. The resulting transformants were streaked on dual indicator plates containing chromogenic substrates X-phos and Red-gal. As expected, cells expressing pBAD24 (negative control) formed colorless colonies on dual indicator plates, while cells expressing PhoALacZα without YegI yielded red/pink colonies indicative of cytoplasmic location (Fig.4.6B). Consistent with the *in silico* prediction, PhoAlacZα fusions of YegI at amino acid positions 340, 390, 439 and 646 yielded red/pink colored colonies on indicator plates suggestive of high β-galactosidase activity and cytoplasmic localization (Fig.4.6B,C). In contrast, PhoAlacZα fusions of YegI at amino acid positions 414, 432 yielded blue colored colonies on indicator plates suggestive of high alkaline phosphatase activity and periplasmic/TM localization. (Fig.4.6 B,C). In summary, the PhoAlacZα reporter fusions confirmed the bioinformatic prediction that YegI is an integral inner membrane protein containing two TM domains connected by a short periplasmic loop, with both the N- and C-terminus located in the cytosol.

A

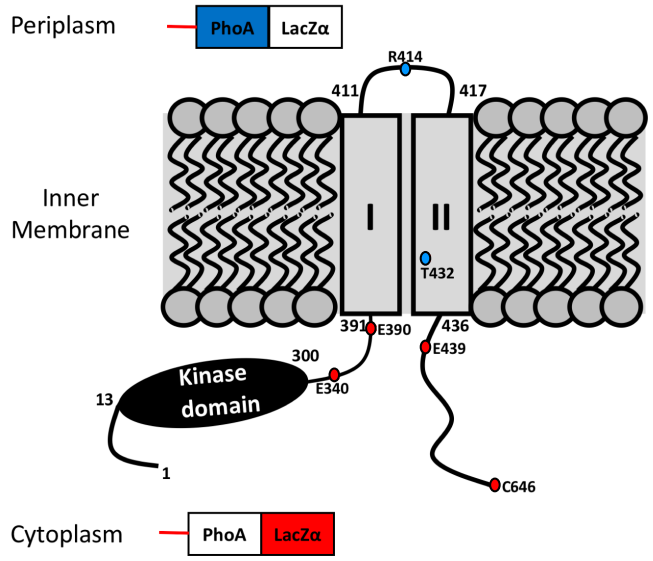

B

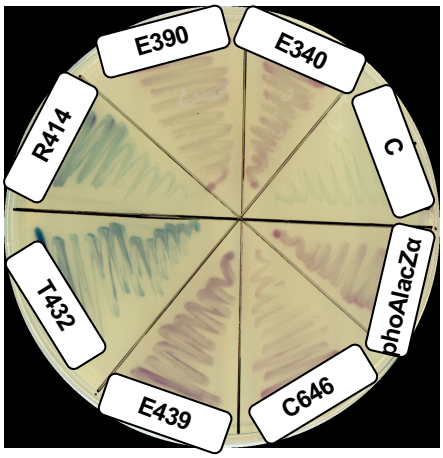

C

YegI fusion	LacZα	PhoA	Localization
E340	+	-	Cytoplasm
E390	+	-	Cytoplasm
R414	+	+	Periplasmic or Transmembrane
T432	-	+	Periplasmic or Transmembrane
E439	+	-	Cytoplasm
C646	+	-	Cytoplasm

Figure 4.6 YegI is an inner membrane protein
(A) **Predicted topology of YegI using Phobius.** Amino acid positions at which phoA-lacZα reporters are fused are indicated along with associated phenotypes. Phenotypes of phoAlacZα fusions due to LacZ activity are denoted as red ellipses while PhoA activity are denoted as blue ellipses. Predicted transmembrane domains (I and II) are depicted as grey rectangles.
(B) **Membrane topology analysis:** DH5α transformed with different phoAlacZα reporters were streaked on an LB plate containing 5-bromo-4-chloro-3-indolyl phosphate disodium salt (X-Phos, 80µg/ml), 6-chloro-3-indolyl-β-D-galactoside (Red-Gal, 100 µg/ml, 0.1 % w/v arabinose and 100 µg/ml of ampicillin. C: control strain expressing pBAD24 empty vector, phoAlacZα: strain expressing phoAlacZα in pBAD24 without YegI. Amino acid positions at which phoAlacZα reporters are fused are indicated.
(C) Localization of different phoAlacZα reporter fusions.

4.4.2 YegI contains two predicted Helix-hairpin-Helix motifs in the C terminal domain

Sequence analysis and domain prediction revealed that the YegI cytoplasmic C-terminal domain contains two predicted Helix-hairpin-Helix (HhH) motifs corresponding to aa 516-535 and aa 546-565 respectively (Fig.4.7A). The HhH motif is a 20 amino acid nonspecific DNA binding motif which forms a hydrogen bond with DNA phosphate groups through the backbone protein nitrogen atoms. The HhH motif is formed by two antiparallel α- helices that are connected by a short hairpin loop (194). Sequence alignment of the two HhH motifs (HhH1 and HhH2) in YegI with known HhH containing proteins showed an absolute conservation of glycine residues at position 8 and 10 forming the GXG motif where X corresponds to a hydrophobic residue (Fig.4.7B). GXG motif is responsible for the hairpin formation as well as binding to DNA. Furthermore, positions 3, 6, 9, 17 and 18 in YegI show the presence of small hydrophobic residues (VILMFYWA) which is crucial for orientation of α-helices.

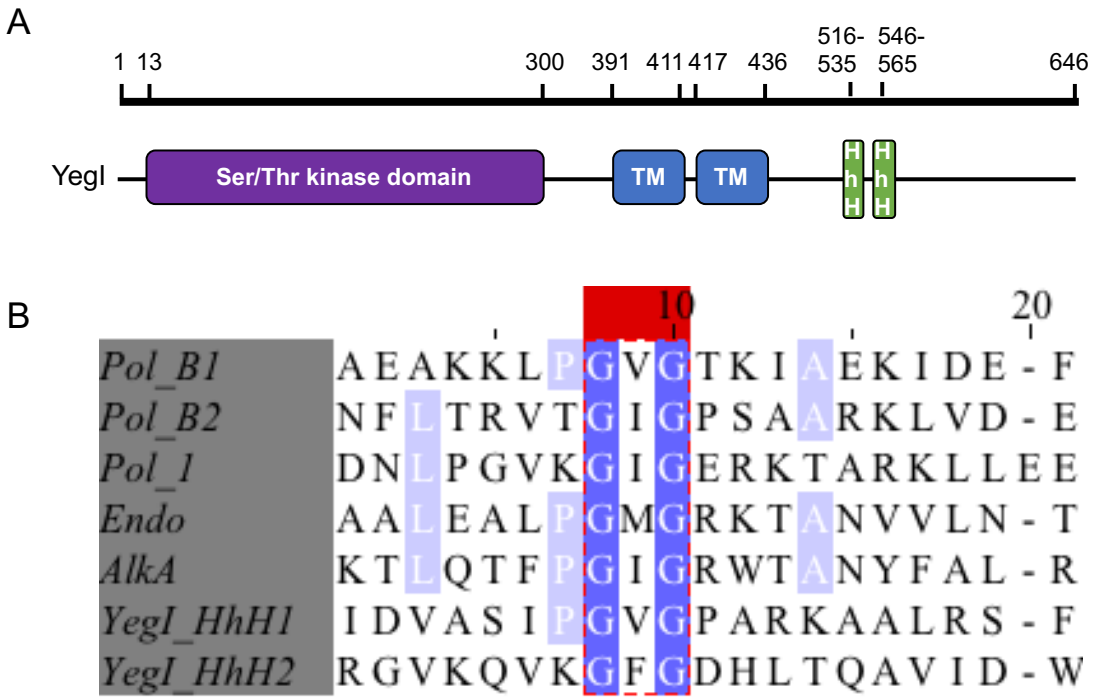

Figure 4.7 YegI contains two Helix-hairpin-helix motifs at the C-terminus.
(A) **Graphical representation of domain architecture of YegI with 2 HhH motifs.** Amino acids corresponding to different domains are indicated at the top. HhH: Helix hairpin helix motif
(B) **Amino acid sequence alignment of YegI HhH motifs and known HhH containing proteins**. Absolutely conserved residues are indicated in dark blue and highlighted by dotted red box. Partially conserved residues (four out of seven motifs) are shaded in light blue. Pol_B1 and Pol_B2: HhH1(aa 59-74)and HhH2 (aa 100-115) from Rat Polymerase β1, Pol_1: *T.aquaticus* polymerase I, Endo: HhH from *E. coli* Endonuclease III (aa 111-126), AlkA: HhH from *E. coli AlkA* (aa 209-224)

4.5 YegI expression

Gene reporter fusions have been widely used to study transcriptional and translational regulation (195). For example, expression of a gene of interest that is translationally fused to the *lac* operon (*lacZY*) can be determined by β-galactosidase assays. To determine when YegI is expressed in *E. coli* REL606, I generated a *yegI* in-frame deletion strain in *E. coli* REL606 where I removed aa 9-624 using Lambda red recombination as described (141). Using FLP/FRT recombinase system, I then constructed a translational fusion of *yegI* to *lacZ* from Δ*yegI*-FRT using pCE40 as described (142) such that *yegI* (aa1-8) fused to FRT site is in-frame with a translational lacZ fusion. I confirmed the conversion of the FRT site in Δ*yegI*-FRT generated from pKD13 (141) to a translational *lacZ* fusion by sequencing. The translational *yegI::lacZ* fusion was made in a Δ*lacZ* background to prevent background β-galactosidase activity due to endogenous *E. coli* LacZ. I observed a slight increase in β-galactosidase activity from *yegI::lacZ* only in stationary phase cultures of LB (24h) as compared to strain lacking the translational fusion (Fig. 4.8) suggesting that YegI might be expressed only in stationary phase. However, the expression was very low (0.01 β-galactosidase Miller units) when to compared endogenous LacZ levels which usually corresponds to 1-2 β -galactosidase miller units in log phase suggesting that when grown in LB, endogenous YegI protein levels are very low.

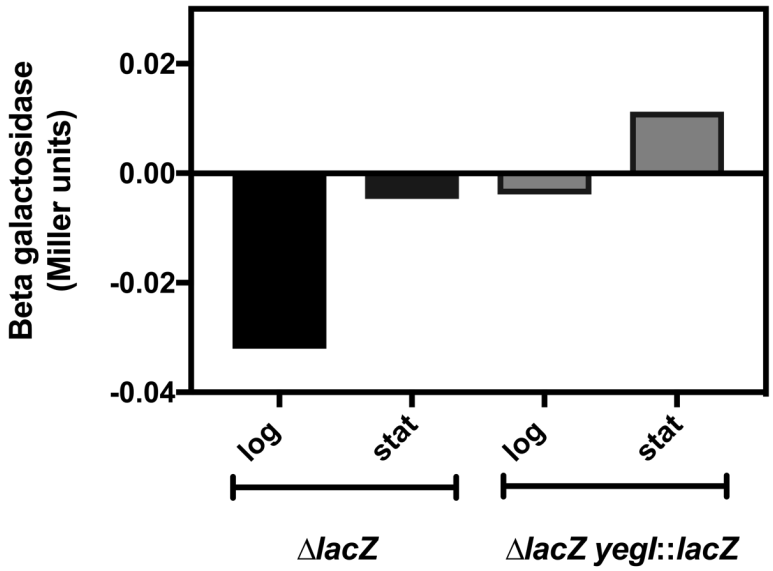

Figure 4.8: YegI is expressed in stationary phase albeit at low levels.
Expression of YegI-lacZ translational fusion was determined using β-galactosidase assay. Strains KR181 (Δ*lacZ*) and KR188 (Δ*lacZ yegI*::lacZ) were grown at 37 ºC in LB to log and stationary phase and β -galactosidase activity (miller units) was calculated.

4.6 Phenotypic analysis of YegI

4.6.1 *yegI* is not essential for growth in minimal media

To determine the physiological role of *yegI*, I used the *yegI* in-frame deletion strain in *E. coli* REL606 where I removed aa 9-624 using Lambda red recombination (141). The resulting strain was confirmed by colony PCR and sequencing. Deletion of eSTKs in *B. subtilis* (106), *S. pyogenes* (170), *E. faecalis* (196) showed significant defects in cell growth. To test if Δ*yegI* also displayed a growth defect, WT and Δ*yegI* strains were grown in chemically defined minimal media (MinA) with glucose or glycerol as a carbon source (144). However, I did not observe any significant difference in growth in minimal media between the WT strain and the Δ*yegI* strain (Fig. 4.9A,B) suggesting that deletion of *yegI* did not have any impact on growth in minimal media.

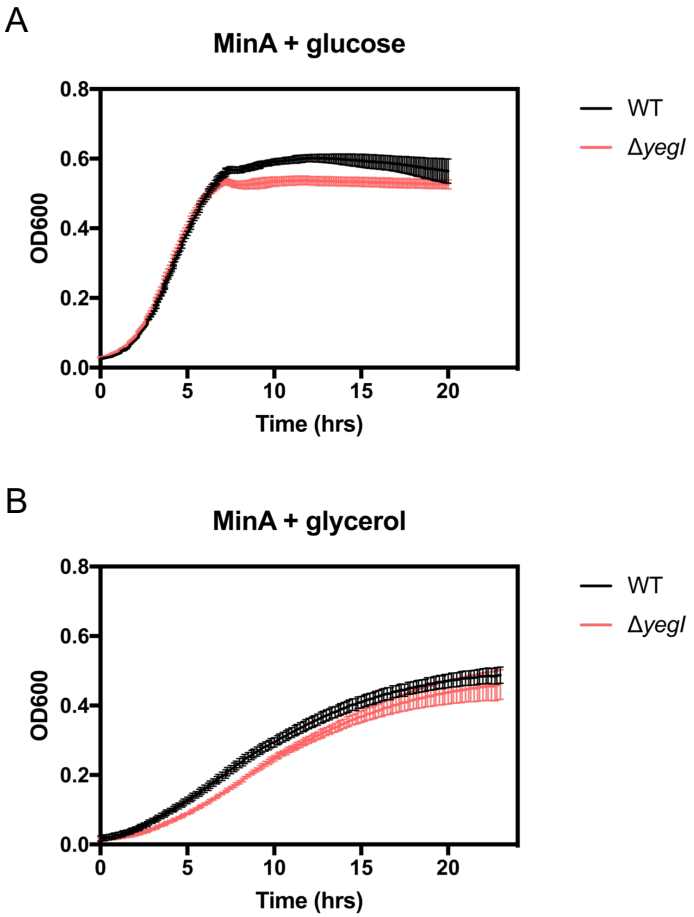

Figure 4.9 Deletion of *yegI* does not affect growth of *E. coli* in minimal media.
(A) Strains WT (JDE2735) and Δ*yegI* (KR160) were grown in MinA medium with 0.4% w/v glucose for 20h in a plate reader and OD_{600} was measured every 10 mins.
(B) Strains WT (JDE2735) and Δ*yegI* (KR160) were grown in MinA medium with 0.4% w/v glycerol for 20h in a plate reader and OD_{600} was measured every 10 mins.

4.6.2 Antibiotic susceptibility

In Gram-positive bacteria, deletion of genes encoding eSTKs results in increased sensitivity to cell wall targeting antibiotics. For example, *E. faecalis* eSTK IreK kinase activity is required for increased resistance to cell wall targeting antibiotics such as cephalosporins (52). Similarly deletion of the *S. aureus* eSTK STK resulted in a marked increase in sensitivity to cephalosporins and carbapenems (49). Based on the rationale that alteration of eSTKs could affect antibiotic susceptibility, I compared *E. coli* REL606 WT and Δ*yegI* strains to screen for differences in susceptibility to ten antibiotics of different classes (listed in Table 4.1).

I used the microtiter broth dilution method for determination of Minimum inhibitory concentrations (MICs) (197). Briefly, bacterial cultures (equivalent to 10^6 cfu/ml) were inoculated into Mueller Hinton Broth containing 2X of the actual concentration of antibiotics tested in a 96 well microplate. The lowest dilution that exhibits minimal inhibition of growth represents the MIC. I observed that the Δ*yegI* strain displayed decreased sensitivity to cell wall targeting antibiotics belonging to the cephalosporin class of β-lactam antibiotics (Table 4.1). Specifically, I observed an 8-16 fold difference in sensitivity to 3rd generation cephalosporins (cefotaxime, ceftriaxone) and a 4-fold decrease in sensitivity to cefoxitin (2nd generation) and cefipime (3rd generation). WT and Δ*yegI* showed little or no difference in susceptibility to inhibitors of protein synthesis (tetracycline, chloramphenicol, gentamycin and kanamycin) or of nucleic acid synthesis (ciprofloxacin). The decreased susceptibility of Δ*yegI* to cephalosporins is in stark contrast to increased antibiotic sensitivity phenotypes seen with *E. faecalis* Δ*ireK* and *S. aureus* Δ*stk* strains, suggesting that the mechanism of regulating antibiotic sensitivity in Δ*yegI* is different from those seen with Gram-positive eSTKs.

No.	Antibiotic	Target	WT (μg/ml)	Δ*yegI* (μg/ml)
1	Cefotaxime	Cell wall	0.0078-0.015	0.125
2	Ceftriaxone	Cell wall	0.0078	0.125
3	Cefoxitin	Cell wall	4	16
4	Cefipime	Cell wall	0.03125	0.125
5	Fosfomycin	Cell wall	4	16
6	Tetracycline	Protein synthesis	1	4
7	Chloramphenicol	Protein synthesis	2	4
8	Ciprofloxacin	Nucleic acid	0.03125	0.03125
9	Gentamycin	Protein synthesis	0.5	0.5
10	Kanamycin	Protein synthesis	4	4

Table 4.1 Antibiotic susceptibility
Median Minimum inhibitory concentrations (MIC) for *E. coli* WT and Δ*yegI* strains

Since the difference in MICs between WT and Δ*yegI* strains were the highest for cefotaxime, I investigated the mechanistic basis of the reduced cefotaxime sensitivity observed in Δ*yegI*. To validate the differential susceptibility to cefotaxime observed in WT and Δ*yegI*, I used Etest strips containing gradients of cefotaxime as an alternate approach to calculate MICs. Consistent with MIC values obtained by Microtiter broth dilution (Table 4.1), I observed striking differences in the MICs of *E. coli* REL606 WT and Δ*yegI* (Fig. 4.10). In the *E. coli* REL606 B strain, *yegI* is contiguous with *pphC* while in the *E. coli* K-12 strain MG1655, an unknown gene, *yegJ*, is found between *yegI* and *pphC* (Fig. 4.1A). I hypothesized that the different genome organization could result in differential sensitivity to antibiotics. To test this hypothesis, I obtained an in-frame deletion strain of *yegI* (Δaa 2-640) in K-12 BW255113 from the Keio collection (145) and transduced this mutation into K-12 MG1655 by P1-mediated transduction. I used cefotaxime Etest strips to calculate MICs of WT and Δ*yegI* to test for differences between B and K strain backgrounds. Since, I observed no difference in sensitivity to cefotaxime between WT and Δ*yegI* in MG1655 (Fig.4.10) there could be differences in the regulation of the *yeg* operon between the closely related *E. coli* K and B strains.

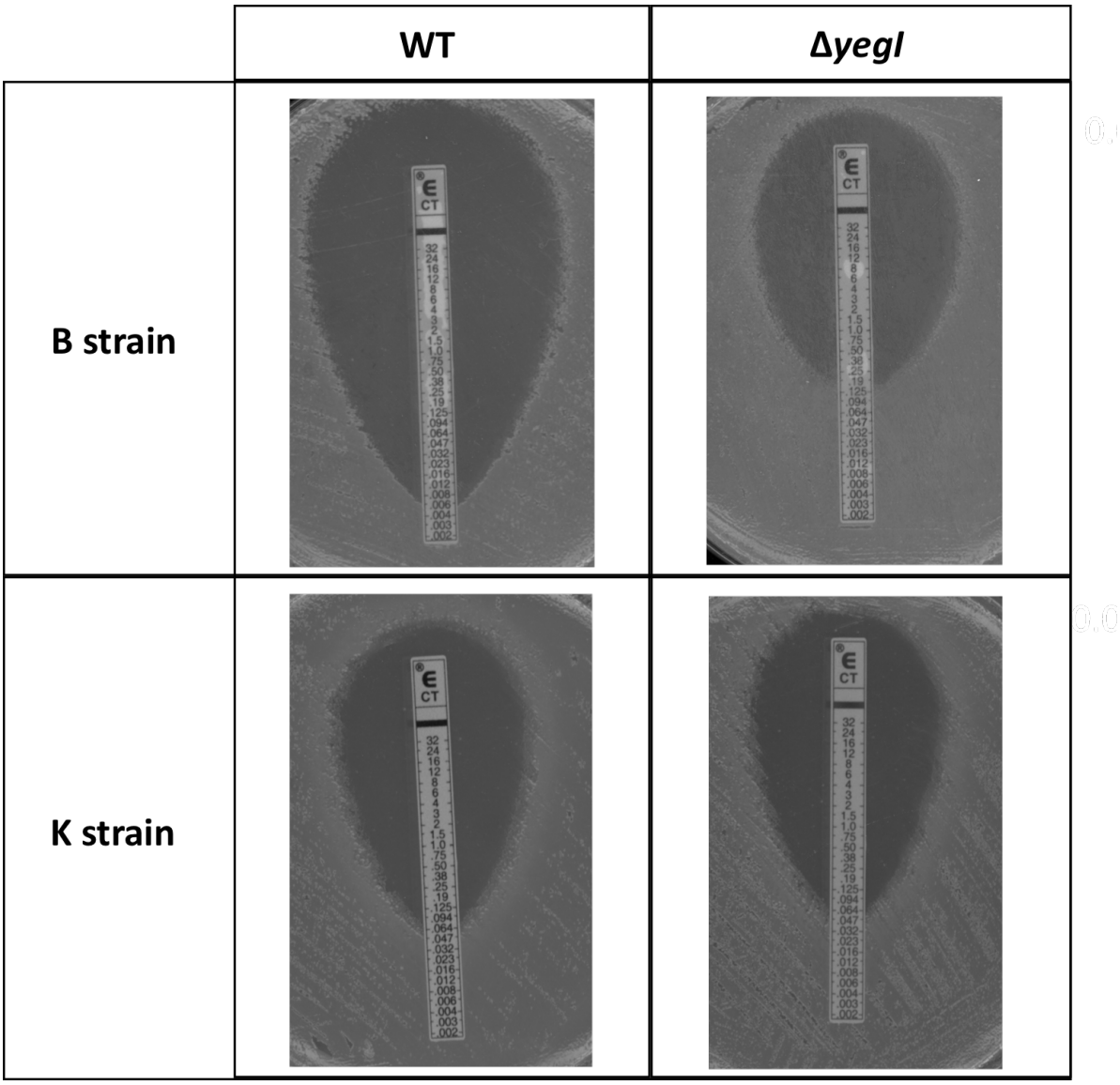

µg/ml	WT	Δ*yegI*
B Strain	0.008	0.125
K Strain	0.064	0.064

Figure 4.10 Deletion of *yegI* decreases sensitivity to cefotaxime in an *E. coli* B strain but not in a K strain.

Determination of MIC of cefotaxime using Etest strips. *For E. coli B strain* WT (JDE2735), Δ*yegI* (KR160) were used while for *E. coli* K strain WT (KR01), Δ*yegI* (KR60) strains were used to calculate MICs using Cefotaxime Etest strips (0.0002-32 µg/ml). E strips were placed on Mueller Hinton II agar plates that were swabbed with bacterial suspension cultures from indicated strains. Plates were incubated at 37 ºC for 20h and MIC were determined by eye. MIC values for B and K strains are indicated in µg/ml.

To confirm that the decreased sensitivity to cefotaxime was indeed due to *yegI*, I transformed both the WT and Δ*yegI* strains in REL606 background with a control vector (pBAD24) or plasmid expressing YegI under control of an arabinose inducible promoter and examined sensitivity to cefotaxime. As expected, I saw a complete restoration of sensitivity to cefotaxime only when expression of YegI-WT was induced in Δ*yegI* strain suggesting that the YegI may play a role in modulating cefotaxime sensitivity (Fig.4.11). To test if the kinase activity of YegI was required for this phenotype, I expressed a ATP binding mutant YegI-K39D or the catalytic mutant YegI-D141N in Δ*yegI* strain. Surprisingly, mutation of K39D or D141N, both which result in an inactive kinase, still restored sensitivity to cefotaxime suggesting that kinase activity of YegI is not required for sensitivity to cefotaxime. As shown in (Fig. 4.2.A) YegI is a 646aa protein with an N-terminal kinase domain (aa 13-300), two TM domains (aa 391-436) and a 210aa C-terminal domain with two HhH motifs. Thus, the TM domains or the C-terminal domain may be involved in restoring cefotaxime sensitivity.

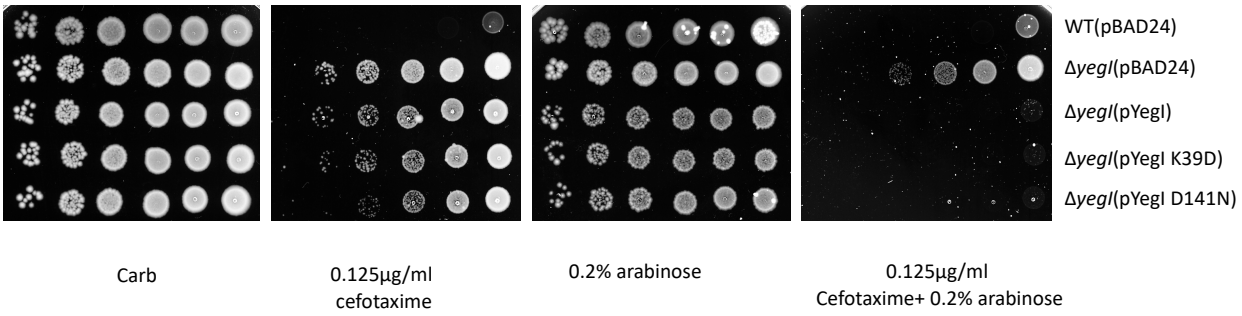

Figure 4.11 Kinase activity of YegI is not required for decreased sensitivity to cefotaxime.
To test if YegI kinase activity is required for decreased sensitivity to cefotaxime, strains KR199: WT (pBAD24), KR200: Δ*yegI* (pBAD24), KR206: Δ*yegI* (pYegI), KR247: Δ*yegI* (pYegI K39D) and KR250: Δ*yegI* (pYegI D141N) were grown at 37 ºC in LB with carbenicillin overnight. Cultures of strains expressing plasmids were serially diluted 10-fold and spotted from right to left (10^{0}-10^{-5}) on LB plates containing indicated concentrations of either cefotaxime or arabinose or both. Carbenicillin (100 µg/ml) was used for plasmid selection. Plasmids used are indicated in parentheses. pBAD24: backbone vector used for complementation. pYegI: pBAD24 expressing WT-YegI, pYegI K39D: pBAD24 expressing K39D-YegI and pYegI D141N: pBAD24 expressing D141N-YegI.

To identify the domain required for restoring cefotaxime sensitivity of Δ*yegI*, I generated pBAD24 derivatives expressing either full-length YegI or truncated versions of YegI (Fig. 4.15A) under the control of an arabinose inducible promoter. YegI protein sequence boundaries for truncation were determined based on secondary structure and domain predictions from InterPro (198). I transformed Δ*yegI* strains with different truncations corresponding to various regions of YegI and examined sensitivity to cefotaxime in the presence of arabinose. Similar to Fig. 4.11, I observed complete restoration of cefotaxime sensitivity when full length protein (pYegI) was induced (Fig 4.12B). Consistent with a kinase independent role of YegI, I did not see any restoration of sensitivity to cefotaxime when the N-terminal domain of YegI alone was expressed (pYegI 1-390, pYegI 1-300) suggesting that the C-terminal domain is involved. Expression of just the C-terminal domain (pYegI 301-646) restored sensitivity to cefotaxime further validating a kinase independent role of YegI. Furthermore, expression of the pYegI 436-646 truncation that lacks the TM domains also restored cefotaxime sensitivity suggesting that TM domains are not required for restoration of cefotaxime sensitivity. However, expression of pYegI 536-646 or pYegI 566-646 lacking one or both HhH motifs respectively failed to restore cefotaxime sensitivity. These results suggest that the HhH motifs in YegI (436-646) are important for restoration of cefotaxime sensitivity to Δ*yegI* strains, although the molecular mechanism of how the HhH motifs affect sensitivity to cefotaxime remains unclear.

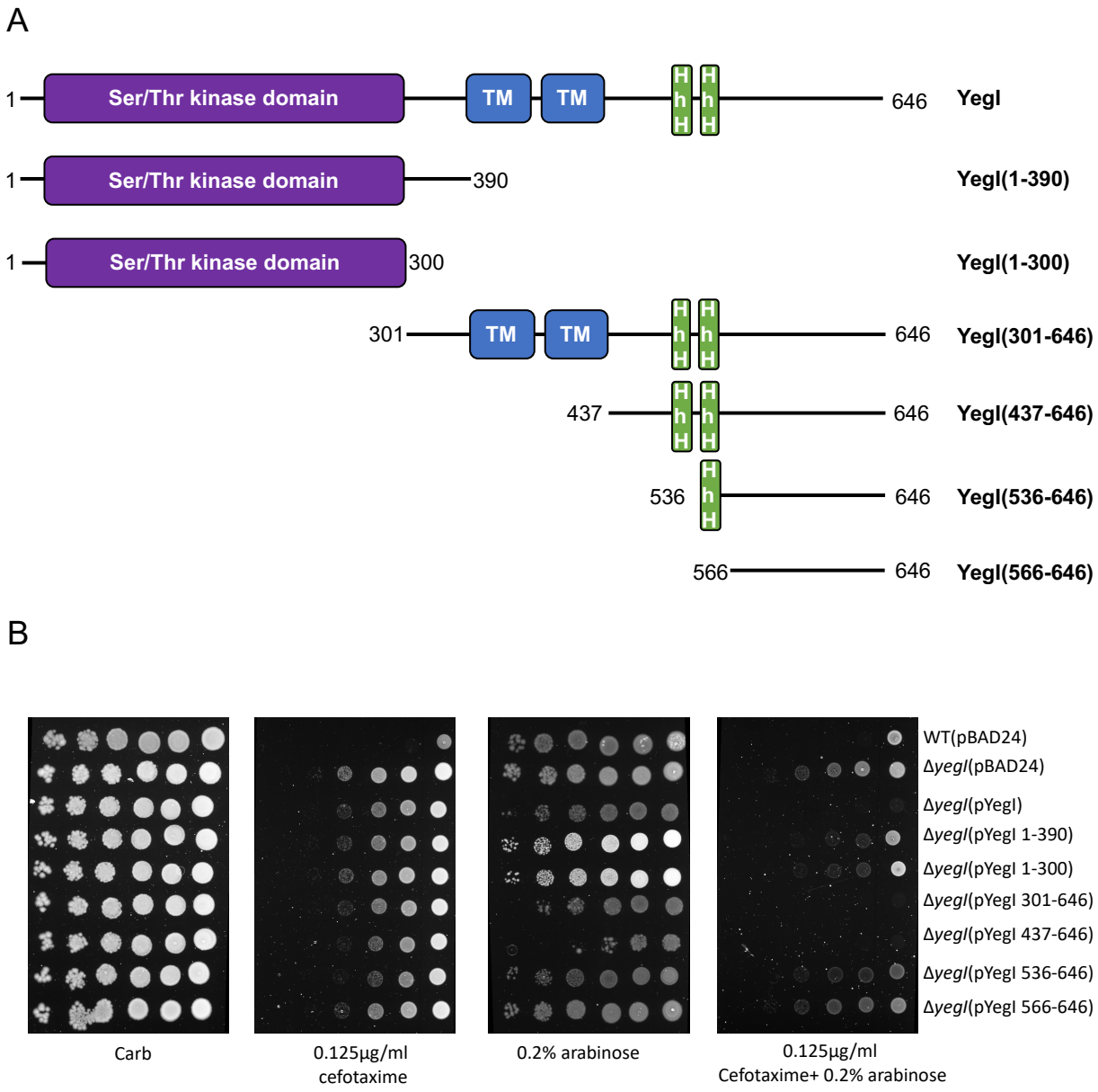

Figure 4.12 HhH motifs in the C-terminal domain are important for decreased sensitivity to cefotaxime

(A) **Domain organization:** Graphical representation of YegI and various truncation mutants used to determine which domain is required for complementation of cefotaxime resistance. Amino acid boundaries are domains included in WT and truncation mutants are indicated. depicting phosphorylation sites following mass spectrometry analysis of autophosphorylation.

(B) Strains KR199: WT (pBAD24), KR200: Δ*yegI* (pBAD24), KR206: Δ*yegI* (pYegI), KR230: Δ*yegI* (pYegI 1-390), KR231: Δ*yegI* (pYegI 1-300), KR292: Δ*yegI* (pYegI 301-646), KR295: Δ*yegI* (pYegI 437-646), KR309: Δ*yegI* (pYegI 536-646) and KR311: Δ*yegI* (pYegI 566-646) were grown at 37 ºC in LB with carbenicillin overnight. Cultures of strains expressing plasmids were serially diluted 10-fold and spotted from right to left (10^{0}-10^{-5}) on LB plates containing indicated concentrations of either cefotaxime or arabinose or both. Carbenicillin (100 µg/ml) was used for plasmid selection. Plasmids used are indicated in parentheses.

4.6.3 Sensitivity to DNA damaging agents

The C-terminal domain of YegI contains two predicted HhH motifs (Fig.4.7A,B). Interestingly, HhH motifs are commonly present in DNA repair proteins (199, 200). For example, *E. coli* DNA-3-methyl adenine glycosylase (AlkA) is a base excision repair glycosylase that contains HhH motifs that likely to mediate DNA affinity during base excision repair of alkylated bases (194, 201, 202). Therefore, YegI could play a role in DNA damage response or repair. To test this hypothesis, I used a deletion strain of *yegI* to test sensitivity to DNA damage caused by UV radiation. The *E. coli* DH5α strain which lacks the HhH containing DNA repair protein recombinase A (*recA*-) displays increased sensitivity to UV and was therefore used as a positive control. Unlike DH5α, both the WT and Δ*yegI* showed no sensitivity to UV radiation even at high UV exposure (60J/m^2) (Fig.4.13) demonstrating that deletion of *yegI* does not affect sensitivity to UV radiation.

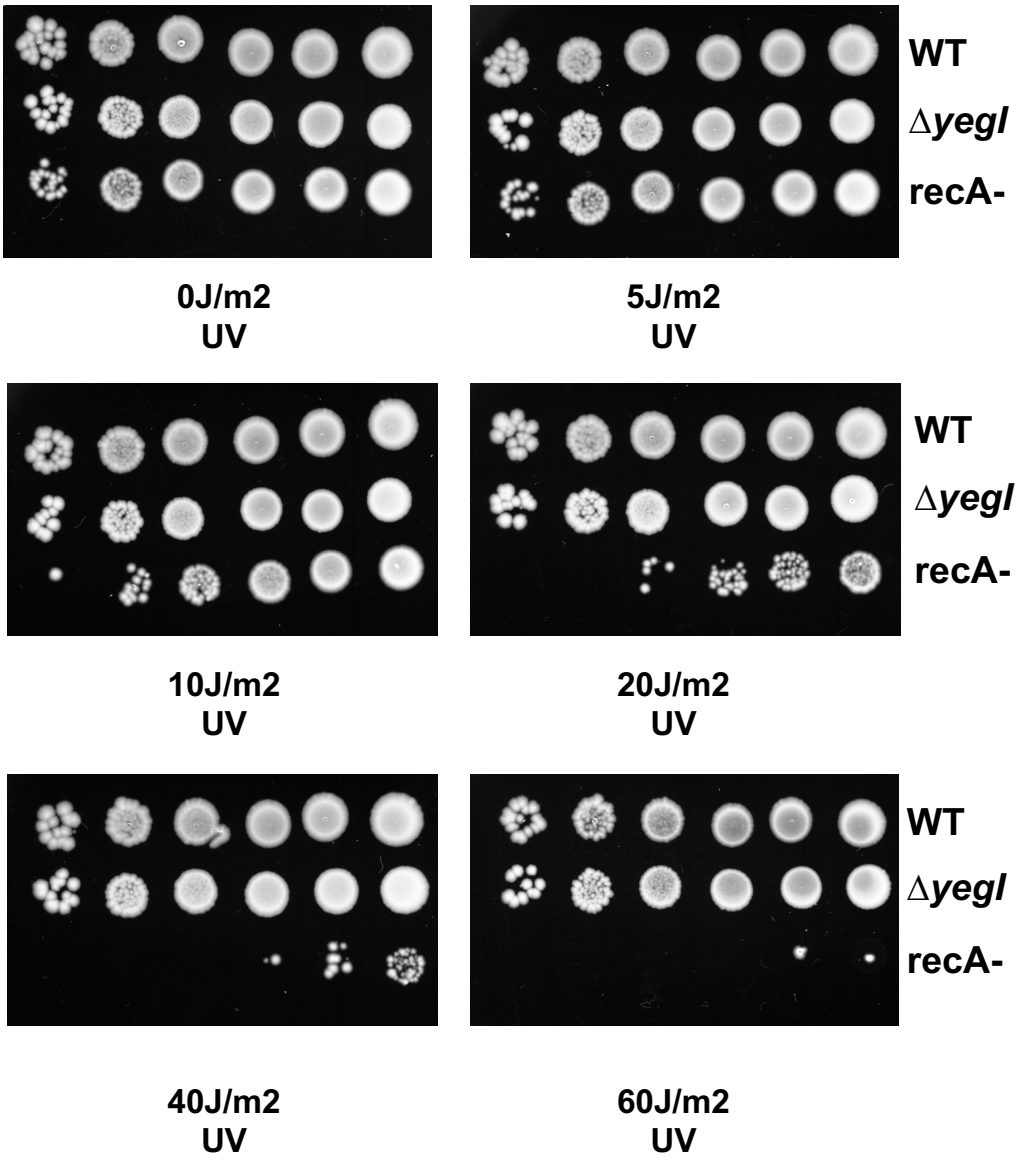

Figure 4.13 Deletion of *yegI* doesn't affect sensitivity to UV radiation
WT (JDE2735), Δ*yegI* (KR160) and *recA*- (JDE12) strains were grown at 37 ºC in LB overnight. Cultures were serially diluted 10-fold and spotted from right to left (10^{0}-10^{-5}) on LB plates. Plates were exposed to indicated doses of UV using UV crosslinker.

I then examined if deletion of YegI affected the response to DNA damage induced by a 4-quinolone antibiotic nalidixic acid. Nalidixic acid inhibits DNA synthesis by directly forming a cleavage complex with DNA gyrase causing DNA damage and activation of the bacterial SOS response (203). Mutations in HhH motif-containing nucleotide excision proteins such as UvrB and UvrC result in decreased sensitivity to nalidixic acid (204, 205). Therefore, I hypothesized that deletion of *yegI* might affect sensitivity to nalidixic acid. To test this hypothesis, I used the same approach as that for assessing cefotaxime sensitivity. First, I determined any differences in sensitivity to nalidixic acid between WT and Δ*yegI* from both REL606 and MG1655 backgrounds. Deletion of *yegI* in REL606 decreased sensitivity by 2-log to nalidixic acid at 1 μg/ml as compared to WT (Fig.4.14A). However I saw no difference between WT and Δ*yegI* in MG1655 suggesting differential response of Δ*yegI* in these closely related *E. coli* strains.

To ensure that decreased sensitivity to nalidixic acid was due to *yegI*, I transformed WT and Δ*yegI* strains with either an empty vector (pBAD24) or a plasmid expressing YegI (pYegI). I observed that expression of WT-YegI restored partial sensitivity to nalidixic acid (Fig.4.14B). To test if kinase activity is required for restoration of nalidixic acid sensitivity, I expressed YegI mutant proteins carrying inactivating mutations (pYegI-K39D or pYegI-D141N) in a Δ*yegI* strain. Similar to the cefotaxime results, expression of a catalytically inactive kinase still restored sensitivity to nalidixic acid similar to YegI-WT (Fig.4.14B). Thus, the kinase activity of YegI is not important for restoring nalidixic acid sensitivity.

To identify the domain required for increasing nalidixic acid sensitivity of Δ*yegI*, I expressed full length YegI or truncated versions of YegI in a Δ*yegI* strain as described previously (Fig.4.12). Similar to cefotaxime results, I observed restoration of nalidixic acid sensitivity in Δ*yegI* strains only when full length YegI, or the YegI 301-646, YegI 436-646 truncations were expressed

(Fig.4.14C). Deletion of one or both HhH motifs failed to restore nalidixic acid sensitivity. Thus, the C-terminal domain (aa 436-646) containing the HhH motifs is likely required for restoration of sensitivity to nalidixic acid.

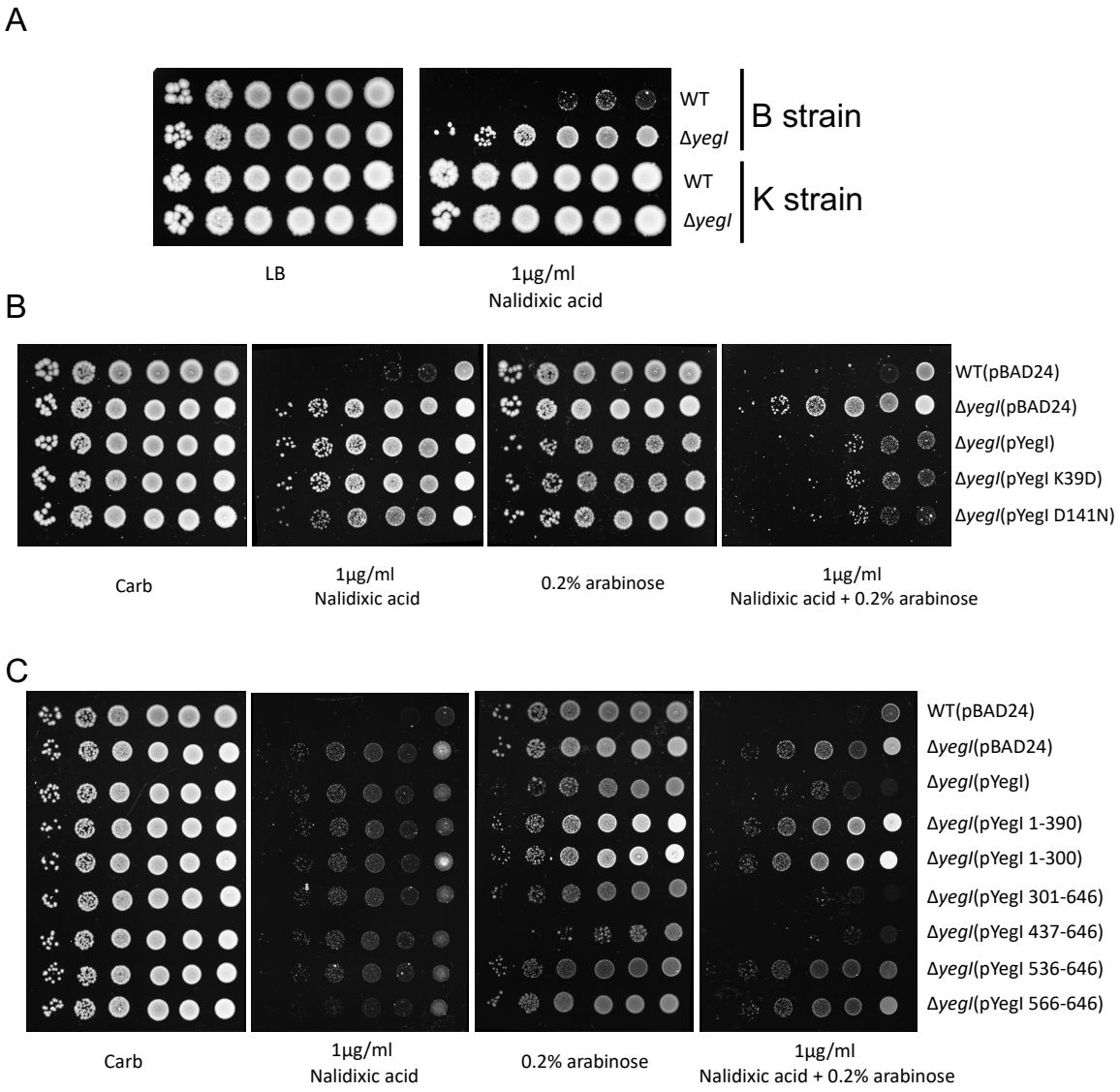

Figure 4.14 Deletion of *yegI* decreases sensitivity to nalidixic acid

(A) **Susceptibility of B and K strains to nalidixic acid.** *E. coli* REL606 (B strain) and MG1655 (K strain) were used to determine differences in nalidixic acid sensitivity \. B strains WT (JDE2735), Δ*yegI* (KR160) and K strains WT (KR01), Δ*yegI* (KR60) were used to calculate sensitivity to nalidixic acid. Strains were grown at 37 ºC in LB overnight. Cultures were serially diluted 10-fold and spotted from right to left (10^0-10^{-5}) on LB plates with or without nalidixic acid (1µg/ml).

(B) **Kinase activity is not required for sensitivity to nalidixic acid.** Strains KR199: WT (pBAD24), KR200: Δ*yegI* (pBAD24), KR206: Δ*yegI* (pYegI), KR247: Δ*yegI* (pYegI K39D) and KR250: Δ*yegI* (pYegI D141N) were grown at 37 ºC in LB with carbenicillin overnight. Cultures of strains expressing plasmids were serially diluted 10-fold and spotted from right to left (10^0-10^{-5}) on LB plates containing indicated concentrations of either nalidixic acid or arabinose or both. Carbenicillin (100 µg/ml) was used for plasmid selection. Plasmids used are indicated in parentheses. pBAD24: backbone vector used for complementation. pYegI: pBAD24 expressing WT-YegI, pYegI K39D: pBAD24 expressing K39D-YegI and pYegI D141N: pBAD24 expressing D141N-YegI.

(C) Indicated strains were grown at 37 ºC in LB with carbenicillin overnight. Cultures of strains expressing plasmids were serially diluted 10-fold and spotted from right to left (10^0-10^{-5}) on LB plates containing indicated concentrations of either nalidixic acid or arabinose or both. Carbenicillin (100 µg/ml) was used for plasmid selection. Plasmids used are indicated in parentheses.

So far, my results indicate that deletion of *yegI* in *E. coli* REL606 decreases sensitivity to cefotaxime and nalidixic acid and expression of YegI in a Δ*yegI* strain restored sensitivity. However, the mechanism by which *yegI* regulates sensitivity to these antibiotics is unclear. One possibility for decreased sensitivity to nalidixic acid or cefotaxime could be due to changes in membrane permeability. In Gram-negative bacteria, membrane permeability can be affected by altering expression of genes encoding outer membrane porin proteins that form channels, efflux pumps or multidrug transporters. Proteomic studies in *E. coli* revealed that expression of multidrug transporters and efflux pumps were enhanced in nalidixic acid resistant strains (206). Specifically, expression of the outer membrane protein TolC, which forms protein complexes with multidrug transporters, is upregulated in nalidixic acid resistant *E. coli* strains.

Therefore, I asked if decreased sensitivity of Δ*yegI* strain to nalidixic acid or cefotaxime is affected by the presence or absence of *tolC*. I constructed an in-frame deletion of *tolC* using **λ** red recombination (141) and confirmed the strain construction by sequencing. I introduced this mutation into a Δ*yegI* strain using P1-mediated transduction to get a double mutant strain Δ*yegI* Δ*tolC* and examined sensitivity of this strain to nalidixic acid and cefotaxime. In case of nalidixic acid, I observed that deletion of *tolC* in a Δ*yegI* background completely restored sensitivity to both cefotaxime and nalidixic acid. However, deletion of *tolC* alone also showed increased sensitivity to nalidixic acid suggesting that deletion of *tolC* is a dominant effect and therefore cannot explain the decreased sensitivity phenotype of Δ*yegI* to nalidixic acid (Fig.4.15). A similar effect of the *tolC* deletion was observed in the case of cefotaxime. Future experiments aimed at determining the expression of *tolC* or determining the transcriptome profiles in WT and Δ*yegI* strains may provide a better explanation for decreased susceptibility to nalidixic acid/cefotaxime.

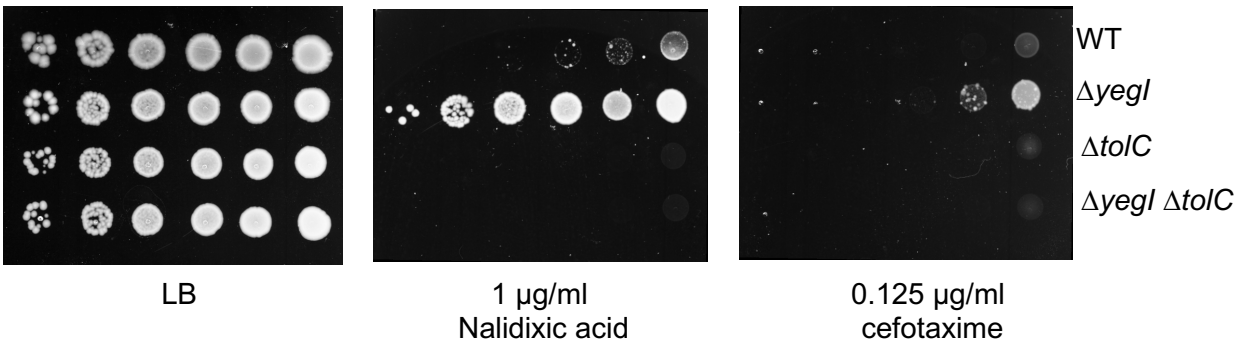

Figure 4.15 Deletion of *tolC* abolishes decreased sensitivity phenotype of Δ*yegI*
WT (JDE2735), Δ*yegI* (KR160), Δ*tolC* (KR337) and Δ*yegI*Δ*tolC* (KR338) strains were grown at 37 ºC in LB overnight. Cultures were serially diluted 10-fold and spotted from right to left (10^{0}-10^{-5}) on LB plates in the absence or presence of indicated antibiotics.

4.7 Potential physiological substrates for YegI

4.7.1 Comparative phosphoproteomics shows enolase as a substrate of YegI

Phosphoproteomic studies have been widely used to identify phosphorylated proteins in bacteria (113). Recent studies with bacterial eSTKs have used comparative phosphoproteomics to identify targets that are specific to the kinase of interest by comparing phosphoproteomes of a kinase null strain is compared to a control strain with intact kinase (136, 207). To identify the substrates of YegI kinase at a more global scale, we performed comparative phosphoproteomics in collaboration with the laboratory of Dr. Ljiljana Pasa-Tolic at Pacific Northwest National Laboratories, WA who has reported successful enrichment of phosphopeptides in *E. coli* using immobilized metal affinity chromatography (IMAC) (146).

I used an in frame deletion strain of *yegI* (Δaa 9-624) in *E. coli* REL606. Both WT and Δ*yegI* strains were grown in defined minimal medium MinA with 0.4% glucose (144) and samples were collected at either log or stationary phase (Fig. 4.16A). Frozen pellets (in triplicates) were submitted to Dr. Pasa-Tolic for subsequent lysis and enrichment of phosphopeptides using IMAC (Fig. 4.16B). Although 1700-2000 proteins were identified in each of the samples, only 38 phosphopeptides corresponding to 34 phosphoproteins were detected, a yield of phosphoproteins much lower than what has been previously reported (~100 phosphoproteins) in *E. coli* phosphoproteomic studies (114, 123, 146). Of the 34 phosphoproteins detected, differential phosphorylation was observed only in the case of the glycolytic enzyme enolase, that catalyzes the conversion of 2-phosphoglycerate to phosphoenolpyruvate. We observed a growth phase dependent increase in enolase phosphorylation at Ser-400 in stationary phase (Fig.4.16C). Interestingly, this increase in phosphorylation was not observed in a Δ*yegI* strain suggesting that enolase could be a target for *yegI in vivo*. However, since enolase phosphorylation was only

detected in one of the three replicates that were used for phosphoproteomic analysis, this result may not be representative.

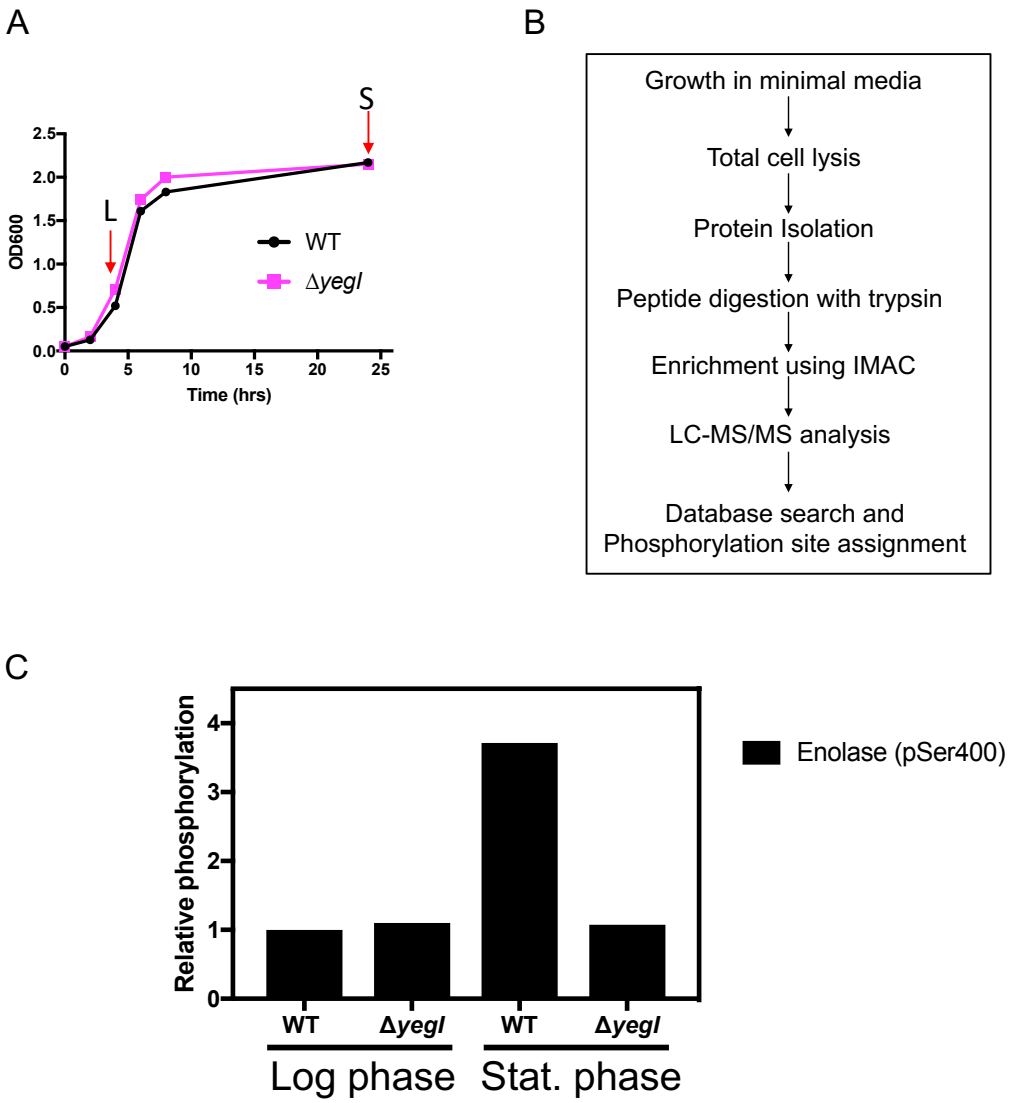

Figure 4.16 Comparative phosphoproteomics shows enolase as a substrate for YegI *in vivo.*
(A) **Growth curves of control strain WT (JDE2735) and Δ*yegI* (KR160)**. For comparative phosphoproteomics, cultures were grown in triplicates in minimal media (MinA) with 0.4% glucose for 24 h at 37 ºC with aeration in baffled flasks. Growth was monitored by measuring optical density (OD) at 600nm. Samples were collected at a log OD:0.8 (L) and stationary phase OD:2.3-2.5 (S) as denoted by red arrows.
(B) **Experimental scheme for comparative phosphoproteomics** Immobilized metal affinity chromatography (IMAC) was used for phosphopeptide enrichment.
(C) **Comparative phosphoproteomics showed differential phosphorylation of enolase.** Change in phosphorylation levels of enolase is calculated relative to WT under log phase. Data represented is from one of the three replicates.

Although enolase phosphorylation was observed in only one of the three replicates, we were encouraged by the results as enolase has been reported to be phosphorylated in several global *E. coli* phosphoproteomic studies (114, 119, 123). Although phosphorylation on Ser-400 has not been reported, enolase was shown to be phosphorylated on Thr-322, Ser-369, Ser-372, Thr-375, Thr-379, depending on the specific study. To validate our phosphoproteomics finding and show directly that enolase is a substrate of YegI, I expressed and purified an N-terminal His tagged enolase (Eno) using Ni^{2+}- affinity chromatography. To confirm the phosphorylation site at Ser-400, I generated a serine to alanine point mutation at position 400 (S400A) and purified it in the same manner as WT. Using radioactive *in vitro* kinase assay, I observed robust phosphorylation of Eno-WT in the presence of YegI-NTD (Fig. 4.17, lane 3) as compared to a reaction without YegI-NTD (Fig. 4.17, lane 2). However, I observed phosphorylation of Eno-S400A to a similar extent (Fig. 4.17, lane 4) suggesting that Ser-400 is not the only phosphorylation site.

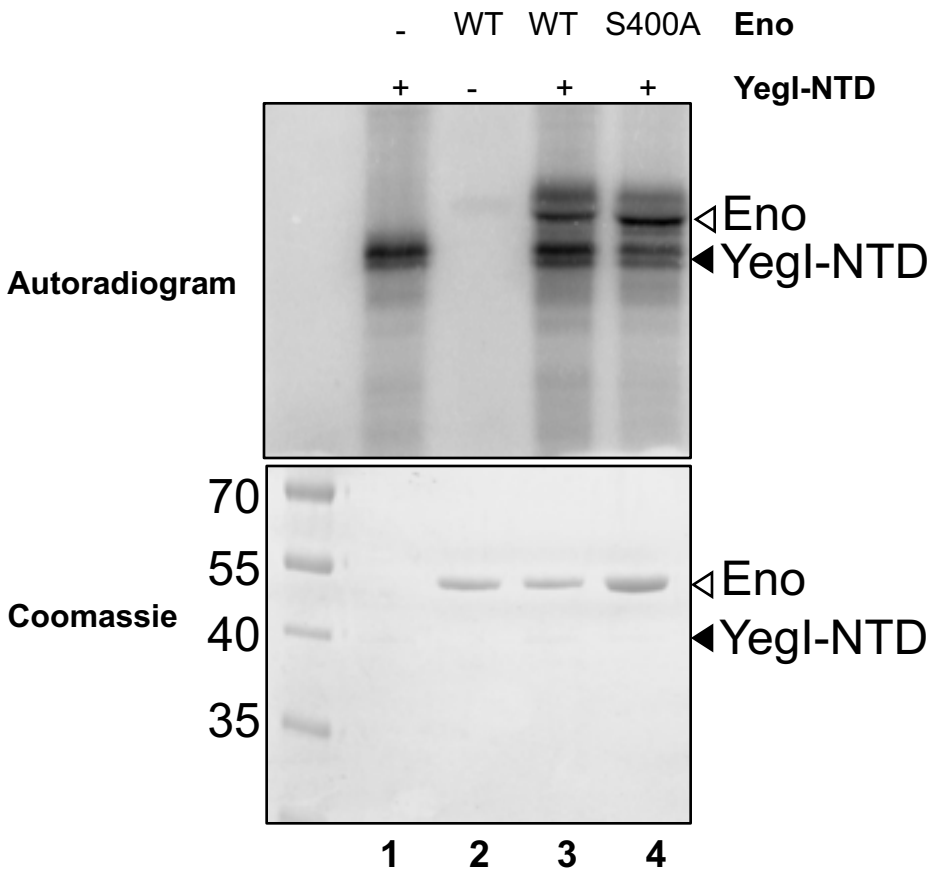

Figure 4.17 Enolase is phosphorylated by YegI *in vitro*.
Reactions were carried out at 37 ºC with 4 µM of Eno (WT or S400A) in the absence or presence of 2 µM of YegI-NTD as indicated on the top of the gel. Reactions were carried out in kinase buffer and stopped at t=60 mins. Samples were resolved on 12% SDS-PAGE followed by autoradiography. Molecular weights (kDa) are indicated on the right of the gel.

4.7.2 YegI regulates protein translation via phosphorylation of elongation factor-Tu

The GTPase elongation factor-Tu (EF-Tu) is one of the most abundant proteins in the cell and plays an essential role in the elongation step of protein translation. In its GTP-bound form, EF-Tu binds aminoacyl tRNA and delivers it to the ribosome. Upon correct codon-anticodon matching, the ribosome activates the GTPase activity of EF-Tu thereby allowing release of EF-Tu-GDP from the ribosome, resulting in peptide elongation. The elongation step in eukaryotic cells is a tightly controlled process and is subject to both transcriptional and translational regulation (208). Several bacterial phosphoproteomics studies, including in *E. coli,* have reported phosphorylation of EF-Tu *in vivo* (114, 115, 207, 209, 210), suggesting that phosphorylation of EF-Tu in bacteria is physiologically relevant.

EF-Tu is phosphorylated *in vitro* by the *M. tuberculosis* eSTK PknB at multiple threonine residues distributed across the full length of EF-Tu. Phosphorylation of Thr-118 resulted in decreased binding affinity to GTP which could impact protein synthesis (132) although whether this modification occurs *in vivo* is not known. More recently, a study from Dworkin lab showed that the *B. subtilis* eSTK YabT phosphorylates EF-Tu on multiple Ser/Thr residues including Ser-11, Thr-63, Ser-300, Ser-385 with Thr-63 being the primary site of phosphorylation. Interestingly phosphorylation of *B. subtilis* Thr-63 (corresponds to *E. coli* Thr-62) inhibits GTP hydrolysis and translation elongation (133). Since YegI is also an eSTK, I hypothesized that EF-Tu could be a YegI substrate.

I used a radioactive *in vitro* kinase assay to test if YegI phosphorylates EF-Tu. YegI-NTD was used in the kinase assay instead of YegI since transphosphorylation of substrates (PphC, Chapter 3) was more robust than YegI. YegI-NTD and EF-Tu migrate at the same molecular weight (~45kDa), so to distinguish between the two proteins, I expressed and purified a GST-tagged EF-

Tu which migrates at ~70kDa ensuring separation on SDS-PAGE. I used GST alone without EF-Tu as a control. Different concentrations of YegI-NTD were used to identify ideal kinase::substrate ratio. Robust phosphorylation of GST-EF-Tu was observed in the presence of equimolar concentrations of YegI-NTD (Fig.4.18A, lane 7) as compared to the no kinase control (Fig.4.18A, lane 6). Phosphorylation levels dropped with lower kinase concentrations (Fig.4.18A, lane 8-10). However, I also observed robust phosphorylation of GST tag in the presence of YegI-NTD (Fig.4.18A, lane 2-5) indicating that YegI-NTD might be phosphorylating the GST tag alone or both the GST tag and EF-Tu.

To determine the site(s) of phosphorylation of GST-EF-Tu, *in vitro* kinase assay sample of GST-EF-Tu that has been incubated with YegI-NTD was submitted to the Columbia University Medical Center Herbert Irving Cancer Center Proteomics Center. Dr. Emily Chen performed mass spectrometry analysis and identified three phosphopeptides corresponding to threonine residue at position 94 and serine residues at position 198 and 220 (Fig. 4.18B) of which Ser-220 has been observed in global phosphoproteomic studies in *E. coli*. (114, 123) Consistent with the *in vitro* kinase assay (Fig.4.18A), Dr. Emily Chen also identified two phosphoserine residues in the GST tag and in the PreScission cleavage site located between the GST tag and EF-Tu.

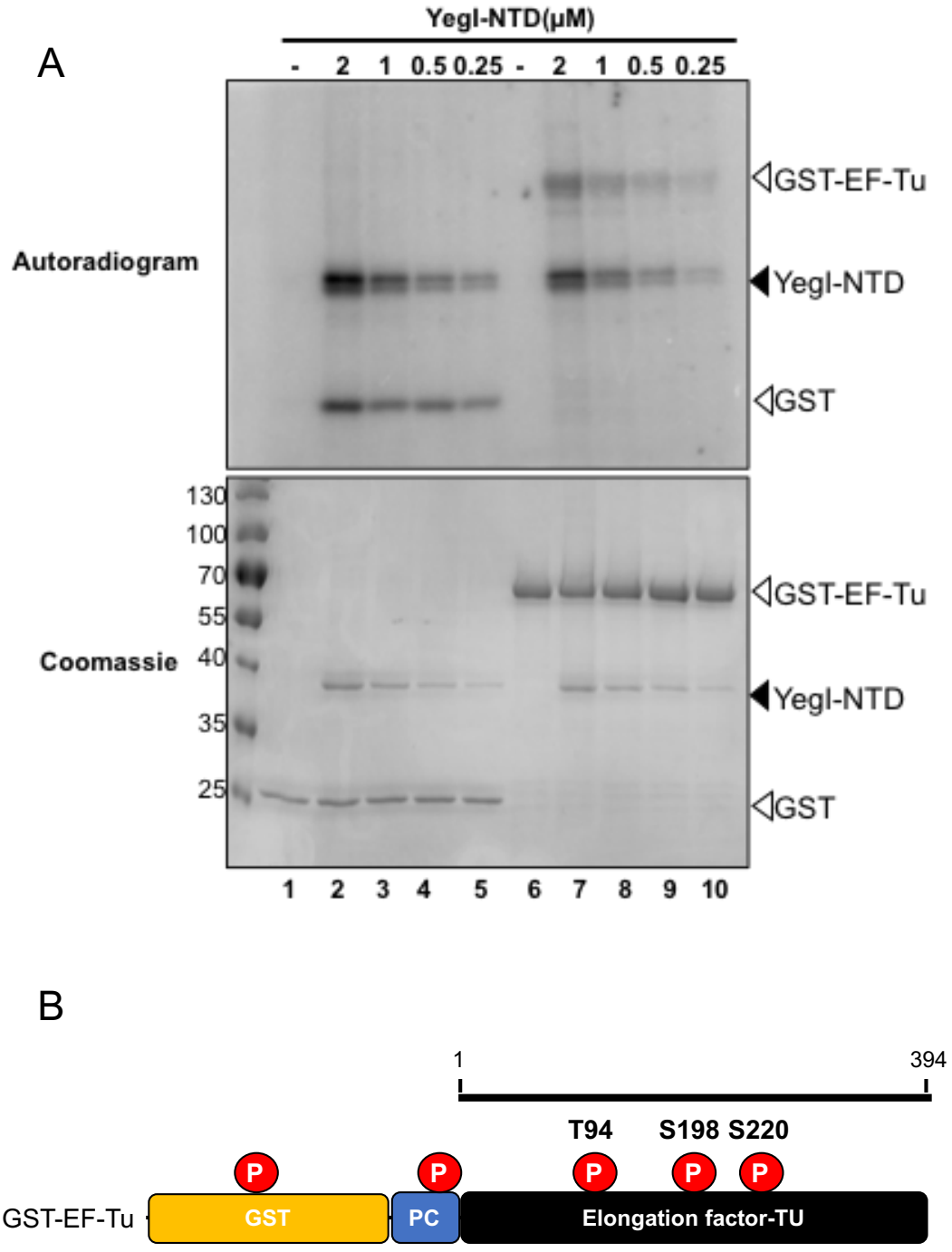

Figure 4.18 YegI phosphorylates elongation factor Tu (EF-Tu) *in vitro.*
(A) Reactions were carried out at 37 ºC with 2 μM of GST(lane 1-5) or GST-EF-Tu(lane 6-10) in the absence (lane 1 and lane 6) or presence of different concentrations of YegI-NTD as indicated on the top of the gel. Reactions were carried out in kinase buffer and stopped at t=60 mins. Samples were resolved on 12 % SDS-PAGE followed by autoradiography. Molecular weights (kda) are indicated on the right of the gel.
(B) Graphical representation of phosphorylation sites on GST-EF-Tu following mass spectrometry analysis of *in vitro* kinase assay with YegI-NTD. Phosphorylated residues are indicated by red circles. PC: PreScission cleavage site is located between GST and EF-Tu.

To test the impact of YegI-dependent phosphorylation of EF-Tu on protein synthesis, I expressed and purified His-tagged EF-Tu in the absence or presence of tagless YegI-NTD in a pETDUET vector to yield an *in vivo* phosphorylated form of EF-Tu. Purified protein was resolved on SDS-PAGE to assess purity (Fig. 4.19A) and was used in the *in vitro* PURExpress transcription/translation assay which contains all the necessary components except EF-Tu as described (133). Briefly, the *in vitro* transcription/ translation reaction was performed in the presence of recombinant EF-Tu or EF-Tu coexpressed with YegI-NTD and all the reconstituted *E. coli* components required for translation. A plasmid expressing a *B. subtilis* spore coat protein carrying a C-terminal FLAG tag (*cotE-FLAG*) was used as a template for the *in vitro* transcription/ translation assay (133). CotE-FLAG synthesis was assayed using western blot with α-flag antibody. Synthesis of CotE-flag decreased (~70%) in the presence of EF-Tu purified from a strain co-expressing YegI-NTD (Fig. 4.19B, lane 2) as compared to EF-Tu purified from a strain expressing EF-Tu by itself (Fig. 4.19B,lane 1) indicating that EF-Tu that had been phosphorylated by YegI inhibits protein translation.

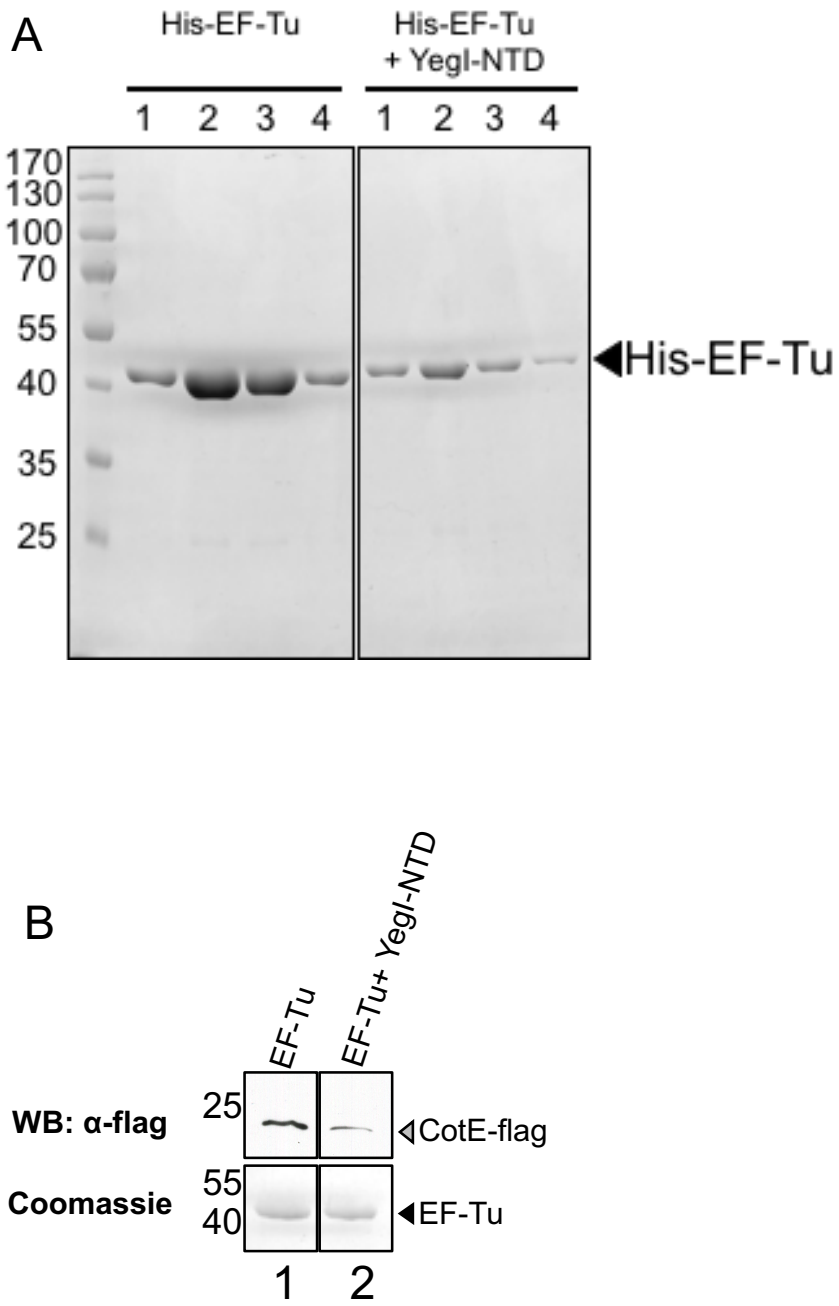

Figure 4.19 Phosphorylation of EF-Tu by YegI inhibits protein translation *in vitro.*
(A) Purification of His_6-EF-Tu and His_6-EF-Tu coexpressed with YegI-NTD. Lanes 1-4 indicate samples after elution from Ni^{2+}-beads using 300 mM imidazole. Samples were resolved on 12% SDS-PAGE followed by Coomassie staining. Molecular weights (kDa) are indicated on the right of the gel.
(B) *In vitro* synthesis of CotE-FLAG in the presence of EF-Tu. PURExpress reactions were carried out at 37 ºC for 10 mins with 2 μM of EF-Tu alone (lane 1) or EF-Tu co-expressed with YegI-NTD (lane 2). Synthesis of CotE-FLAG was detected by anti-flag antibody using Western blot analysis. Coomassie stained gel indicates the amount of EF-Tu added to each reaction.

4.8 Discussion

Ser/Thr phosphorylation is an important post translational modification that is capable of regulating protein function both in eukaryotes (211) and prokaryotes (150). Advent of genomic sequencing of several prokaryotic genomes have identified several open reading frames that encode serine/threonine kinases and cognate protein phosphatases that are responsible for reversible phosphorylation indicating widespread prevalence of Ser/Thr phosphorylation in bacteria (30). Although Ser/Thr phosphorylation in the Gram-negative bacterium *Escherichia coli* has been known for >10 years, little is known about the enzymes responsible for this reversible modification and their specific substrates. In this chapter, I have described the characterization of a novel Ser/Thr kinase YegI in *E. coli* and the identification of several potential substrates

In silico analysis revealed that YegI belongs to the class of eukaryotic-like Ser/Thr kinases (eSTKs) that contain all the 11 key structural subdomains that are characteristic of eukaryotic protein kinases (28). Homology search using YegI kinase domain revealed that it was similar to kinase domains of several bacterial eSTKs (Fig.4.1D). Unlike other bacterial eSTKs, however YegI includes only seven of the ten absolutely conserved residues responsible for ATP binding, catalysis, and substrate recognition (13, 28) (Fig.4.1B). Despite the absence of these conserved residues, YegI encodes an active protein kinase (Fig. 4.3) that undergoes autophosphorylation primarily on serine residues (Fig.4.5A) Similar to most bacterial eSTKs, autophosphorylation of YegI on serine residues in the activation loop is critical for catalytic activity of YegI (Fig. 4.5B). A notable feature of YegI is that it lacks the conserved DFG loop which is important for Mg^{2+} binding. The orientation of DFG loop with respect to the activation loop dictates active or inactive conformation of the kinase and susceptibility to kinase inhibitors (212). I speculated that addition of DFG loop could help kinase activation. However, since I observed that replacing the DSD loop

with DFG completely abolished YegI activity (Fig.4.4C), the DSD motif is likely important for YegI activity.

Unlike Gram-positive eSTKs, YegI lacks a C-terminal extracellular sensing domain and instead has a cytoplasmic domain at the C-terminus (Fig.4.6). This suggests that the kinase senses a cytoplasmic signal. Since sequence analysis revealed the presence of two conserved non-specific DNA binding Helix-hairpin-Helix motifs (Fig.4.7A,B) which is commonly found in DNA repair proteins, I hypothesized that YegI plays a role in DNA repair. Consistently, I found that deletion of YegI decreases sensitivity to DNA damaging agent nalidixic acid (Fig.4.14). This is the first example of an eSTK with HhH motifs. The only other example of an eSTK directly interacting with DNA is *B. subtilis* YabT which contains a putative DNA binding site characterized by stretch of lysine-arginine residues (213). Understanding the possible role of HhH motif in activation of YegI will help understand the physiological role of YegI.

An interesting feature of the genome organization of *yegI* is that it differs in closely related *E. coli* strains (Fig.4.1.A). In most pathogenic strains and lab B strains of *E. coli, yegI* occurs immediately downstream of *pphC*, a PP2C-like phosphatase with a four nucleotide overlap while in K strains this locus is disrupted by unknown protein *yegJ* suggesting potential regulatory differences between strains. Interestingly, deletion of *yegI* in REL606 (B strain) displayed reduced sensitivity to cell wall acting antibiotic cefotaxime as compared to WT strain (Fig.4.10). However this was not observed in an MG1655 (K strain) background allowing us to speculate that *yegI* kinase expression in K strain background might resemble a kinase null mutant. In REL606 strains, *yegI* expression was detected only in stationary phase but at very low levels (Fig.4.8). However, the absence of physiological stimulus that initiates *yegI* expression and activation makes it difficult to interpret the functional implications of the altered gene locus.

Although Ser/Thr kinases have been previously identified in *E. coli* and impact various cellular processes like antibiotic persistence and the stress response, the physiological targets for these kinases have largely not been identified. One of the main aims of this study was to identify physiological substrates of YegI. Using comparative phosphoproteomics (Fig.4.16) and an *in vitro* kinase assay (Fig.4.17), I identified enolase as a potential substrate for YegI kinase. Enolase has been previously reported to be phosphorylated on multiple Ser/Thr/Tyr residues (114, 123) consistent with my results. Identification of the sites of phosphorylation and their effect on enolase function would help to understand the possible role of phosphorylation in the regulation of enolase. In addition to its function in glycolysis, enolase also forms a part of the RNA degradosome assembly complex that is responsible for degradation of mRNAs. The function of enolase in the RNA degradosome is not well studied although enolase can mediate degradation of glucose transporter mRNA in response to phosphosugar stress (126). Therefore, phosphorylation of enolase could affect either its role in glycolysis or in the RNA degradosome.

In vivo, E. coli elongation factor-Tu is phosphorylated on multiple Ser/Thr residues (114, 134, 146) but the specific *E. coli* kinase responsible for this modification is not known. Recent studies have shown that phosphorylation of EF-Tu at a single site Thr 383 by the P1 phage encoded Doc kinase inactivates EF-Tu (214, 215). I found that phosphorylation of EF-Tu by YegI impaired EF-Tu function in protein synthesis (Fig.4.19B) consistent with previous findings in *E. coli* (134). However, the mechanistic basis for this effect remains unclear. Mass spectrometry analysis revealed that YegI phosphorylated EF-Tu at residues Thr-94, Ser-194 and Ser-220 (Fig.4.18). Lys-89 and Asp-90 have been previously shown to be important for amino acyl tRNA binding and mutation of either of these residues leads to loss of tRNA binding (216). Thus, phosphorylation of Thr-94 could impact tRNA binding. Similarly, Gly-223 is involved in ribosome dependent

activation of GTPase activity of EF-Tu since mutation of this residue, which contacts the ribosome, inhibits GTP hydrolysis and subsequently protein synthesis (217, 218). Therefore, phosphorylation of EF-Tu at Ser-220, a nearby residue, could indirectly affect GTP hydrolysis.

In summary, this chapter presents the first report of an integral membrane Ser/Thr kinase in *E. coli*. Additionally, I showed that activation of YegI requires autophosphorylation of serine residues near the activation loop. Furthermore, I have demonstrated that YegI phosphorylates EF-Tu and inhibits its function in protein translation. YegI also phosphorylate enolase *in vitro* however the sites of phosphorylation and the effect of phosphorylation on enolase function are yet to be investigated. I found that YegI contains two HhH motif and the presence of HhH motif was essential for sensitivity to cell wall antibiotic cefotaxime and DNA synthesis inhibitor nalidixic acid. Further studies will be required to fully understand how YegI mediates sensitivity to cell wall acting antibiotics and DNA damaging agents.

CHAPTER 5

Summary and Future Directions

5.1 General summary

The work presented in this thesis has identified and characterized novel enzymes that mediate Ser/Thr phosphorylation in *E. coli*. First, I identified a gene *yegK(pphC)* encoding a PP2C-like Ser/Thr phosphatase in *E. coli* using a homology based search. I then biochemically characterized PphC and showed that it is an active Ser/Thr phosphatase. This is the first report of a PP2C-like Ser/Thr phosphatase in *E. coli.* Additionally, I identified a downstream gene, *yegI,* that encodes a putative integral membrane eukaryotic-like Ser/Thr kinase with two helix-hairpin-helix motifs. I showed that YegI is an active kinase *in vitro* and identified two substrates. Phosphorylation of one of these substrates, the essential elongation factor-Tu (EF-Tu), appears to inhibit its activity in protein translation, suggesting that this Ser/Thr kinase/phosphatase pair may be involved in regulating protein synthesis.

5.1.1 PphC (YegK) is a novel PP2C-like Ser/Thr phosphatase in *E. coli*

Chapter 3 describes the characterization of a novel PP2C-like Ser/Thr phosphatase encoded by the gene *yegK* that I have reannotated as *pphC.* Despite the presence of only six of the eight key conserved residues associated with PP2C-like phosphatases (Fig.3.1), I found that PphC was an active phosphatase (Fig.3.3). PphC was able to effectively dephosphorylate Ser residues on phosphorylated β-casein substrate suggesting that PphC is a serine phosphatase (Fig.3.7). Consistent with the observation that the primary substrate for PP2C phosphatases are partner kinases that are often encoded in the same operon, I observed PphC-dependent dephosphorylation of YegI, a putative Ser/Thr kinase encoded by a gene adjacent to *pphC* (Fig.3.9).

5.1.2 YegI is a novel eukaryotic-like Ser/Thr kinase in *E. coli*

Chapter 4 of this thesis describes the characterization of a novel eukaryotic-like Ser/Thr kinase encoded by *yegI* located downstream of *pphC*. Consistent with previous reports from other bacteria (30, 150), eukaryotic-like Ser/Thr kinases and their cognate phosphatase are often encoded in the same operon and the kinase activity is regulated by the phosphatase. YegI differs in amino acid sequence with previously characterized eSTKs especially in conserved residues in both the catalytic loop and the metal binding loop (Fig.4.1B). However, my biochemical analysis revealed that YegI is an active kinase (Fig.4.3) which requires the bivalent cations Mg^{2+}/Mn^{2+} for activity (Fig.4.4). Similar to previously characterized eSTKs, YegI undergoes autophosphorylation of residues in the activation loop which is absolutely essential for YegI kinase activity (Fig.4.5). Unlike previously identified Ser/Thr kinases *in E. coli*, YegI is an integral membrane protein with both the N-terminal kinase domain and the C-terminus located in the cytoplasm (Fig.4.6). Interestingly, the C-terminal domain contains non-specific DNA binding helix-hairpin-helix motifs (Fig.4.7). Phenotypic analysis revealed that deletion of *yegI* resulted in decreased sensitivity to cell wall antibiotic cefotaxime (Fig.4.10) and DNA synthesis inhibitor nalidixic acid (Fig.4.14), and that the DNA binding domain of YegI was required for this decreased sensitivity (Fig.4.12, Fig.4.14). Finally, phosphoproteomic analysis and *in vitro* kinase assays reveal two potential substrates for YegI kinase: enolase (Fig.4.16) and elongation factor-Tu (Fig.4.18).

5.2 Future Directions

5.2.1 Differences in activity of PphC between closely related *E. coli* strains

Results in Chapter 3 showed a significant difference in phosphatase activity of PphC when purified from closely related *E. coli* strains (B and K strains) (Fig. 3.6) despite ~92% amino acid sequence identity (Fig. 3.5). Interestingly, all of the absolutely conserved residues that dictate catalysis and metal coordination in bacterial PP2Cs are 100% identical between REL606 and MG1655 PphC. However, there are differences in non-conserved residues that are broadly distributed throughout the protein. I speculate that these changes in amino acid sequence could reflect the difference in phosphatase activity. Generating amino acid substitutions in MG1655 PphC in these non-conserved regions such that it resembles REL606 PphC and assessing phosphatase activity could give us additional insight into the biochemical differences between the closely related phosphatases. Since the differences are in residues not currently known to impact catalytic activity, this work could help in understanding the role of non-canonical residues that contribute to activity.

5.2.2 How is PphC activity regulated?

Unlike other classes of Ser/Thr phosphatases (e.g., PPP), PP2C-like phosphatases are metal dependent phosphatases that do not contain additional regulatory motifs raising the question of how these enzymes are regulated (152). One possibility is regulation at the transcriptional level; however, in most cases both the eSTK and eSTP occur in same operon indicating probable co-transcription. Therefore, regulation of PP2C activity may be more complex. So far, two mechanisms of regulation of bacterial PP2C activity have been proposed: phosphorylation by partner eSTKs in the case of *M. tuberculosis* PstP (174) or regulation by dimer induced conformational change in the broadly conserved switch region as seen in the *B. subtilis* PP2C-like

phosphatase SpoIIE (175). However, PphC shows poor conservation in the switch region indicating that this mechanism may not be relevant

YegI phosphorylates PphC on Ser-174 (Fig.3.11), reminiscent of previous findings in *M. tuberculosis*, where the PP2C-like phosphatase PstP is phosphorylated by eSTK PknA and PknB (174). To test whether Ser-174 phosphorylation has a role in regulating phosphatase activity, I generated a phosphoablative mutant (PphC-S174A). This mutation however did not have a significant impact on phosphatase activity against pNPP or phosphorylated β-casein (Fig.3.12). Furthermore, phosphorylating PphC with YegI *in vitro* and subsequent analysis of phosphatase activity against pNPP showed no difference in activity as compared to unphosphorylated PphC (Fig.3.12). It is possible that *in vitro* phosphorylation may not yield a sufficiently high stoichiometry of phosphorylated PphC to impact enzyme kinetics. Co-expression of the kinase and putative substrate in pETDuet-1 systems have been successfully utilized to understand the dynamics of kinase-substrate interaction and phosphorylation in *E. coli* (133, 174, 219, 220). Therefore, co-expression of PphC with YegI followed by phosphoenrichment could be used to generate *in vivo* phosphorylated PphC which might serve as a better candidate for testing impact of phosphorylation on PphC activity.

5.2.3 Autophosphorylation-mediated regulation of YegI

Although the predicted structure of YegI closely resembled the structure of the bacterial eSTK PknB (Fig. 4.1D), the YegI sequence shows striking deviations in the conserved regions particularly in the catalytic loop and the Mg^{2+}-binding DFG loop (Fig. 4.1B). Specifically, the YegI sequence contains the catalytic loop VGDXXQXS as opposed to the canonical catalytic loop HRDXXPXN found in almost all other bacterial eSTKs. The conserved histidine residue in the

catalytic loop is crucial for binding both the carbonyl group of catalytic aspartate in the catalytic loop and making a hydrophobic contact with the phenylalanine in the DFG loop. Additionally, YegI lacks the highly conserved DFG (aspartate-phenylalanine-glycine) loop in motif VII which recognizes the Mg^{2+}-bound ATP (221). Instead, YegI contains a DSD (aspartate-serine-aspartate) sequence suggesting either that YegI might be an inactive kinase or that the DFG loop is not essential for every kinase. My results suggest the latter, since, despite these differences in highly conserved residues, YegI is an active kinase (Fig.4.3) that requires bivalent cations Mg^{2+}/Mn^{2+} for activity with increased preference to Mn^{2+} ion (Fig.4.4A, B). Replacing the DSD loop in YegI with the canonical DFG loop failed to increase activity or preference for Mg^{2+} ion and instead completely abolished activity (Fig.4.4C). This result suggests that the presence of a serine and an aspartic acid residue in the DSD loop might be critical for activity and could affect YegI autophosphorylation. Consistently, I observed that the serine residue in the DSD loop is one of the three serine residues that undergoes autophosphorylation and is required for activity of the kinase (Fig.4.5A). Substitution of all three serine residues with alanine residues (Ser153ASer160ASer162A) abolished YegI kinase activity indicating that these residues are important for autophosphorylation of YegI (Fig.4.5C). In the future, generating single phosphoablative mutants of these autophosphorylated serine residues will help uncover the contribution of each site to the activity of YegI.

5.2.4 Impact of DNA binding on YegI activity

The typical domain architecture of membrane eSTKs comprises of a cytoplasmic N-terminal kinase domain connected to a single transmembrane domain and an extracellular C-terminal domain responsible for ligand recognition and binding (30). However, unlike membrane eSTKs,

YegI lacks an extracellular C-terminal domain. Instead, membrane topology analysis of YegI revealed the presence of two transmembrane domains with both the N-terminal kinase domain and C-terminus located in the cytosol (Fig. 4.6). Interestingly, I observed that the YegI C-terminus contains two predicted helix-hairpin-helix (HhH) motifs (Fig. 4.7A,B) that in other proteins are responsible for non-specific DNA binding (194). This observation raises an important question: Is DNA binding important for the function of YegI? More specifically, could binding to DNA serve as a signal for activation of YegI kinase? To test this, I will first test DNA binding of YegI by using YegI and YegI-NTD protein that lacks the transmembrane and C-terminal domain and examine the effect of DNA binding on YegI autophosphorylation and transphosphorylation. DNA binding could alter the conformation of YegI which may favor an active/inactive conformation. Therefore, dissecting the function of these HhH motifs in YegI could possibly provide clues about the functional role of YegI in *E. coli*.

5.2.5 Phenotypic characterization of *yegI*

Similar to other bacterial eSTKs, YegI is a non-essential protein. Phenotypic evaluation of Δ*yegI* strain revealed no significant difference in growth in minimal media as compared to WT strain (Fig.4.9). I observed decreased susceptibility of Δ*yegI* strain to cell wall antibiotic cefotaxime (Table 4.1, Fig.4.10) as well as to the DNA gyrase inhibitor nalidixic acid (Fig.4.14). This difference in susceptibility was seen only in the B strain REL606 and not in the K strain MG1655 suggesting potential regulatory differences in the *yegI* locus between the closely related *E. coli* strains (Fig.4.10, Fig.4.14A). While the kinase activity did not account for this reduced susceptibility (Fig.4.11, Fig.4.14B), the C-terminal domain including the HhH motifs were required to restore sensitivity to both antibiotics (Fig.4.12B, Fig.4.14C). This observation is in

marked contrast to previously reported roles of eSTKs in antibiotic resistance. For example, deletion of the *E. faecalis* eSTK IreK resulted in increased susceptibility to cephalosporins and this susceptibility was dependent on the kinase activity of IreK (52). Similarly, deletion of the *S. aureus* eSTK Stk increased susceptibility to cephalosporins (49). Thus, why are Δ*yegI* strains *less* susceptible to antibiotics?

Common mechanisms of antibiotic resistance include increased efflux of antibiotics, decreased membrane permeability or decreased affinity of target to antibiotics (222). Membrane permeability and antibiotic efflux are regulated by outer membrane proteins. Furthermore, overexpression of outer membrane proteins including the multidrug efflux pump TolC, were observed in nalidixic acid resistant strains (206). Interestingly, the operon adjacent to the *yeg* locus encodes multidrug transporters (MdtA, MdtB, MdtC) (Fig.3.5) which forms a complex with TolC to mediate efflux of antibiotics (223, 224). Thus, I hypothesized that deletion of *yegI* could affect TolC levels either by direct regulation or by an indirect mechanism. I therefore examined if there were differences in antibiotic susceptibility between WT and Δ*yegI* strains in a Δ*tolC* background. However, deletion of *tolC* completely sensitized both WT and Δ*yegI* strains to the indicated concentrations of antibiotics therefore making it not possible to determine differences in sensitivity (Fig.4.15). In future experiments, I will test if the reduced susceptibility of Δ*yegI* is a result of high TolC levels by examining expression of *tolC* mRNA using qRT-PCR in WT and Δ*yegI* in the absence or presence of antibiotics. Identifying this mechanism of decreased susceptibility to antibiotics could help understand the role of YegI in maintaining antibiotic sensitivity.

5.2.6 Potential YegI substrates

Comparative phosphoproteomics of WT and Δ*yegI* strains revealed differential phosphorylation of enolase, a key glycolytic enzyme, at Ser-400 (Fig.4.16C). Glycolysis breaks down glucose into pyruvate which is used to generate ATP and NADH and is therefore essential for maintaining optimal growth and production of various biomolecules. During glycolysis, enolase catalyzes the interconversion between 2-phosphoglycerate to phosphoenol pyruvate. Previously published global phosphoproteomes from phylogenetically diverse bacteria also report Ser/Thr phosphorylation of enolase (114, 115, 117, 122, 123). Consistent with the comparative phosphoproteomics analysis, I observed YegI-dependent *in vitro* phosphorylation of enolase (Fig.4.17). However, since YegI still phosphorylated the phosphoablative mutant enolase-S400A, there are likely additional sites of phosphorylation. Mass spectrometry analysis of enolase phosphorylation by YegI will help identify these sites of phosphorylation.

The more pertinent question is whether phosphorylation of enolase affects its function. The lack of a commercially available substrate 2-phosphoglycerate makes the study of the impact of phosphorylation on enolase glycolytic activity challenging. Alternatively, in addition to its role in glycolysis, enolase is part of the multicomponent RNA degradosome complex that is responsible for regulating half-life of RNA transcripts (124). Although its exact role in RNA degradation is unknown, the presence of enolase in the RNA degradosome complex is required for degradation of glucose transporter *ptsG* mRNA levels under phosphosugar stress (126). Rapid degradation of *ptsG* mRNA was observed only when glycolytic pathway was blocked early on by deletion of phosphoglucose isomerase *pgi*. Pgi mediates the interconversion of glucose-6-phosphate to fructose-6-phosphate and deletion of *pgi* leads to accumulation of glucose-6-phosphate in cells resulting in phosphosugar stress. However how enolase in the RNA degradosome complex stimulates rapid degradation is still unknown. It is possible that phosphorylation could affect

protein-protein interactions between enolase and degradosome complex. Therefore, I speculate that phosphorylation of enolase could impact the formation of RNA degradosome complex *in vivo* which could in turn affect *ptsG* mRNA degradation. Future experiments will test whether phosphorylation of enolase affects activity in RNA degradosome by examining *ptsG* mRNA levels in WT or Δ*yegI* strain under phosphosugar stress using qRT-PCR. If indeed YegI phosphorylates enolase and inhibits enolase activity then we should observe stabilization of *ptsG* mRNA in Δ*yegI* strain even in the presence of phosphosugar stress. Alternatively, if YegI phosphorylation has no impact on enolase activity in the degredasome, then we would observe decreased *ptsG* levels due to rapid degradation.

Phosphorylation of elongation factor-Tu (EF-Tu) is observed in multiple phosphoproteomics studies (130). In *E. coli,* EF-Tu is reported to be phosphorylated on multiple Ser/Thr residues (114, 123, 134) but the kinase responsible for this phosphorylation is not known. Using *in vitro* kinase assay, I demonstrated YegI-dependent phosphorylation of EF-Tu (Fig. 4.18). Furthermore, EF-Tu purified from an *E. coli* strain co-expressing an active YegI truncation was less active in stimulating protein synthesis than EF-Tu that has been purified from *E. coli* in the absence of co-expressed YegI (Fig.4.19B). This result hints at a possible role of phosphorylation mediated regulation of EF-Tu activity in protein translation. In the future, I would like to dissect the exact mechanism by which YegI dependent phosphorylation of EF-Tu affects protein synthesis. To address this question, I would like to first ensure that co-expression of EF-Tu with YegI-NTD leads to phosphorylation of EF-Tu using mass spectrometry. While several commercially available non-radioactive phosphorylation detection methods such as Phos-tag (172, 225), pIMAGO (226) as well as phosphospecific antibodies exist, I have been unable to detect any specific phosphorylation event using these methodologies. Thus, following validation of phosphorylation

of EF-Tu using mass spectrometry, I will compare the sites of phosphorylation obtained from *in vitro* phosphorylated EF-Tu (Thr-94, Ser-198, Ser-220) to the *in vivo* phosphorylated EF-Tu and assess the impact of single phosphoablative mutants on protein translation. While Thr-94 is located in the GTP binding domain, Ser-198 and Ser-220 are located in the C-terminal domain responsible for functional interaction with the ribosome. If Thr-94 is phosphorylated, then one could directly assess the impact of this modification on GTP hydrolysis. The adjacent glycine residue (Gly-95) is crucial for release of inorganic phosphate after GTP hydrolysis which is a crucial step for function of GTPases like EF-Tu (227), therefore I speculate that phosphorylation of Thr-94 could affect EF-Tu GTPase activity. Similarly if Ser-220 is phosphorylated, then one could assess the impact of this modification on GTP hydrolysis. Since Gly-223 is necessary for ribosome dependent activation of GTP hydrolysis (217, 218), phosphorylation of Ser-220 could affect ribosome dependent activation of GTPase activity. Together, these studies would offer insight into phosphorylation mediated regulation of *E. coli* EF-Tu function.

References

1. **Pawson T, Scott JD.** 2005. Protein phosphorylation in signaling--50 years and counting. Trends Biochem Sci **30:**286-290.
2. **Fischer EH, Krebs EG.** 1955. Conversion of phosphorylase b to phosphorylase a in muscle extracts. J Biol Chem **216:**121-132.
3. **Krebs EG, Fischer EH.** 1955. Phosphorylase activity of skeletal muscle extracts. J Biol Chem **216:**113-120.
4. **Krebs EG, Fischer EH.** 1956. The phosphorylase b to a converting enzyme of rabbit skeletal muscle. Biochim Biophys Acta **20:**150-157.
5. **Sutherland EW, Jr., Wosilait WD.** 1955. Inactivation and activation of liver phosphorylase. Nature **175:**169-170.
6. **Bakal CJ, Davies JE.** 2000. No longer an exclusive club: eukaryotic signalling domains in bacteria. Trends Cell Biol **10:**32-38.
7. **Kuo JF, Greengard P.** 1969. An adenosine 3',5'-monophosphate-dependent protein kinase from Escherichia coli. J Biol Chem **244:**3417-3419.
8. **Khandelwal RL, Spearman TN, Hamilton IR.** 1973. Protein kinase activity in cariogenic and non-cariogenic oral streptococci: Activation and inhibition by cyclic AMP. FEBS Lett **31:**246-250.
9. **Garnak M, Reeves HC.** 1979. Phosphorylation of Isocitrate dehydrogenase of Escherichia coli. Science **203:**1111-1112.
10. **Manai M, Cozzone AJ.** 1979. Analysis of the protein-kinase activity of Escherichia coli cells. Biochem Biophys Res Commun **91:**819-826.
11. **Garland D, Nimmo HG.** 1984. A comparison of the phosphorylated and unphosphorylated forms of isocitrate dehydrogenase from Escherichia coli ML308. FEBS Lett **165:**259-264.
12. **Nimmo GA, Nimmo HG.** 1984. The regulatory properties of isocitrate dehydrogenase kinase and isocitrate dehydrogenase phosphatase from Escherichia coli ML308 and the roles of these activities in the control of isocitrate dehydrogenase. Eur J Biochem **141:**409-414.
13. **Hanks SK, Hunter T.** 1995. Protein kinases 6. The eukaryotic protein kinase superfamily: kinase (catalytic) domain structure and classification. FASEB J **9:**576-596.
14. **Stock JB, Ninfa AJ, Stock AM.** 1989. Protein phosphorylation and regulation of adaptive responses in bacteria. Microbiol Rev **53:**450-490.
15. **Stock JB, Stock AM, Mottonen JM.** 1990. Signal transduction in bacteria. Nature **344:**395-400.
16. **Hoch JA.** 2000. Two-component and phosphorelay signal transduction. Curr Opin Microbiol **3:**165-170.
17. **Stock AM, Robinson VL, Goudreau PN.** 2000. Two-component signal transduction. Annu Rev Biochem **69:**183-215.
18. **Stock J, Da Re S.** 2000. Signal transduction: response regulators on and off. Curr Biol **10:**R420-424.
19. **Huynh TN, Stewart V.** 2011. Negative control in two-component signal transduction by transmitter phosphatase activity. Molecular Microbiology **82:**275-286.

20. **Galperin MY, Nikolskaya AN, Koonin EV.** 2001. Novel domains of the prokaryotic two-component signal transduction systems. FEMS Microbiol Lett **203:**11-21.
21. **Chang C, Kwok SF, Bleecker AB, Meyerowitz EM.** 1993. Arabidopsis ethylene-response gene ETR1: similarity of product to two-component regulators. Science **262:**539-544.
22. **Ota IM, Varshavsky A.** 1993. A yeast protein similar to bacterial two-component regulators. Science **262:**566-569.
23. **Munoz-Dorado J, Inouye S, Inouye M.** 1991. A gene encoding a protein serine/threonine kinase is required for normal development of M. xanthus, a gram-negative bacterium. Cell **67:**995-1006.
24. **Zhang W, Munoz-Dorado J, Inouye M, Inouye S.** 1992. Identification of a putative eukaryotic-like protein kinase family in the developmental bacterium Myxococcus xanthus. J Bacteriol **174:**5450-5453.
25. **Nariya H, Inouye S.** 2005. Identification of a protein Ser/Thr kinase cascade that regulates essential transcriptional activators in Myxococcus xanthus development. Mol Microbiol **58:**367-379.
26. **Inouye S, Jain R, Ueki T, Nariya H, Xu CY, Hsu MY, Fernandez-Luque BA, Munoz-Dorado J, Farez-Vidal E, Inouye M.** 2000. A large family of eukaryotic-like protein Ser/Thr kinases of Myxococcus xanthus, a developmental bacterium. Microb Comp Genomics **5:**103-120.
27. **Kannan N, Taylor SS, Zhai Y, Venter JC, Manning G.** 2007. Structural and functional diversity of the microbial kinome. PLoS Biol **5:**e17.
28. **Hanks SK, Quinn AM, Hunter T.** 1988. The protein kinase family: conserved features and deduced phylogeny of the catalytic domains. Science **241:**42-52.
29. **Bork P, Brown NP, Hegyi H, Schultz J.** 1996. The protein phosphatase 2C (PP2C) superfamily: detection of bacterial homologues. Protein science : a publication of the Protein Society **5:**1421-1425.
30. **Pereira SF, Goss L, Dworkin J.** 2011. Eukaryote-like serine/threonine kinases and phosphatases in bacteria. Microbiology and molecular biology reviews : MMBR **75:**192-212.
31. **Taylor SS, Radzio-Andzelm E.** 1994. Three protein kinase structures define a common motif. Structure **2:**345-355.
32. **Huse M, Kuriyan J.** 2002. The conformational plasticity of protein kinases. Cell **109:**275-282.
33. **Nolen B, Taylor S, Ghosh G.** 2004. Regulation of protein kinases; controlling activity through activation segment conformation. Mol Cell **15:**661-675.
34. **Boitel B, Ortiz-Lombardia M, Duran R, Pompeo F, Cole ST, Cervenansky C, Alzari PM.** 2003. PknB kinase activity is regulated by phosphorylation in two Thr residues and dephosphorylation by PstP, the cognate phospho-Ser/Thr phosphatase, in *Mycobacterium tuberculosis*. Mol Microbiol **49:**1493-1508.
35. **Young TA, Delagoutte B, Endrizzi JA, Falick AM, Alber T.** 2003. Structure of Mycobacterium tuberculosis PknB supports a universal activation mechanism for Ser/Thr protein kinases. Nat Struct Biol **10:**168-174.
36. **Duran R, Villarino A, Bellinzoni M, Wehenkel A, Fernandez P, Boitel B, Cole ST, Alzari PM, Cervenansky C.** 2005. Conserved autophosphorylation pattern in activation

loops and juxtamembrane regions of Mycobacterium tuberculosis Ser/Thr protein kinases. Biochem Biophys Res Commun **333:**858-867.
37. **Taylor SS, Radzio-Andzelm E, Hunter T.** 1995. How do protein kinases discriminate between serine/threonine and tyrosine? Structural insights from the insulin receptor protein-tyrosine kinase. FASEB J **9:**1255-1266.
38. **Ortiz-Lombardia M, Pompeo F, Boitel B, Alzari PM.** 2003. Crystal structure of the catalytic domain of the PknB serine/threonine kinase from Mycobacterium tuberculosis. J Biol Chem **278:**13094-13100.
39. **Greenstein AE, Echols N, Lombana TN, King DS, Alber T.** 2007. Allosteric activation by dimerization of the PknD receptor Ser/Thr protein kinase from Mycobacterium tuberculosis. J Biol Chem **282:**11427-11435.
40. **Hsu F, Schwarz S, Mougous JD.** 2009. TagR promotes PpkA-catalysed type VI secretion activation in Pseudomonas aeruginosa. Mol Microbiol **72:**1111-1125.
41. **Mieczkowski C, Iavarone AT, Alber T.** 2008. Auto-activation mechanism of the Mycobacterium tuberculosis PknB receptor Ser/Thr kinase. EMBO J **27:**3186-3197.
42. **Jones G, Dyson P.** 2006. Evolution of transmembrane protein kinases implicated in coordinating remodeling of gram-positive peptidoglycan: inside versus outside. J Bacteriol **188:**7470-7476.
43. **Yeats C, Finn RD, Bateman A.** 2002. The PASTA domain: a beta-lactam-binding domain. Trends Biochem Sci **27:**438.
44. **Shah IM, Laaberki MH, Popham DL, Dworkin J.** 2008. A Eukaryotic-like Ser/Thr Kinase Signals Bacteria to Exit Dormancy in Response to Peptidoglycan Fragments. Cell **135:**486-496.
45. **Fernandez P, Saint-Joanis B, Barilone N, Jackson M, Gicquel B, Cole ST, Alzari PM.** 2006. The Ser/Thr protein kinase PknB is essential for sustaining mycobacterial growth. J Bacteriol **188:**7778-7784.
46. **Fleurie A, Manuse S, Zhao C, Campo N, Cluzel C, Lavergne JP, Freton C, Combet C, Guiral S, Soufi B, Macek B, Kuru E, VanNieuwenhze MS, Brun YV, Di Guilmi AM, Claverys JP, Galinier A, Grangeasse C.** 2014. Interplay of the serine/threonine-kinase StkP and the paralogs DivIVA and GpsB in pneumococcal cell elongation and division. PLoS Genet **10:**e1004275.
47. **Fleurie A, Lesterlin C, Manuse S, Zhao C, Cluzel C, Lavergne JP, Franz-Wachtel M, Macek B, Combet C, Kuru E, VanNieuwenhze MS, Brun YV, Sherratt D, Grangeasse C.** 2014. MapZ marks the division sites and positions FtsZ rings in Streptococcus pneumoniae. Nature **516:**259-262.
48. **Tamber S, Schwartzman J, Cheung AL.** 2010. Role of PknB kinase in antibiotic resistance and virulence in community-acquired methicillin-resistant Staphylococcus aureus strain USA300. Infect Immun **78:**3637-3646.
49. **Beltramini AM, Mukhopadhyay CD, Pancholi V.** 2009. Modulation of cell wall structure and antimicrobial susceptibility by a *Staphylococcus aureus* eukaryote-like serine/threonine kinase and phosphatase. Infection and immunity **77:**1406-1416.
50. **Pensinger DA, Boldon KM, Chen GY, Vincent WJ, Sherman K, Xiong M, Schaenzer AJ, Forster ER, Coers J, Striker R, Sauer JD.** 2016. The Listeria monocytogenes PASTA Kinase PrkA and Its Substrate YvcK Are Required for Cell Wall Homeostasis, Metabolism, and Virulence. PLoS Pathog **12:**e1006001.

51. **Pensinger DA, Aliota MT, Schaenzer AJ, Boldon KM, Ansari IU, Vincent WJ, Knight B, Reniere ML, Striker R, Sauer JD.** 2014. Selective pharmacologic inhibition of a PASTA kinase increases Listeria monocytogenes susceptibility to beta-lactam antibiotics. Antimicrob Agents Chemother **58:**4486-4494.
52. **Kristich CJ, Little JL, Hall CL, Hoff JS.** 2011. Reciprocal regulation of cephalosporin resistance in Enterococcus faecalis. MBio **2:**e00199-00111.
53. **Hall CL, Tschannen M, Worthey EA, Kristich CJ.** 2013. IreB, a Ser/Thr kinase substrate, influences antimicrobial resistance in Enterococcus faecalis. Antimicrob Agents Chemother **57:**6179-6186.
54. **Manuse S, Fleurie A, Zucchini L, Lesterlin C, Grangeasse C.** 2016. Role of eukaryotic-like serine/threonine kinases in bacterial cell division and morphogenesis. FEMS Microbiol Rev **40:**41-56.
55. **Hussain H, Branny P, Allan E.** 2006. A eukaryotic-type serine/threonine protein kinase is required for biofilm formation, genetic competence, and acid resistance in Streptococcus mutans. J Bacteriol **188:**1628-1632.
56. **Zhang W, Inouye M, Inouye S.** 1996. Reciprocal regulation of the differentiation of Myxococcus xanthus by Pkn5 and Pkn6, eukaryotic-like Ser/Thr protein kinases. Mol Microbiol **20:**435-447.
57. **Udo H, Munoz-Dorado J, Inouye M, Inouye S.** 1995. Myxococcus xanthus, a gram-negative bacterium, contains a transmembrane protein serine/threonine kinase that blocks the secretion of beta-lactamase by phosphorylation. Genes Dev **9:**972-983.
58. **Nariya H, Inouye S.** 2002. Activation of 6-phosphofructokinase via phosphorylation by Pkn4, a protein Ser/Thr kinase of Myxococcus xanthus. Mol Microbiol **46:**1353-1366.
59. **Hanlon WA, Inouye M, Inouye S.** 1997. Pkn9, a Ser/Thr protein kinase involved in the development of Myxococcus xanthus. Mol Microbiol **23:**459-471.
60. **Nariya H, Inouye S.** 2006. A protein Ser/Thr kinase cascade negatively regulates the DNA-binding activity of MrpC, a smaller form of which may be necessary for the Myxococcus xanthus development. Mol Microbiol **60:**1205-1217.
61. **Galyov EE, Hakansson S, Forsberg A, Wolf-Watz H.** 1993. A secreted protein kinase of Yersinia pseudotuberculosis is an indispensable virulence determinant. Nature **361:**730-732.
62. **Wang J, Li C, Yang H, Mushegian A, Jin S.** 1998. A novel serine/threonine protein kinase homologue of *Pseudomonas aeruginosa* is specifically inducible within the host infection site and is required for full virulence in neutropenic mice. J Bacteriol **180:**6764-6768.
63. **Mougous JD, Gifford CA, Ramsdell TL, Mekalanos JJ.** 2007. Threonine phosphorylation post-translationally regulates protein secretion in *Pseudomonas aeruginosa*. Nat Cell Biol **9:**797-803.
64. **Pan J, Zha Z, Zhang P, Chen R, Ye C, Ye T.** 2017. Serine/threonine protein kinase PpkA contributes to the adaptation and virulence in Pseudomonas aeruginosa. Microb Pathog **113:**5-10.
65. **Blattner FR, Plunkett G, 3rd, Bloch CA, Perna NT, Burland V, Riley M, Collado-Vides J, Glasner JD, Rode CK, Mayhew GF, Gregor J, Davis NW, Kirkpatrick HA, Goeden MA, Rose DJ, Mau B, Shao Y.** 1997. The complete genome sequence of Escherichia coli K-12. Science **277:**1453-1462.

66. **Tagourti J, Landoulsi A, Richarme G.** 2008. Cloning, expression, purification and characterization of the stress kinase YeaG from Escherichia coli. Protein Expression and Purification **59:**79-85.
67. **Weber H, Polen T, Heuveling J, Wendisch VF, Hengge R.** 2005. Genome-wide analysis of the general stress response network in Escherichia coli: sigmaS-dependent genes, promoters, and sigma factor selectivity. J Bacteriol **187:**1591-1603.
68. **Fischer C, Geourjon C, Bourson C, Deutscher J.** 1996. Cloning and characterization of the Bacillus subtilis prkA gene encoding a novel serine protein kinase. Gene **168:**55-60.
69. **Tagourti J, Gautier V, Beaujouan JC, Gauchy C, Landoulsi A, Richarme G.** 2011. Phosphorylation of a 65 kDa cytoplasmic protein by the Escherichia coli YeaG kinase. Annals of Microbiology **61:**499-503.
70. **Figueira R, Brown DR, Ferreira D, Eldridge MJ, Burchell L, Pan Z, Helaine S, Wigneshweraraj S.** 2015. Adaptation to sustained nitrogen starvation by *Escherichia coli* requires the eukaryote-like serine/threonine kinase YeaG. Sci Rep **5:**17524.
71. **Switzer A, Evangelopoulos D, Figueira R, de Carvalho LPS, Brown DR, Wigneshweraraj S.** 2018. A novel regulatory factor affecting the transcription of methionine biosynthesis genes in Escherichia coli experiencing sustained nitrogen starvation. Microbiology doi:10.1099/mic.0.000683.
72. **Scheeff ED, Bourne PE.** 2005. Structural evolution of the protein kinase-like superfamily. PLoS Comput Biol **1:**e49.
73. **Correia FF, D'Onofrio A, Rejtar T, Li L, Karger BL, Makarova K, Koonin EV, Lewis K.** 2006. Kinase activity of overexpressed HipA is required for growth arrest and multidrug tolerance in Escherichia coli. J Bacteriol **188:**8360-8367.
74. **Stancik IA, Sestak MS, Ji B, Axelson-Fisk M, Franjevic D, Jers C, Domazet-Loso T, Mijakovic I.** 2018. Serine/Threonine Protein Kinases from Bacteria, Archaea and Eukarya Share a Common Evolutionary Origin Deeply Rooted in the Tree of Life. J Mol Biol **430:**27-32.
75. **Moyed HS, Broderick SH.** 1986. Molecular cloning and expression of hipA, a gene of Escherichia coli K-12 that affects frequency of persistence after inhibition of murein synthesis. J Bacteriol **166:**399-403.
76. **Moyed HS, Bertrand KP.** 1983. hipA, a newly recognized gene of Escherichia coli K-12 that affects frequency of persistence after inhibition of murein synthesis. J Bacteriol **155:**768-775.
77. **Bokinsky G, Baidoo EE, Akella S, Burd H, Weaver D, Alonso-Gutierrez J, Garcia-Martin H, Lee TS, Keasling JD.** 2013. HipA-triggered growth arrest and beta-lactam tolerance in Escherichia coli are mediated by RelA-dependent ppGpp synthesis. J Bacteriol **195:**3173-3182.
78. **Kaspy I, Rotem E, Weiss N, Ronin I, Balaban NQ, Glaser G.** 2013. HipA-mediated antibiotic persistence via phosphorylation of the glutamyl-tRNA-synthetase. Nat Commun **4:**3001.
79. **Germain E, Castro-Roa D, Zenkin N, Gerdes K.** 2013. Molecular mechanism of bacterial persistence by HipA. Mol Cell **52:**248-254.
80. **Zheng J, He C, Singh VK, Martin NL, Jia Z.** 2007. Crystal structure of a novel prokaryotic Ser/Thr kinase and its implication in the Cpx stress response pathway. Mol Microbiol **63:**1360-1371.

81. **De Wulf P, McGuire AM, Liu X, Lin EC.** 2002. Genome-wide profiling of promoter recognition by the two-component response regulator CpxR-P in Escherichia coli. J Biol Chem **277:**26652-26661.
82. **Dorsey-Oresto A, Lu T, Mosel M, Wang X, Salz T, Drlica K, Zhao X.** 2013. YihE kinase is a central regulator of programmed cell death in bacteria. Cell Rep **3:**528-537.
83. **Machuca J, Recacha E, Briales A, Diaz-de-Alba P, Blazquez J, Pascual A, Rodriguez-Martinez JM.** 2017. Cellular Response to Ciprofloxacin in Low-Level Quinolone-Resistant Escherichia coli. Front Microbiol **8:**1370.
84. **Shi L, Carmichael WW, Kennelly PJ.** 1999. Cyanobacterial PPP family protein phosphatases possess multifunctional capabilities and are resistant to microcystin-LR. J Biol Chem **274:**10039-10046.
85. **Zhuo S, Clemens JC, Hakes DJ, Barford D, Dixon JE.** 1993. Expression, purification, crystallization, and biochemical characterization of a recombinant protein phosphatase. J Biol Chem **268:**17754-17761.
86. **Av-Gay Y, Everett M.** 2000. The eukaryotic-like Ser/Thr protein kinases of Mycobacterium tuberculosis. Trends Microbiol **8:**238-244.
87. **Adler E, Donella-Deana A, Arigoni F, Pinna LA, Stragler P.** 1997. Structural relationship between a bacterial developmental protein and eukaryotic PP2C protein phosphatases. Mol Microbiol **23:**57-62.
88. **Kennelly PJ.** 2002. Protein kinases and protein phosphatases in prokaryotes: a genomic perspective. FEMS Microbiol Lett **206:**1-8.
89. **Shi L, Potts M, Kennelly PJ.** 1998. The serine, threonine, and/or tyrosine-specific protein kinases and protein phosphatases of prokaryotic organisms: a family portrait. FEMS Microbiol Rev **22:**229-253.
90. **Zhang W, Shi L.** 2004. Evolution of the PPM-family protein phosphatases in Streptomyces: duplication of catalytic domain and lateral recruitment of additional sensory domains. Microbiology **150:**4189-4197.
91. **Duncan L, Alper S, Arigoni F, Losick R, Stragier P.** 1995. Activation of cell-specific transcription by a serine phosphatase at the site of asymmetric division. Science **270:**641-644.
92. **Yang X, Kang CM, Brody MS, Price CW.** 1996. Opposing pairs of serine protein kinases and phosphatases transmit signals of environmental stress to activate a bacterial transcription factor. Genes Dev **10:**2265-2275.
93. **Dutta S, Lewis RJ.** 2003. Crystallization and preliminary crystallographic analysis of the kinase-recruitment domain of the PP2C-type phosphatase RsbU. Acta Crystallogr D Biol Crystallogr **59:**191-193.
94. **Das AK, Helps NR, Cohen PT, Barford D.** 1996. Crystal structure of the protein serine/threonine phosphatase 2C at 2.0 A resolution. EMBO J **15:**6798-6809.
95. **Schlicker C, Fokina O, Kloft N, Grune T, Becker S, Sheldrick GM, Forchhammer K.** 2008. Structural analysis of the PP2C phosphatase tPphA from *Thermosynechococcus elongatus*: a flexible flap subdomain controls access to the catalytic site. J Mol Biol **376:**570-581.
96. **Pullen KE, Ng HL, Sung PY, Good MC, Smith SM, Alber T.** 2004. An alternate conformation and a third metal in PstP/Ppp, the *M. tuberculosis* PP2C-Family Ser/Thr protein phosphatase. Structure **12:**1947-1954.

97. **Bellinzoni M, Wehenkel A, Shepard W, Alzari PM.** 2007. Insights into the catalytic mechanism of PPM Ser/Thr phosphatases from the atomic resolution structures of a mycobacterial enzyme. Structure **15:**863-872.
98. **Rantanen MK, Lehtio L, Rajagopal L, Rubens CE, Goldman A.** 2007. Structure of *Streptococcus agalactiae* serine/threonine phosphatase. The subdomain conformation is coupled to the binding of a third metal ion. FEBS J **274:**3128-3137.
99. **Zheng W, Cai X, Xie M, Liang Y, Wang T, Li Z.** 2016. Structure-Based Identification of a Potent Inhibitor Targeting Stp1-Mediated Virulence Regulation in *Staphylococcus aureus*. Cell Chem Biol **23:**1002-1013.
100. **Obuchowski M, Madec E, Delattre D, Boel G, Iwanicki A, Foulger D, Seror SJ.** 2000. Characterization of PrpC from *Bacillus subtilis*, a member of the PPM phosphatase family. J Bacteriol **182:**5634-5638.
101. **Rajagopal L, Clancy A, Rubens CE.** 2003. A eukaryotic type serine/threonine kinase and phosphatase in *Streptococcus agalactiae* reversibly phosphorylate an inorganic pyrophosphatase and affect growth, cell segregation, and virulence. J Biol Chem **278:**14429-14441.
102. **Chopra P, Singh B, Singh R, Vohra R, Koul A, Meena LS, Koduri H, Ghildiyal M, Deol P, Das TK, Tyagi AK, Singh Y.** 2003. Phosphoprotein phosphatase of *Mycobacterium tuberculosis* dephosphorylates serine-threonine kinases PknA and PknB. Biochem Biophys Res Commun **311:**112-120.
103. **Beilharz K, Novakova L, Fadda D, Branny P, Massidda O, Veening JW.** 2012. Control of cell division in Streptococcus pneumoniae by the conserved Ser/Thr protein kinase StkP. Proc Natl Acad Sci U S A **109:**E905-913.
104. **Novakova L, Bezouskova S, Pompach P, Spidlova P, Saskova L, Weiser J, Branny P.** 2010. Identification of multiple substrates of the StkP Ser/Thr protein kinase in Streptococcus pneumoniae. J Bacteriol **192:**3629-3638.
105. **Libby EA, Goss LA, Dworkin J.** 2015. The Eukaryotic-Like Ser/Thr Kinase PrkC Regulates the Essential WalRK Two-Component System in *Bacillus subtilis*. PLoS Genet **11:**e1005275.
106. **Gaidenko TA, Kim TJ, Price CW.** 2002. The PrpC serine-threonine phosphatase and PrkC kinase have opposing physiological roles in stationary-phase *Bacillus subtilis* cells. J Bacteriol **184:**6109-6114.
107. **Treuner-Lange A, Ward MJ, Zusman DR.** 2001. Pph1 from *Myxococcus xanthus* is a protein phosphatase involved in vegetative growth and development. Mol Microbiol **40:**126-140.
108. **Cameron DR, Ward DV, Kostoulias X, Howden BP, Moellering RC, Jr., Eliopoulos GM, Peleg AY.** 2012. Serine/Threonine Phosphatase Stp1 Contributes to Reduced Susceptibility to Vancomycin and Virulence in *Staphylococcus aureus*. The Journal of infectious diseases doi:10.1093/infdis/jis252.
109. **Passalacqua KD, Satola SW, Crispell EK, Read TD.** 2012. A mutation in the PP2C phosphatase gene in a Staphylococcus aureus USA300 clinical isolate with reduced susceptibility to vancomycin and daptomycin. Antimicrob Agents Chemother **56:**5212-5223.
110. **Faucher SP, Viau C, Gros PP, Daigle F, Le Moual H.** 2008. The prpZ gene cluster encoding eukaryotic-type Ser/Thr protein kinases and phosphatases is repressed by

oxidative stress and involved in Salmonella enterica serovar Typhi survival in human macrophages. FEMS Microbiol Lett **281:**160-166.

111. **Shakir SM, Bryant KM, Larabee JL, Hamm EE, Lovchik J, Lyons CR, Ballard JD.** 2010. Regulatory interactions of a virulence-associated serine/threonine phosphatase-kinase pair in *Bacillus anthracis*. J Bacteriol **192:**400-409.
112. **Breitkreutz A, Choi H, Sharom JR, Boucher L, Neduva V, Larsen B, Lin ZY, Breitkreutz BJ, Stark C, Liu G, Ahn J, Dewar-Darch D, Reguly T, Tang X, Almeida R, Qin ZS, Pawson T, Gingras AC, Nesvizhskii AI, Tyers M.** 2010. A global protein kinase and phosphatase interaction network in yeast. Science **328:**1043-1046.
113. **Mijakovic I, Macek B.** 2012. Impact of phosphoproteomics on studies of bacterial physiology. FEMS Microbiol Rev **36:**877-892.
114. **Macek B, Gnad F, Soufi B, Kumar C, Olsen JV, Mijakovic I, Mann M.** 2008. Phosphoproteome analysis of *E. coli* reveals evolutionary conservation of bacterial Ser/Thr/Tyr phosphorylation. Mol Cell Proteomics **7:**299-307.
115. **Macek B, Mijakovic I, Olsen JV, Gnad F, Kumar C, Jensen PR, Mann M.** 2007. The serine/threonine/tyrosine phosphoproteome of the model bacterium *Bacillus subtilis*. Mol Cell Proteomics **6:**697-707.
116. **Ravichandran A, Sugiyama N, Tomita M, Swarup S, Ishihama Y.** 2009. Ser/Thr/Tyr phosphoproteome analysis of pathogenic and non-pathogenic *Pseudomonas* species. Proteomics **9:**2764-2775.
117. **Schmidl SR, Gronau K, Pietack N, Hecker M, Becher D, Stulke J.** 2010. The phosphoproteome of the minimal bacterium *Mycoplasma pneumoniae*: Analysis of the complete known Ser/ Thr kinome suggests the existence of novel kinases. Mol Cell Proteomics doi:10.1074/mcp.M900267-MCP200.
118. **Prisic S, Dankwa S, Schwartz D, Chou MF, Locasale JW, Kang CM, Bemis G, Church GM, Steen H, Husson RN.** 2010. Extensive phosphorylation with overlapping specificity by *Mycobacterium tuberculosis* serine/threonine protein kinases. Proc Natl Acad Sci U S A **107:**7521-7526.
119. **Lim S, Marcellin E, Jacob S, Nielsen LK.** 2015. Global dynamics of *Escherichia coli* phosphoproteome in central carbon metabolism under changing culture conditions. J Proteomics **126:**24-33.
120. **Lin MH, Sugiyama N, Ishihama Y.** 2015. Systematic profiling of the bacterial phosphoproteome reveals bacterium-specific features of phosphorylation. Sci Signal **8:**rs10.
121. **Lin MH, Hsu TL, Lin SY, Pan YJ, Jan JT, Wang JT, Khoo KH, Wu SH.** 2009. Phosphoproteomics of Klebsiella pneumoniae NTUH-K2044 reveals a tight link between tyrosine phosphorylation and virulence. Mol Cell Proteomics **8:**2613-2623.
122. **Voisin S, Watson DC, Tessier L, Ding W, Foote S, Bhatia S, Kelly JF, Young NM.** 2007. The cytoplasmic phosphoproteome of the Gram-negative bacterium *Campylobacter jejuni:* evidence for modification by unidentified protein kinases. Proteomics **7:**4338-4348.
123. **Soares NC, Spat P, Krug K, Macek B.** 2013. Global dynamics of the *Escherichia coli* proteome and phosphoproteome during growth in minimal medium. J Proteome Res **12:**2611-2621.

124. **Miczak A, Kaberdin VR, Wei CL, Lin-Chao S.** 1996. Proteins associated with RNase E in a multicomponent ribonucleolytic complex. Proc Natl Acad Sci U S A **93:**3865-3869.
125. **Mackie GA.** 2013. RNase E: at the interface of bacterial RNA processing and decay. Nat Rev Microbiol **11:**45-57.
126. **Morita T, Kawamoto H, Mizota T, Inada T, Aiba H.** 2004. Enolase in the RNA degradosome plays a crucial role in the rapid decay of glucose transporter mRNA in the response to phosphosugar stress in Escherichia coli. Mol Microbiol **54:**1063-1075.
127. **Murashko ON, Lin-Chao S.** 2017. Escherichia coli responds to environmental changes using enolasic degradosomes and stabilized DicF sRNA to alter cellular morphology. Proc Natl Acad Sci U S A **114:**E8025-E8034.
128. **Soung GY, Miller JL, Koc H, Koc EC.** 2009. Comprehensive analysis of phosphorylated proteins of Escherichia coli ribosomes. J Proteome Res **8:**3390-3402.
129. **Soufi B, Gnad F, Jensen PR, Petranovic D, Mann M, Mijakovic I, Macek B.** 2008. The Ser/Thr/Tyr phosphoproteome of Lactococcus lactis IL1403 reveals multiply phosphorylated proteins. Proteomics **8:**3486-3493.
130. **Macek B, Mijakovic I.** 2011. Site-specific analysis of bacterial phosphoproteomes. Proteomics **11:**3002-3011.
131. **Kavaliauskas D, Nissen P, Knudsen CR.** 2012. The busiest of all ribosomal assistants: elongation factor Tu. Biochemistry **51:**2642-2651.
132. **Sajid A, Arora G, Gupta M, Singhal A, Chakraborty K, Nandicoori VK, Singh Y.** 2011. Interaction of Mycobacterium tuberculosis elongation factor Tu with GTP is regulated by phosphorylation. J Bacteriol **193:**5347-5358.
133. **Pereira SF, Gonzalez RL, Jr., Dworkin J.** 2015. Protein synthesis during cellular quiescence is inhibited by phosphorylation of a translational elongation factor. Proc Natl Acad Sci U S A **112:**E3274-3281.
134. **Lippmann C, Lindschau C, Vijgenboom E, Schroder W, Bosch L, Erdmann VA.** 1993. Prokaryotic elongation factor Tu is phosphorylated in vivo. J Biol Chem **268:**601-607.
135. **Alexander C, Bilgin N, Lindschau C, Mesters JR, Kraal B, Hilgenfeld R, Erdmann VA, Lippmann C.** 1995. Phosphorylation of elongation factor Tu prevents ternary complex formation. J Biol Chem **270:**14541-14547.
136. **Ravikumar V, Shi L, Krug K, Derouiche A, Jers C, Cousin C, Kobir A, Mijakovic I, Macek B.** 2014. Quantitative phosphoproteome analysis of *Bacillus subtilis* reveals novel substrates of the kinase PrkC and phosphatase PrpC. Mol Cell Proteomics **13:**1965-1978.
137. **Zhang CC.** 1996. Bacterial signalling involving eukaryotic-type protein kinases. Mol Microbiol **20:**9-15.
138. **Chambers MC, Maclean B, Burke R, Amodei D, Ruderman DL, Neumann S, Gatto L, Fischer B, Pratt B, Egertson J, Hoff K, Kessner D, Tasman N, Shulman N, Frewen B, Baker TA, Brusniak MY, Paulse C, Creasy D, Flashner L, Kani K, Moulding C, Seymour SL, Nuwaysir LM, Lefebvre B, Kuhlmann F, Roark J, Rainer P, Detlev S, Hemenway T, Huhmer A, Langridge J, Connolly B, Chadick T, Holly K, Eckels J, Deutsch EW, Moritz RL, Katz JE, Agus DB, MacCoss M, Tabb DL, Mallick P.** 2012. A cross-platform toolkit for mass spectrometry and proteomics. Nat Biotechnol **30:**918-920.

139. **Tanner S, Shu H, Frank A, Wang LC, Zandi E, Mumby M, Pevzner PA, Bafna V.** 2005. InsPecT: identification of posttranslationally modified peptides from tandem mass spectra. Anal Chem **77:**4626-4639.
140. **Horton RM, Hunt HD, Ho SN, Pullen JK, Pease LR.** 1989. Engineering hybrid genes without the use of restriction enzymes: gene splicing by overlap extension. Gene **77:**61-68.
141. **Datsenko KA, Wanner BL.** 2000. One-step inactivation of chromosomal genes in Escherichia coli K-12 using PCR products. Proc Natl Acad Sci U S A **97:**6640-6645.
142. **Ellermeier CD, Janakiraman A, Slauch JM.** 2002. Construction of targeted single copy lac fusions using lambda Red and FLP-mediated site-specific recombination in bacteria. Gene **290:**153-161.
143. **Thomason LC, Costantino N, Court DL.** 2007. E. coli genome manipulation by P1 transduction. Curr Protoc Mol Biol **Chapter 1:**Unit 1 17.
144. **Miller JH.** 1992. A short course in bacterial genetics : a laboratory manual and handbook for Escherichia coli and related bacteria. Cold Spring Harbor Laboratory Press, Plainview, N.Y.
145. **Baba T, Ara T, Hasegawa M, Takai Y, Okumura Y, Baba M, Datsenko KA, Tomita M, Wanner BL, Mori H.** 2006. Construction of Escherichia coli K-12 in-frame, single-gene knockout mutants: the Keio collection. Mol Syst Biol **2:**2006 0008.
146. **Qu Y, Wu S, Zhao R, Zink E, Orton DJ, Moore RJ, Meng D, Clauss TR, Aldrich JT, Lipton MS, Pasa-Tolic L.** 2013. Automated immobilized metal affinity chromatography system for enrichment of *Escherichia coli* phosphoproteome. Electrophoresis **34:**1619-1626.
147. **Canova MJ, Kremer L, Molle V.** 2008. pETPhos: a customized expression vector designed for further characterization of Ser/Thr/Tyr protein kinases and their substrates. Plasmid **60:**149-153.
148. **Perla-Kajan J, Lin X, Cooperman BS, Goldman E, Jakubowski H, Knudsen CR, Mandecki W.** 2010. Properties of Escherichia coli EF-Tu mutants designed for fluorescence resonance energy transfer from tRNA molecules. Protein Eng Des Sel **23:**129-136.
149. **Hunter T.** 1995. Protein kinases and phosphatases: the yin and yang of protein phosphorylation and signaling. Cell **80:**225-236.
150. **Dworkin J.** 2015. Ser/Thr phosphorylation as a regulatory mechanism in bacteria. Curr Opin Microbiol **24C:**47-52.
151. **Shi L.** 2004. Manganese-dependent protein O-phosphatases in prokaryotes and their biological functions. Front Biosci **9:**1382-1397.
152. **Shi Y.** 2009. Serine/threonine phosphatases: mechanism through structure. Cell **139:**468-484.
153. **Arora G, Sajid A, Arulanandh MD, Misra R, Singhal A, Kumar S, Singh LK, Mattoo AR, Raj R, Maiti S, Basu-Modak S, Singh Y.** 2013. Zinc regulates the activity of kinase-phosphatase pair (BasPrkC/BasPrpC) in *Bacillus anthracis*. Biometals **26:**715-730.
154. **Claywell JE, Fisher DJ.** 2016. CTL0511 from *Chlamydia trachomatis* Is a Type 2C Protein Phosphatase with Broad Substrate Specificity. J Bacteriol **198:**1827-1836.
155. **Lai SM, Le Moual H.** 2005. PrpZ, a *Salmonella enterica serovar Typhi* serine/threonine protein phosphatase 2C with dual substrate specificity. Microbiology **151:**1159-1167.

156. **Menegatti AC, Vernal J, Terenzi H.** 2015. The unique serine/threonine phosphatase from the minimal bacterium *Mycoplasma synoviae*: biochemical characterization and metal dependence. J Biol Inorg Chem **20:**61-75.
157. **Mukhopadhyay S, Kapatral V, Xu W, Chakrabarty AM.** 1999. Characterization of a Hank's type serine/threonine kinase and serine/threonine phosphoprotein phosphatase in *Pseudomonas aeruginosa*. Journal of bacteriology **181:**6615-6622.
158. **Su J, Forchhammer K.** 2013. Determinants for substrate specificity of the bacterial PP2C protein phosphatase tPphA from *Thermosynechococcus elongatus*. FEBS J **280:**694-707.
159. **Notredame C, Higgins DG, Heringa J.** 2000. T-Coffee: A novel method for fast and accurate multiple sequence alignment. J Mol Biol **302:**205-217.
160. **Kelley LA, Mezulis S, Yates CM, Wass MN, Sternberg MJ.** 2015. The Phyre2 web portal for protein modeling, prediction and analysis. Nat Protoc **10:**845-858.
161. **Guzman LM, Belin D, Carson MJ, Beckwith J.** 1995. Tight regulation, modulation, and high-level expression by vectors containing the arabinose PBAD promoter. J Bacteriol **177:**4121-4130.
162. **Missiakas D, Raina S.** 1997. Signal transduction pathways in response to protein misfolding in the extracytoplasmic compartments of *E. coli*: role of two new phosphoprotein phosphatases PrpA and PrpB. EMBO J **16:**1670-1685.
163. **MacKintosh C, MacKintosh RW.** 1994. Inhibitors of protein kinases and phosphatases. Trends Biochem Sci **19:**444-448.
164. **Zheng W, Liang Y, Zhao H, Zhang J, Li Z.** 2015. 5,5'-Methylenedisalicylic Acid (MDSA) Modulates SarA/MgrA Phosphorylation by Targeting Ser/Thr Phosphatase Stp1. Chembiochem **16:**1035-1040.
165. **Aburai N, Yoshida M, Ohnishi M, Kimura K.** 2010. Sanguinarine as a potent and specific inhibitor of protein phosphatase 2C in vitro and induces apoptosis via phosphorylation of p38 in HL60 cells. Biosci Biotechnol Biochem **74:**548-552.
166. **Studier FW, Daegelen P, Lenski RE, Maslov S, Kim JF.** 2009. Understanding the differences between genome sequences of *Escherichia coli* B strains REL606 and BL21(DE3) and comparison of the E. coli B and K-12 genomes. J Mol Biol **394:**653-680.
167. **Kimura Y, Mori Y, Ina Y, Takegawa K.** 2011. Enzymatic and functional analysis of a protein phosphatase, Pph3, from *Myxococcus xanthus*. J Bacteriol **193:**2657-2661.
168. **Su J, Schlicker C, Forchhammer K.** 2011. A third metal is required for catalytic activity of the signal-transducing protein phosphatase M tPphA. J Biol Chem **286:**13481-13488.
169. **Halbedel S, Busse J, Schmidl SR, Stulke J.** 2006. Regulatory protein phosphorylation in *Mycoplasma pneumoniae*. A PP2C-type phosphatase serves to dephosphorylate HPr(Ser-P). J Biol Chem **281:**26253-26259.
170. **Jin H, Pancholi V.** 2006. Identification and biochemical characterization of a eukaryotic-type serine/threonine kinase and its cognate phosphatase in *Streptococcus pyogenes*: their biological functions and substrate identification. J Mol Biol **357:**1351-1372.
171. **Bingham EW.** 1976. Modification of casein by phosphatases and protein kinases. J Agric Food Chem **24:**1094-1099.
172. **Kinoshita E, Kinoshita-Kikuta E, Takiyama K, Koike T.** 2006. Phosphate-binding tag, a new tool to visualize phosphorylated proteins. Mol Cell Proteomics **5:**749-757.

173. **Schumacher MA, Min J, Link TM, Guan Z, Xu W, Ahn YH, Soderblom EJ, Kurie JM, Evdokimov A, Moseley MA, Lewis K, Brennan RG.** 2012. Role of unusual P loop ejection and autophosphorylation in HipA-mediated persistence and multidrug tolerance. Cell Rep **2:**518-525.
174. **Sajid A, Arora G, Gupta M, Upadhyay S, Nandicoori VK, Singh Y.** 2011. Phosphorylation of Mycobacterium tuberculosis Ser/Thr phosphatase by PknA and PknB. PLoS One **6:**e17871.
175. **Bradshaw N, Levdikov VM, Zimanyi CM, Gaudet R, Wilkinson AJ, Losick R.** 2017. A widespread family of serine/threonine protein phosphatases shares a common regulatory switch with proteasomal proteases. Elife **6**.
176. **Barrick JE, Yu DS, Yoon SH, Jeong H, Oh TK, Schneider D, Lenski RE, Kim JF.** 2009. Genome evolution and adaptation in a long-term experiment with *Escherichia coli*. Nature **461:**1243-1247.
177. **Soares NC, Spat P, Mendez JA, Nakedi K, Aranda J, Bou G.** 2014. Ser/Thr/Tyr phosphoproteome characterization of Acinetobacter baumannii: comparison between a reference strain and a highly invasive multidrug-resistant clinical isolate. J Proteomics **102:**113-124.
178. **Rajagopalan K, Dworkin J.** 2018. Identification and biochemical characterization of a novel PP2C-like Ser/Thr phosphatase in E. coli. J Bacteriol doi:10.1128/JB.00225-18.
179. **Waterhouse A, Bertoni M, Bienert S, Studer G, Tauriello G, Gumienny R, Heer FT, de Beer TAP, Rempfer C, Bordoli L, Lepore R, Schwede T.** 2018. SWISS-MODEL: homology modelling of protein structures and complexes. Nucleic Acids Res **46:**W296-W303.
180. **Massiah MA, Wright KM, Du H.** 2016. Obtaining Soluble Folded Proteins from Inclusion Bodies Using Sarkosyl, Triton X-100, and CHAPS: Application to LB and M9 Minimal Media. Curr Protoc Protein Sci **84:**6 13 11-16 13 24.
181. **Andersen KR, Leksa NC, Schwartz TU.** 2013. Optimized *E. coli* expression strain LOBSTR eliminates common contaminants from His-tag purification. Proteins **81:**1857-1861.
182. **Ruegg UT, Burgess GM.** 1989. Staurosporine, K-252 and UCN-01: potent but nonspecific inhibitors of protein kinases. Trends Pharmacol Sci **10:**218-220.
183. **Meggio F, Donella Deana A, Ruzzene M, Brunati AM, Cesaro L, Guerra B, Meyer T, Mett H, Fabbro D, Furet P, et al.** 1995. Different susceptibility of protein kinases to staurosporine inhibition. Kinetic studies and molecular bases for the resistance of protein kinase CK2. Eur J Biochem **234:**317-322.
184. **Liu Q, Fan J, Niu C, Wang D, Wang J, Wang X, Villaruz AE, Li M, Otto M, Gao Q.** 2011. The eukaryotic-type serine/threonine protein kinase Stk is required for biofilm formation and virulence in Staphylococcus epidermidis. PLoS One **6:**e25380.
185. **Srinivasan VB, Vaidyanathan V, Mondal A, Venkataramaiah M, Rajamohan G.** 2012. Functional characterization of a novel Mn2+ dependent protein serine/threonine kinase KpnK, produced by Klebsiella pneumoniae strain MGH78578. FEBS Lett **586:**3778-3786.
186. **Knighton DR, Zheng JH, Ten Eyck LF, Ashford VA, Xuong NH, Taylor SS, Sowadski JM.** 1991. Crystal structure of the catalytic subunit of cyclic adenosine monophosphate-dependent protein kinase. Science **253:**407-414.

187. **Zheng W, Cai X, Li S, Li Z.** 2018. Autophosphorylation Mechanism of the Ser/Thr Kinase Stk1 From Staphylococcus aureus. Front Microbiol **9:**758.
188. **Ravala SK, Singh S, Yadav GS, Kumar S, Karthikeyan S, Chakraborti PK.** 2015. Evidence that phosphorylation of threonine in the GT motif triggers activation of PknA, a eukaryotic-type serine/threonine kinase from Mycobacterium tuberculosis. FEBS J **282:**1419-1431.
189. **Kall L, Krogh A, Sonnhammer EL.** 2007. Advantages of combined transmembrane topology and signal peptide prediction--the Phobius web server. Nucleic Acids Res **35:**W429-432.
190. **Alexeyev MF, Winkler HH.** 1999. Membrane topology of the Rickettsia prowazekii ATP/ADP translocase revealed by novel dual pho-lac reporters. J Mol Biol **285:**1503-1513.
191. **Islam ST, Taylor VL, Qi M, Lam JS.** 2010. Membrane topology mapping of the O-antigen flippase (Wzx), polymerase (Wzy), and ligase (WaaL) from Pseudomonas aeruginosa PAO1 reveals novel domain architectures. MBio **1**.
192. **Karimova G, Ladant D.** 2017. Defining Membrane Protein Topology Using pho-lac Reporter Fusions. Methods Mol Biol **1615:**129-142.
193. **Karimova G, Robichon C, Ladant D.** 2009. Characterization of YmgF, a 72-residue inner membrane protein that associates with the Escherichia coli cell division machinery. J Bacteriol **191:**333-346.
194. **Doherty AJ, Serpell LC, Ponting CP.** 1996. The helix-hairpin-helix DNA-binding motif: a structural basis for non-sequence-specific recognition of DNA. Nucleic Acids Res **24:**2488-2497.
195. **Slauch JM, Silhavy TJ.** 1991. Genetic fusions as experimental tools. Methods Enzymol **204:**213-248.
196. **Kristich CJ, Wells CL, Dunny GM.** 2007. A eukaryotic-type Ser/Thr kinase in Enterococcus faecalis mediates antimicrobial resistance and intestinal persistence. Proc Natl Acad Sci U S A **104:**3508-3513.
197. **Wiegand I, Hilpert K, Hancock RE.** 2008. Agar and broth dilution methods to determine the minimal inhibitory concentration (MIC) of antimicrobial substances. Nat Protoc **3:**163-175.
198. **Finn RD, Attwood TK, Babbitt PC, Bateman A, Bork P, Bridge AJ, Chang HY, Dosztanyi Z, El-Gebali S, Fraser M, Gough J, Haft D, Holliday GL, Huang H, Huang X, Letunic I, Lopez R, Lu S, Marchler-Bauer A, Mi H, Mistry J, Natale DA, Necci M, Nuka G, Orengo CA, Park Y, Pesseat S, Piovesan D, Potter SC, Rawlings ND, Redaschi N, Richardson L, Rivoire C, Sangrador-Vegas A, Sigrist C, Sillitoe I, Smithers B, Squizzato S, Sutton G, Thanki N, Thomas PD, Tosatto SC, Wu CH, Xenarios I, Yeh LS, Young SY, Mitchell AL.** 2017. InterPro in 2017-beyond protein family and domain annotations. Nucleic Acids Res **45:**D190-D199.
199. **Aravind L, Walker DR, Koonin EV.** 1999. Conserved domains in DNA repair proteins and evolution of repair systems. Nucleic Acids Res **27:**1223-1242.
200. **Thayer MM, Ahern H, Xing D, Cunningham RP, Tainer JA.** 1995. Novel DNA binding motifs in the DNA repair enzyme endonuclease III crystal structure. EMBO J **14:**4108-4120.
201. **Bowman BR, Lee S, Wang S, Verdine GL.** 2010. Structure of Escherichia coli AlkA in complex with undamaged DNA. J Biol Chem **285:**35783-35791.

202. **Hollis T, Ichikawa Y, Ellenberger T.** 2000. DNA bending and a flip-out mechanism for base excision by the helix-hairpin-helix DNA glycosylase, Escherichia coli AlkA. EMBO J **19:**758-766.
203. **Newmark KG, O'Reilly EK, Pohlhaus JR, Kreuzer KN.** 2005. Genetic analysis of the requirements for SOS induction by nalidixic acid in Escherichia coli. Gene **356:**69-76.
204. **Drlica K, Kreiswirth B.** 1994. 4-quinolones and the physiology of DNA gyrase. Adv Pharmacol **29A:**263-283.
205. **Moolenaar GF, Uiterkamp RS, Zwijnenburg DA, Goosen N.** 1998. The C-terminal region of the Escherichia coli UvrC protein, which is homologous to the C-terminal region of the human ERCC1 protein, is involved in DNA binding and 5'-incision. Nucleic Acids Res **26:**462-468.
206. **Lin XM, Li H, Wang C, Peng XX.** 2008. Proteomic analysis of nalidixic acid resistance in Escherichia coli: identification and functional characterization of OM proteins. J Proteome Res **7:**2399-2405.
207. **Parandhaman DK, Sharma P, Bisht D, Narayanan S.** 2014. Proteome and phosphoproteome analysis of the serine/threonine protein kinase E mutant of Mycobacterium tuberculosis. Life Sci **109:**116-126.
208. **Gralla JD.** 2005. Escherichia coli ribosomal RNA transcription: regulatory roles for ppGpp, NTPs, architectural proteins and a polymerase-binding protein. Mol Microbiol **55:**973-977.
209. **Misra SK, Milohanic E, Ake F, Mijakovic I, Deutscher J, Monnet V, Henry C.** 2011. Analysis of the serine/threonine/tyrosine phosphoproteome of the pathogenic bacterium Listeria monocytogenes reveals phosphorylated proteins related to virulence. Proteomics **11:**4155-4165.
210. **Ouidir T, Jouenne T, Hardouin J.** 2016. Post-translational modifications in Pseudomonas aeruginosa revolutionized by proteomic analysis. Biochimie **125:**66-74.
211. **Manning G, Plowman GD, Hunter T, Sudarsanam S.** 2002. Evolution of protein kinase signaling from yeast to man. Trends Biochem Sci **27:**514-520.
212. **Hari SB, Merritt EA, Maly DJ.** 2013. Sequence determinants of a specific inactive protein kinase conformation. Chem Biol **20:**806-815.
213. **Bidnenko V, Shi L, Kobir A, Ventroux M, Pigeonneau N, Henry C, Trubuil A, Noirot-Gros MF, Mijakovic I.** 2013. Bacillus subtilis serine/threonine protein kinase YabT is involved in spore development via phosphorylation of a bacterial recombinase. Mol Microbiol **88:**921-935.
214. **Cruz JW, Rothenbacher FP, Maehigashi T, Lane WS, Dunham CM, Woychik NA.** 2014. Doc toxin is a kinase that inactivates elongation factor Tu. J Biol Chem **289:**7788-7798.
215. **Talavera A, Hendrix J, Versees W, Jurenas D, Van Nerom K, Vandenberk N, Singh RK, Konijnenberg A, De Gieter S, Castro-Roa D, Barth A, De Greve H, Sobott F, Hofkens J, Zenkin N, Loris R, Garcia-Pino A.** 2018. Phosphorylation decelerates conformational dynamics in bacterial translation elongation factors. Sci Adv **4:**eaap9714.
216. **Wiborg O, Andersen C, Knudsen CR, Clark BF, Nyborg J.** 1996. Mapping Escherichia coli elongation factor Tu residues involved in binding of aminoacyl-tRNA. J Biol Chem **271:**20406-20411.

217. **Swart GW, Parmeggiani A, Kraal B, Bosch L.** 1987. Effects of the mutation glycine-222----aspartic acid on the functions of elongation factor Tu. Biochemistry **26:**2047-2054.
218. **Vorstenbosch E, Pape T, Rodnina MV, Kraal B, Wintermeyer W.** 1996. The G222D mutation in elongation factor Tu inhibits the codon-induced conformational changes leading to GTPase activation on the ribosome. EMBO J **15:**6766-6774.
219. **Khan S, Nagarajan SN, Parikh A, Samantaray S, Singh A, Kumar D, Roy RP, Bhatt A, Nandicoori VK.** 2010. Phosphorylation of enoyl-acyl carrier protein reductase InhA impacts mycobacterial growth and survival. J Biol Chem **285:**37860-37871.
220. **Kumar P, Kumar D, Parikh A, Rananaware D, Gupta M, Singh Y, Nandicoori VK.** 2009. The Mycobacterium tuberculosis protein kinase K modulates activation of transcription from the promoter of mycobacterial monooxygenase operon through phosphorylation of the transcriptional regulator VirS. J Biol Chem **284:**11090-11099.
221. **Fabbro D, Cowan-Jacob SW, Moebitz H.** 2015. Ten things you should know about protein kinases: IUPHAR Review 14. Br J Pharmacol **172:**2675-2700.
222. **McKeegan KS, Borges-Walmsley MI, Walmsley AR.** 2002. Microbial and viral drug resistance mechanisms. Trends Microbiol **10:**S8-14.
223. **Nikaido H.** 1996. Multidrug efflux pumps of gram-negative bacteria. J Bacteriol **178:**5853-5859.
224. **Nishino K, Yamada J, Hirakawa H, Hirata T, Yamaguchi A.** 2003. Roles of TolC-dependent multidrug transporters of Escherichia coli in resistance to beta-lactams. Antimicrob Agents Chemother **47:**3030-3033.
225. **Kinoshita E, Kinoshita-Kikuta E, Sugiyama Y, Fukada Y, Ozeki T, Koike T.** 2012. Highly sensitive detection of protein phosphorylation by using improved Phos-tag Biotin. Proteomics **12:**932-937.
226. **Iliuk A, Liu XS, Xue L, Liu X, Tao WA.** 2012. Chemical visualization of phosphoproteomes on membrane. Mol Cell Proteomics **11:**629-639.
227. **Kothe U, Rodnina MV.** 2006. Delayed release of inorganic phosphate from elongation factor Tu following GTP hydrolysis on the ribosome. Biochemistry **45:**12767-12774.

Appendix A: Strains used in this study

Strains used in Chapter 3

Strain	Relevant Genotype	Description	Reference
DH5α			Invitrogen
C43(DE3)			(1)
BL21(DE3)			Stratagene
LOBSTR (BL21(DE3)			Kerafast (2)
JDE2944	pKR16 amp	C43(DE3) expressing N terminal 6X-His tagged WT PphC from *E.coli* REL606	This study
JDE2946	pKR17 amp	C43(DE3) expressing N terminal 6X-His tagged D46N PphC *E.coli* REL606	This study
JDE2908	pKR02 amp	C43(DE3) expressing N terminal 6X-His tagged WT PphC from *E.coli* MG1655	This study
JDE3039	pKR60 amp	C43(DE3) expressing N terminal 6X-His tagged S174A PphC from *E.coli* REL606	This study
JDE1715	pSFP65	BL21(DE3) expressing C terminal StrepII tagged WT PrpC from *B.subtilis*	(3)
KR81	pKR31 amp	LOBSTR-BL21 (DE3) expressing N terminal 6X-His tagged WT YegI from *E.coli* REL606	This study
KR87	pKR29 amp	LOBSTR-BL21 (DE3) expressing N terminal 6X-His tagged WT YegI-NTD from *E.coli* REL606	This study
JDE2117	pEN03 amp	C43(DE3) expressing N terminal 6X-His tagged WT HipA from *E.coli* MG1655	This study
JDE2916	pKR07 amp	C43(DE3) expressing N terminal 6X-His tagged WT GltX from *E.coli* MG1655	This study

Strains used in Chapter 4

Strain	Relevant Genotype	Description	Reference
DH5α			Laboratory stock
JDE2735	REL606		(4)

JDE2487	MG1655		Laboratory stock
KR70	pKR31 amp	C43 (DE3) expressing N terminal 6X-His tagged WT YegI from *E.coli* REL606	This study
KR81	pKR31 amp	LOBSTR-BL21 (DE3) expressing N terminal 6X-His tagged WT YegI from *E.coli* REL606	Chapter 3
KR71	pKR29 amp	C43 (DE3) expressing N terminal 6X-His tagged WT YegI-NTD from *E.coli* REL606	This study
KR87	pKR29 amp	LOBSTR-BL21 (DE3) expressing N terminal 6X-His tagged WT YegI-NTD from *E.coli* REL606	Chapter 3
KR245	pKR81 amp	LOBSTR-BL21 (DE3) expressing N terminal 6X-His tagged K39D YegI from *E.coli* REL606	This study
KR251	pKR83 amp	LOBSTR-BL21 (DE3) expressing N terminal 6X-His tagged D141N YegI from *E.coli* REL606	This study
KR289	pKR90 amp	LOBSTR-BL21 (DE3) expressing N terminal 6X-His tagged K39A YegI from *E.coli* REL606	This study
KR314	pKR97 amp	LOBSTR-BL21 (DE3) expressing N terminal 6X-His tagged S160FD161G YegI from *E.coli* REL606	This study
KR135	pKR64 amp	LOBSTR-BL21 (DE3) expressing N terminal 6X-His tagged S602SS644A YegI from *E.coli* REL606	This study
KR137	pKR67 amp	LOBSTR-BL21 (DE3) expressing N terminal 6X-His tagged S153AS160AS162A YegI- NTD from *E.coli* REL606	This study
KR03	pBAD24 amp	DH5α expressing pBAD24 plasmid	This study
KR223	pKR78 amp	DH5α expressing N terminal 6X-His tagged PhoA (aa 21-471) lacZα (aa 5-60)	This study
KR221	pKR72 amp	DH5α expressing N terminal 6X-His tagged YegI (aa 1-646) fused with PhoA lacZα from *E.coli* REL606	This study
KR211	pKR73 amp	DH5α expressing N terminal 6X-His tagged YegI (aa 1-439) fused with PhoAlacZα from *E.coli* REL606	This study

KR213	pKR74 amp	DH5α expressing N terminal 6X-His tagged YegI (aa 1-432) fused with PhoA lacZα from *E.coli* REL606	This study
KR215	pKR75 amp	DH5α expressing N terminal 6X-His tagged YegI (aa 1-414) fused with PhoA lacZα from *E.coli* REL606	This study
KR218	pKR76 amp	DH5α expressing N terminal 6X-His tagged YegI (aa 1-390) fused with PhoA lacZα from *E.coli* REL606	This study
KR219	pKR77 amp	DH5α expressing N terminal 6X-His tagged YegI (aa 1-340) fused with PhoA lacZα from *E.coli* REL606	This study
KR154	Δ*yegI*::[FRT-kan-FRT]	In frame deletion of (Δaa 9-624) of *yegI* in JDE2735 (*E.coli* REL606)	This study
KR156	Δ*yegI*::FRT/pcp20	Removal of kan marker from KR154 using pcp20 flippase	This study
KR160	Δ*yegI*	ΔyegI in JDE2735	
KR168	Δ*yegI* ::[FRT-*lacZY* kan]	Generation of *yegI (aa 1-8)* translational fusion to lacZ by transforming pCE40 into KR156	This study
KR178	Δ*lacZ*::[FRT-kan-FRT]	In frame deletion (Δaa 10-1011) of *lacZ* in JDE2735	This study
KR181	Δ*lacZ*	Removal of kan marker from KR178 using pcp20 flippase	This study
KR188	Δ*lacZ* Δ*yegI* ::[FRT-*lacZY* kan]	*yegI lacZ* translational fusion in Δ*lacZ* strain.	This study
KR257	Δ*yegI*	Δ*yegI* in JDE2487 (*E.coli* MG1655)	This study
KR199	pBAD24 amp	REL606 WT (JDE2735) expressing pBAD24 empty vector	This study
KR200	pBAD24 amp	REL606 Δ*yegI* (KR160) expressing pBAD24 empty vector	This study
KR206	pKR31 amp	REL606 Δ*yegI* (KR160) expressing N terminal 6X-His tagged WT YegI from *E.coli* REL606	This study
KR244	pKR81 amp	REL606 Δ*yegI* (KR160) expressing N terminal 6X-His tagged K39D YegI from *E.coli* REL606	This study
KR250	pKR83 amp	REL606 Δ*yegI* (KR160) expressing N terminal 6X-His tagged D141N YegI from *E.coli* REL606	This study
KR230	pKR29 amp	REL606 Δ*yegI* (KR160) expressing N terminal 6X-His tagged YegI-NTD from *E.coli* REL606	This study

KR231	pKR30 amp	REL606 Δ*yegI* (KR160) expressing N terminal 6X-His tagged YegI (aa 1-300) from *E.coli* REL606	This study
KR292	pKR93 amp	REL606 Δ*yegI* (KR160) expressing N terminal 6X-His tagged YegI (aa 301-646) from *E.coli* REL606	This study
KR295	pKR92 amp	REL606 Δ*yegI* (KR160) expressing N terminal 6X-His tagged YegI (aa 436-646) from *E.coli* REL606	This study
KR309	pKR95 amp	REL606 Δ*yegI* (KR160) expressing N terminal 6X-His tagged YegI (aa 536-646) from *E.coli* REL606	This study
KR311	pKR96 amp	REL606 Δ*yegI* (KR160) expressing N terminal 6X-His tagged YegI (aa 566-646) from *E.coli* REL606	This study
KR329	Δ*tolC::Kan*	In frame deletion of (Δaa 10-475) of *tolC* in JDE2735	This study
KR337	Δ*tolC*	Removal of kan marker from KR329 using pcp20 flippase	This study
KR338	Δ*yegI* Δ*tolC*	ΔtolC in Δ*yegI* (KR160) strain	This study
KR205	pKR71 amp	BL21 (DE3) expressing N terminal 6X-His tagged WT Eno from *E.coli* REL606	This study
KR255	pKR85 amp	BL21 (DE3) expressing N terminal 6X-His tagged S400A Eno from *E.coli* REL606	This study
KR114	pGEX6p-1 amp	BL21(DE3) expressing GST tag alone from pGEX6p-1 vector	This study
KR113	pKR61 amp	BL21(DE3) expressing N terminal GST tagged EF-Tu from *E.coli* MG1655	This study
KR322	pKR103 amp	BL21(DE3) expressing N terminal 6X-His tagged EF-Tu from *E.coli* *E.coli* MG1655	This study
KR324	pKR105 amp	BL21(DE3) expressing N terminal 6X-His tagged EF-Tu from *E.coli* MG1655 and YegI-NTD (aa 1-300) from *E.coli* REL606	This study

Appendix B: Plasmids used in this study

Plasmids used in Chapter 3

Plasmid Name	Description	Reference
pBAD24	Cloning vector, ampR	(5)
pET11a	Cloning vector, ampR	Novagen
pKR02	*yegK(pphC)* was amplified from MG1655 genomic DNA using KR08/KR02 primers, digested with NcoI/PstI and ligated into pBAD24	This study
pKR16	*yegK(pphC)* was amplified from REL606 genomic DNA using KR38/KR39 primers, digested with NcoI/PstI and ligated into pBAD24	This study
pKR17	REL606 D46N *yegK(pphC)* was generated by two step PCR using KR38/KR41 and KR39/KR40 primer pairs followed by amplification with KR38/KR39. Resulting product was digested with NcoI/PstI and ligated into pBAD24	This study
pKR29	*yegI* (aa 1-390) was amplified from REL606 genomic DNA using KR58/KR60 primers, digested with NcoI/SphI and ligated into pBAD24	This study
pKR31	*yegI* was amplified from REL606 genomic DNA using KR58/KR59 primers, digested with NcoI/SphI and ligated into pBAD24	This study
pKR60	REL606 S174A *yegK(pphC)* was generated by two step PCR using KR38/KR129 and KR128/KR40 primer pairs followed by amplification with KR38/KR39. Resulting product was digested with NcoI/PstI and ligated into pBAD24	This study
pEN3	*hipA* was amplified from MG1655 genomic DNA using EN05/EN02 primers, digested with XbaI/PstI and ligated into pBAD24	Laboratory Stock (Liz Nagle)
pKR07	*gltX* was amplified from MG1655 genomic DNA using KR23/KR25 primers, digested with NdeI/BamhI and ligated into pET11a	This study

Plasmids used in Chapter 4

Plasmid Name	Description	Reference
pBAD24	Cloning vector, ampR	(5)
pGEX6p-1	Cloning vector, ampR	GE healthcare
pETduet-1	Cloning vector, ampR	Novagen
pCE40	*oriR6K**γ** kan* FRT *lacZ*$^{+}$ *lacY*$^{+}$	(6)
pETPhos	Cloning vector, ampR	(7)
pKD13	*oriR6K**γ** kan FRT kan bla , ampR*	(8)
pKD46	repA101^{ts} araBp-gam-bet-exo oriR101 bla, ampR	(8)
Pcp20	λpR-FLP λcI857+ Rep^{ts} bla cat	(8)
pKR81	REL606 K39D *yegI* was generated by two step PCR using KR58/KR246 and KR245/KR59 primer pairs followed by amplification with KR58/KR59. Resulting product was digested with NcoI/SphI and ligated into pBAD24	This study
pKR83	REL606 D141N *yegI* was generated by two step PCR using KR58/KR248 and KR247/KR59 primer pairs followed by amplification with KR58/KR59. Resulting product was digested with NcoI/SphI and ligated into pBAD24	This study
pKR90	REL606 K39A *yegI* was generated by two step PCR using KR58/KR264 and KR263/KR59 primer pairs followed by amplification with KR58/KR59. Resulting product was digested with NcoI/SphI and ligated into pBAD24	This study
pKR97	REL606 S160FD161G *yegI* was generated by Q5 site directed mutagenesis using KR285/KR286 and pKR31 as a template.	This study
pKR62	REL606 S602A *yegI* was generated by two step PCR using KR58/KR153 and KR152/KR59 primer pairs followed by amplification with KR58/KR59. Resulting product was digested with NcoI/SphI and ligated into pBAD24	This study
pKR64	REL606 S602AS644A *yegI* was generated by two step PCR using pKR62 as template and KR58/KR155 and KR154/59 primer pairs followed by amplification with KR58/KR59.	This study

	Resulting product was digested with NcoI/SphI and ligated into pBAD24	
pKR65	REL606 S153A *yegI* (aa 1-390) was generated by two step PCR using KR58/KR158 and KR157/60 primer pairs followed by amplification with KR58/KR60. Resulting product was digested with NcoI/SphI and ligated into pBAD24	This study
pKR67	REL606 S153AS160AS162A *yegI* (aa 1-390) was generated by two step PCR using pKR65 as template KR58/KR160 and KR159/60 primer pairs followed by amplification with KR58/KR60. Resulting product was digested with NcoI/SphI and ligated into pBAD24	This study
pKR72	REL606 *yegI-phoA-lacZ fusion* was generated by overlap extension PCR using KR223/KR224 , KR225/KR226, KR227/KR228 primer pairs followed by amplification with KR229/KR228. Resulting product was digested with NheI/KpnI and ligated into pBAD24	This study
pKR73	REL606 YegI E439-phoA lacZ was generated by Q5 site directed mutagenesis using KR230/KR231 and pKR72 as a template.	This study
pKR74	REL606 YegI T432-phoA lacZ was generated by Q5 site directed mutagenesis using KR230/KR232 and pKR72 as a template.	This study
pKR75	REL606 YegI R414-phoA lacZ was generated by Q5 site directed mutagenesis using KR230/KR233 and pKR72 as a template.	This study
pKR76	REL606 YegI E390-phoA lacZ was generated by Q5 site directed mutagenesis using KR230/KR234 and pKR72 as a template.	This study
pKR77	REL606 YegI E340-phoA lacZ was generated by Q5 site directed mutagenesis using KR230/KR235 and pKR72 as a template.	This study
pKR78	Control phoA lacZ was generated by Q5 site directed mutagenesis using KR230/KR240 and pKR72 as a template.	This study
pKR30	*yegI(1-300)* was amplified from REL606 genomic DNA using KR58/KR61 primers, digested with NcoI/SphI and ligated into pBAD24	This study
pKR93	REL606 YegI (301-436) was generated by Q5 site directed mutagenesis using KR274/KR275 and pKR31 as a template.	This study

pKR92	REL606 YegI (436-646) was generated by Q5 site directed mutagenesis using KR276/KR275 and pKR31 as a template.	This study
pKR95	REL606 YegI (536-646) was generated by Q5 site directed mutagenesis using KR287/KR288 and pKR31 as a template.	This study
pKR96	REL606 YegI (566-646) was generated by Q5 site directed mutagenesis using KR289/KR290 and pKR31 as a template.	This study
pKR71	*eno* was amplified from REL606 genomic DNA using KR211/KR212 primers, digested with NdeI/BamHI and ligated into pETPhos	This study
pKR85	REL606 S400A *eno* was generated by two step PCR using KR211/KR250 and KR249/KR212 primer pairs followed by amplification with KR211/KR212. Resulting product was digested with NdeI/BamHI and ligated into pETPhos	This study
pKR61	*tufB* was amplified from MG1655 genomic DNA using KR145/KR146 primers, digested with BamHI/NotI and ligated into pGEX6p-1	This study
pKR103	*tufB* was amplified from MG1655 genomic DNA using KR293/KR294 primers, digested with BamHI/NotI and ligated into pETDUET-1	This study
pKR105	*yegI(aa 1-390)* was amplified from REL606 genomic DNA using KR62/KR64 primers, digested with BglII/ Xho1 and ligated into pKR103	This study

Appendix C: Oligos used in this study

Oligos used in Chapter 3

Oligo	Sequence (5'-3')	Features	Origin
KR02	cgtccactgcagTCACTCTGCCCACAGCGC	PstI;STOP	This study
KR08	ggaaaaccatgg*cacatcatcatcatcatcat*AGCTGGCGTC TGGTCTATG	NcoI; *6X-His tag*	This study
KR38	ggaaaaccatggca*catcatcatcatcatcat*AGCTGGCGTC TGGTTTATGC	NcoI; *6X-His tag*	This study
KR39	cgtccactgcagTCATGGTAACCACAGCGCCA	PstI; STOP	This study
KR40	TTCCTTGCT**AAT**GGCGCAGGT	D46N	This study
KR41	ACCTGCGCC**ATT**AGCAAGGAA	D46N	This study
KR58	ggaaaaccatggca*catcatcatcatcatcat*AAACCCACTT TATATACTGCTAC	NcoI; *6X-His tag*	This study
KR59	cgtccagcatgcTCAGCAGCGGCTTAAATCTG	SphI; STOP	This study
KR60	cgtccagcatgctcaTTCGCGCCGTAACAGGCCT	SphI; STOP	This study
KR128	CTTTCACC**GCC**ACTGAGCG	S174A	This study
KR129	CGCTCAGT**GGC**GGTGAAAG	S174A	This study
EN5	ctaggaattcatggct*catcatcatcatcatcat*tcgcgcCCTAAA CTTGTCACTTGGAT	EcoRI; *6X-His tag*	This study
EN2	aaaactgcagtcaCTTACTACCGTATTCTCGGC	PstI; STOP	This study
KR23	ggaaaacatatgatg*catcatcatcatcatcac*AAAATCAAA ACTCGCTTCGCG	Nde1; *6X-His tag*	This study
KR25	cgtccaggatccTTACTGCTGATTTTCGCGTTCA	BamHI; STOP	This study

Homology sequences to gene are shown in uppercase. Non homology sequences are indicated in lower case including His_6-tag (italics), restriction enzyme sites (underlined). Point mutations are highlighted in bold.

Oligos used in Chapter 4

Oligo	Sequence (5'-3')	Features	Origin
KR58	ggaaaaccatggca*catcatcatcatcatcat*AAACCCA CTTTATATACTGCTAC	NcoI; *6X-His tag*	This study
KR59	cgtccagcatgcTCAGCAGCGGCTTAAATCT G	SphI; STOP	This study
KR60	cgtccagcatgctcaTTCGCGCCGTAACAGGC CT	SphI; STOP	This study
KR61	cgtccagcatgctcaTAGAGAATCCAGTGCTG CTAC	SphI; STOP	This study
KR245	AGCGTCGCC**GAC**ATTTATCAC	K39D	This study
KR246	GTGATAAAT**GTC**GGCGACGCT	K39D	This study
KR247	GTCGTGGGG**AAC**GTAAACCA	D141N	This study
KR248	TGGTTTAC**GTT**CCCCACGAC	D141N	This study
KR263	AGCGTCGCC**GCG**ATTTATCA	K39A	This study
KR264	TGATAAAT**CGC**GGCGACGCT	K39A	This study
KR285	GTTGATCGAT**TTTGGC**TCCTTTCAGAT TAACGCCAATG	S160FD161G	This study
KR286	ACCACTTTGCTGTCGCGA	S160FD161G	This study
KR152	GGCTGGAA**GCG**GCGTTGAC	S602A	This study
KR153	GTCAACGC**CGC**TTCCAGCC	S602A	This study
KR154	GCAGATTTA**GCC**CGCTGCTGA	S644A	This study
KR155	TCAGCAGCG**GGC**TAAATCTGC	S644A	This study
KR157	GTCGCGAC**GCC**AAAGTGGT	S153A	This study
KR158	ACCACTTT**GGC**GTCGCGAC	S153A	This study

KR159	TTGATCGAT**GCT**GAC**GCC**TTTC	S160AS162A	This study
KR160	GAAA**GGC**GTC**AGC**ATCGATCAA	S160AS162A	This study
KR223	ccatggca*catcatcatcatcatcat*AAACCCACTTTATATACTGCTACT	NcoI; *6X-His tag*	This study
KR224	**catttctggtgtccgggc***gctaccgctgccgctacc*GCAGCGGCTTAAATCTGCCTG	PhoA; *Linker*	This study
KR225	GCCCGGACACCAGAAATG	PhoA	This study
KR226	**gacggccagtgaatccgt**TTTCAGCCCCAGAGCGGC	LacZ; PhoA	This study
KR227	ACGGATTCACTGGCCGTCGTT	LacZ	This study
KR228	cgtccaggtaccttaGCGCCATTCGCCATTCAGGC	Kpn1; STOP	This study
KR229	ggaaaagctagcaggaggaattCCATGGCACATCATCATCATCAT	Nhe1; His tag	This study
KR230	GGTAGCGGCAGCGGTAGC	Q5 SDM_Linker	This study
KR231	TTCTGCTTTATAAGCTTTGCTTGTCAGACTG	Q5 SDM_E439	This study
KR232	TGTCAGACTGCCAATAATCCAGATAGC	Q5_SDM_E432	This study
KR233	ACGCGGTTCTGCCTGAAGG	Q5_SDM_E414	This study
KR234	TTCGCGCCGTAACAGGCC	Q5_SDM_E390	This study
KR235	TTCGCCGAGATCAATAAAATAGATAACGCC	Q5_SDM_E340	This study
KR240	ATGATGATGATGATGATGTGCCATGGTG	Q5_SDM_phoAlacZ	This study
KR176	gcgctgtggttaccatgaaacccactttatatactgctacGATCCGTCGACCTGCAGTTC	yegI, pKD13	This study

KR177	ctgagccagtttttctgccgcctgacgtaacggttccatcaaTGTGTAGGCTGGAGCTGCTT	yegI, pKD13	This study
KR185	cacacaggaaacagctatgaccatgattacggattcactgGTGTAGGCTGGAGCTGCTT	lacZ, pKD13	This study
KR186	tttttgacaccagaccaactggtaatggtagcgaccggcCATATGAATATCCTCCTTAGTTC	lacZ, pKD13	This study
KR274	CGCCAACAGTTAAAGAAATG	Q5 SDM_L300	This study
KR275	ATGATGATGATGATGATGTG	Q5 SDM_His	This study
KR276	AAAGCAGAAATCCAGCAAC	Q5 SDM_K437	This study
KR287	ATTGAAACAGCAGCGGATG	Q5 SDM_G536	This study
KR288	ATGATGATGATGATGATGTGC	Q5 SDM_ G536	This study
KR289	GCGAGCTGTGAACGCCGT	Q5 SDM_G566	This study
KR290	ATGATGATGATGATGATGTGCCATGG	Q5 SDM_G566	This study
KR299	aaggaatgcaaatgaagaaattgctccccattcttatcggGATCCGTCGACCTGCAGTTC	tolC, pKD13	This study
KR300	ttatgaccgttactggtggtagtgcgtgcggatgtttgctTGTGTAGGCTGGAGCTGCTT	tolC, pKD13	This study
KR211	ggaaaacatATGTCCAAAATCGTAAAAATCATC	Nde1	This study
KR212	cgtccaggatccTTATGCCTGGCCTTTGATCT	BamH1	This study
KR249	TGAGCCGT**GCT**GACCGTGT	S400A	This study
KR250	ACACGGTC**AGC**ACGGCTCA	S400A	This study
KR145	ggaaaaggatccTCTAAAGAAAAGTTTGAACGTACA	BamH1	This study
KR146	cgtccactcgagTTAGCTCAGAACTTTTGCTACAA	Xho1	This study
KR293	ggaaaaggatccgTCTAAAGAAAAGTTTGAACGTAC	BamH1	This study

KR294	cgtccagcggccgcTTAGCTCAGAACTTTTGCTACAA	Not1	This study
KR62	ggaaaaagatctaAAACCCACTTTATATACTGCTAC	BglII	This study
KR64	cgtccactcgagtcaTTCGCGCCGTAACAGGCCT	Xho1	This study

Homology sequences to gene are shown in uppercase. Non homology sequences are indicated in lower case including His_6-tag (italics), restriction enzyme sites (underlined). Point mutations are highlighted in bold. Homology sequences for deletion of gene (40nt) is highlighted in blue.

1. **Miroux B, Walker JE.** 1996. Over-production of proteins in *Escherichia coli*: mutant hosts that allow synthesis of some membrane proteins and globular proteins at high levels. J Mol Biol **260:**289-298.
2. **Andersen KR, Leksa NC, Schwartz TU.** 2013. Optimized *E. coli* expression strain LOBSTR eliminates common contaminants from His-tag purification. Proteins **81:**1857-1861.
3. **Pereira SF, Gonzalez RL, Jr., Dworkin J.** 2015. Protein synthesis during cellular quiescence is inhibited by phosphorylation of a translational elongation factor. Proc Natl Acad Sci U S A **112:**E3274-3281.
4. **Barrick JE, Yu DS, Yoon SH, Jeong H, Oh TK, Schneider D, Lenski RE, Kim JF.** 2009. Genome evolution and adaptation in a long-term experiment with *Escherichia coli*. Nature **461:**1243-1247.
5. **Guzman LM, Belin D, Carson MJ, Beckwith J.** 1995. Tight regulation, modulation, and high-level expression by vectors containing the arabinose PBAD promoter. J Bacteriol **177:**4121-4130.
6. **Ellermeier CD, Janakiraman A, Slauch JM.** 2002. Construction of targeted single copy lac fusions using lambda Red and FLP-mediated site-specific recombination in bacteria. Gene **290:**153-161.
7. **Canova MJ, Kremer L, Molle V.** 2008. pETPhos: a customized expression vector designed for further characterization of Ser/Thr/Tyr protein kinases and their substrates. Plasmid **60:**149-153.
8. **Datsenko KA, Wanner BL.** 2000. One-step inactivation of chromosomal genes in Escherichia coli K-12 using PCR products. Proc Natl Acad Sci U S A **97:**6640-6645.